國 立 交 通 大 學

土木工程學系

博士論文

載具沿滑軌運動之傾墜分析

Dynamic Analyses of a Vehicle Moving along a Guideway with Considering the Tip-off Effect

研 究 生： 周勝男

指導教授： 黃炯憲 博士

鄭淯平 博士

中華民國一百零一年六月

載具沿滑軌運動之傾墜分析

Dynamic Analyses of a Vehicle Moving along a Guideway with Considering the Tip-off Effect

研 究 生： 周勝男　　Student ： Sheng-Nan Chou

指導教授： 黃炯憲　　Advisors : Chiung-Shiann Huang

鄭復平　　Fu-Ping Cheng

國立交通大學

土木工程學系

博士論文

A Dissertation

Submitted to Department of Civil Engineering

College of Engineering

National Chiao Tung University

in partial Fulfillment of the Requirements

for the Degree of

Doctor of Philosophy

in

Civil Engineering

June 2012

Hsinchu, Taiwan, Republic of China

中華民國一百零一年六月

載具沿滑軌運動之傾墜分析

學生：周勝男　　指導教授：黃炯憲 博士

鄭復平 博士

國立交通大學土木工程學系 博士班

摘 要

本研究考量載具與滑軌間的結構互制行為，發展半解析方法分析載具沿著滑軌運動的傾墜反應。對於飛彈發射系統設計而言，精確的計算其傾墜反應是極為重要的課題，飛彈可視為本研究之載具。本文提出 R.E. 與 E.E. 兩種模型進行動態反應分析。其中 R.E. 模型係將載具視為剛性梁，滑軌視為彈性梁，而在 E.E. 模型中將載具與滑軌皆視為彈性梁。在上述分析模型的解析時，皆考慮了慣性力、科氏力與離心力的影響，同時載具與滑軌之間皆透過兩個剛性滑腳來接觸。

本研究基於 Euler-Bernoulli 梁理論，採用振態疊加法與拉格蘭日乘子法來推導載具與滑軌運動的控制方程式。此系統的運動方程式是由一組非線性的微分方程式所組成，其數值解採用 Petzold-Gear 的後向微分法（Backward Differentiation Formula, BDF）來求算此動態系統的數值模擬結果，所需花費時間較少於一般傳統逐步數值積分的方法，對於載具與滑軌的分析模擬經與文獻實際特殊案例的結果比較，可呈現本研究所提出之方法的優點。

利用此分析方法進一步探討滑軌的長度、載具滑腳的距離、載具與滑軌的質量比與剛性比等各參數對載具傾墜反應的影響，經由本研究之成果，於載具發射系統設計時，可以提供非常有價值的資訊。

關鍵字： 移動荷重; 移動梁; 拉格蘭日法; 振態疊加法; 傾墜效應

Dynamic Analyses of a Vehicle Moving along a Guideway with Considering the Tip-off Effect

Stduent : Sheng-Nan Chou

Advisors : Dr. Chiung-Shiann Huang
Dr. Fu-Ping Cheng

Department of Civil Engineering
National Chiao Tung University

ABSTRACT

A semi-analytical solution for analyzing the tip-off responses of a vehicle moving along a guideway is developed by considering the dynamic interaction between the vehicle and the guideway. Accurately determined tip-off responses are important for designing a launch system for a missile, in which the missile can be treated as the vehicle in the present study. Two models are proposed to determine those dynamic responses, namely, R.E. model and E.E. model. In the R.E. model, the vehicle is assumed rigid and its guideway is modeled as a flexible beam, while both of the vehicle and guideway are modeled as flexible beams in the E.E model. The inertia, Coriolis, and centrifugal forces are considered in these models. The vehicle contacts with its guideway through two rigid shoes.

Equations for governing the motions of the vehicle and the guideway are developed using the Lagrangian approach and the modal superposition method, on the basis of the Euler-Bernoulli beam theory. The governing equations, which are a set of nonlinear differential equations, are solved by the Petzold-Gear backward differentiation formula numerical method. It takes time lower than the traditional step-by-step numerical integration methods. Comparisons of the presented solutions with those based on different published models for the vehicle and guideway reveal the advantages of the present approach.

The solutions are further employed to investigate the effects of the length of the guideway, distance between the shoes of the vehicle, and mass and rigidity ratios of

the vehicle to the guideway on the tip-off responses of the vehicle. The results presented herein provide valuable information for designing vehicle launch systems.

keywords: moving load; moving beam model; Lagrangian approach; mode superposition; tip-off effect.

ACKNOWLEDGEMENTS

年過半百拿到博士學位，心中的喜樂絕對不比一般的年輕學子低，除了全職的上班工作與出差外，論文投稿與寫作期間的日常生活幾乎就是晚上窩在電腦前絞盡腦汁的推導理論與寫程式度過，雖然辛苦，但是收穫卻特別多。回想交大的求學階段，遇到許多的貴人，首先必須感謝我的指導老師鄭復平博士，您亦師亦友多年來持續在生活上的關心與論文研究上的指導，直到老師退休還熱心的將我託付給指導老師黃炯憲博士，使得我在最後關頭還能在研究上找到方向並總結出重要的成果，由於上班的任務繁重與限制，多次有勞黃老師假日來學校指導論文瓶頸與英文論文寫作，兩位指導老師的研究精神讓我如沐春風受益良多，當學生的我在此衷心感謝，期待日後仍能繼續向老師們多方請益。

在求學期間，劉俊秀、林昌佑、王彥博、洪士林、趙文成與陳誠直等諸位老師的學識淵博，讓我藉著修課與討論增加了專業的本質學能，同時在博士班資格考時的研究方向指導，讓我獲得許多寶貴的知識，在此一併致謝。由於工作上與學業上的壓力交雜，曾經萌生放棄學業的念頭，在此要感謝我生命中的貴人與長官姜武英博士，總是在每個階段引領我走出低潮，同時費心協助我選定的論文題目能夠與工作上的任務應用做完美的結合，讓我在工作與學業上能取得最佳的平衡並堅持到底。在畢業論文口試時，非常感謝楊明放院長、姚忠達教授與上述諸位老師的費心指導，並提供許多寶貴的建議與修訂方向，讓這份研究成果更為完整，在此表達衷心的謝忱。

我的高中同窗好友與同事李運璋博士，不僅協助我突破許多研究上的理論瓶頸，還引導我進入 LaTeX 排版與 Beamer 簡報系統等論文寫作工具的大門，由於我對文件品質上的執著，非常感謝他的耐心指導陪我走過初學階段。此外，林仁正學長多年來在每一段時間都會來電關切我的研究進度，雖然備感壓力，但是非常窩心，謝謝您學長。

攻讀博士學位是我人生中非常重要的階段，我很幸運擁有一個非常美滿的家庭，女兒項萱與兒子揚賀在成長與求學階段都能自我管理的很好，讓我不僅無後顧之憂甚至以他們為榮；當然最重要的是我摯愛的妻子淑敏，她為我承擔了大部分的家務與孩子們的瑣事，是我能夠畢業的最大支柱，一世夫妻百世恩，在求學的低潮期感謝她溫馨的陪我走過艱辛歲月，在論文即將付梓之際，我很願意將這份成果與我親愛的家人們共享，由於無法逐一感謝曾經幫助過我的每一個人，謹以誠摯的心向大家致上最真誠的謝意！

周勝男 謹識 07/10/2012

TABLE OF CONTENTS

LIST OF TABLES

LIST OF FIGURES

NOTATION

$\mathrm{P}(t)$	Thrust force acting on vehicle
J	Mass moment of inertia of rigid vehicle
g	Gravitational acceleration
$\theta_{_E}$	Angle of inclination of guideway
E_vI_v	Flexural rigidity of vehicle
E_gI_g	Flexural rigidity of guideway
L_v	Length of vehicle
L_g	Length of guideway
ξ_v	Damping ratio of vehicle
ξ_g	Damping ratio of guideway
ρ_vA_v	Mass per unit length of vehicle
ρ_gA_g	Mass per unit length of guideway
m_v	Mass of vehicle
d	Distance between shoes of vehicle
$d_{_1}$	Distance between the rear shoe and the center of gravity of the vehicle
d_R	Distance between left end to rear shoe of vehicle
d_G	Distance between left end to center of gravity of vehicle
d_F	Distance between left end to front shoe of vehicle
$F(t)$	Front shoe contact forces between vehicle and guideway
$R(t)$	Rear shoe contact forces between vehicle and guideway
$\zeta(t)$	Position coordinate of vehicle on guideway
$\dot{\zeta}(t)$	Velocity of vehicle on guideway
$\ddot{\zeta}(t)$	Acceleration of vehicle on guideway
$\zeta_{_R}$	Distance from left end of guideway to rear shoe of vehicle at $t = 0$
$\zeta_{_F}$	Distance from front shoe of vehicle to right end of guideway at $t = 0$

t_b	Time of thrust build-up
t_F	Time at which front shoe of vehicle loses contact
t_R	Time at which vehicle takes-off
$w(\zeta, t)$	Displacements of the shoe contact point in the y-direction of the guideway at position ζ and time t
y_R	Displacements of the rear shoe contact point in the y-direction of the guideway
y_F	Displacements of the front shoe contact point in the y-direction of the guideway
$\bar{y}(t)$	Displacement of the vehicle's center of gravity at time t
$\bar{\theta}(t)$	Pitch angle of the vehicle's center of gravity at time t
$\dot{\bar{y}}(t)$	Velocity of the vehicle's center of gravity at time t
$\dot{\bar{\theta}}(t)$	Pitch rate of the vehicle's center of gravity at time t
$Y_i(t)$	Generalized coordinate corresponding to the ith mode
$\dot{Y}_i(t)$	Generalized velocity corresponding to the ith mode
$\ddot{Y}_i(t)$	Generalized acceleration corresponding to the ith mode
$\mathbf{Y}$	Matrix of generalized coordinate
$\dot{\mathbf{Y}}$	Matrix of generalized velocity
$\ddot{\mathbf{Y}}$	Matrix of generalized acceleration
$\mathbf{M}$	Matrix of generalized mass
$\mathbf{C}$	Matrix of generalized damping
$\mathbf{K}$	Matrix of generalized stiffness
$\mathbf{Q}$	Matrix of generalized force
$\mathcal{G}_1$	Displacement constraint at rear shoe of vehicle
$\mathcal{G}_2$	Displacement constraint at front shoe of vehicle
λ	Lagrange multiplier
M_r	Mass ratio between vehicle and guideway
R_r	Flexural rigidity ratio between vehicle and guideway

CHAPTER ONE

Introduction

1.1 Background and Motivation

In real designs of all vehicle launch systems, one of the main concerns is to minimize the transverse motions of the vehicle, which can be a missile, moving along its guideway, especially when the vehicle takes off. In the field of control engineering, a vehicle and its guideway are typically modeled as rigid bodies for the tip-off analysis. Although such modeling is quite simple and easily used, it does not consider the dynamic interactions between the vehicle and its guideway. To reduce the transverse motions of the vehicle, it is important to accurately consider the vehicle acting forces and the associated vehicle-guideway interactions during the launch phase.

At present, much research has been devoted to the structural dynamic analysis of a flexible flight vehicle, whereas until now there has been no investigated study for vehicle launch system design considering the vehicle and guideway as flexible bodies in real applications. The bending flexibilities of vehicle and guideway can have a remarkable influence on the behaviors of the vehicle as it leaves the guideway of launcher, and hence on the resulting accuracy of control. The responses of the vehicle at take-off significantly affect its flight control, and accurately determining the responses of the vehicle in the tip-off phase is crucial. The motivation of this study is to develop an analysis method to efficiently and accurately study dynamic behaviors of a vehicle-guideway system with time-dependent constraints between the vehicle

and the guideway.

1.2 Statement of the Problems

When a vehicle moves along the guideway, the vehicle is mainly subjected to thrust, inertia, and gravity forces, and two phases can be identified (see Fig. 1.1). Before the front shoe of the vehicle loses contact with the guideway, the vehicle is in a two-shoe contact phase (see Fig. 1.1). The vehicle rotates with respect to its rear shoe when its front shoe loses contact with the guideway, and this phenomenon is known as tip-off. When the vehicle exhibits tip-off, it is referred to as being "in the tip-off phase" (see Fig. 1.2). In the published literature, such a vehicle and its guideway are typically modeled as rigid bodies for the tip-off analysis, the model is not sufficiently accurate to present the real behaviors of the vehicle. In real applications, the mass of the launched vehicle substantially exceeds that of its guideway, and both of the vehicle and the guideway are flexible.

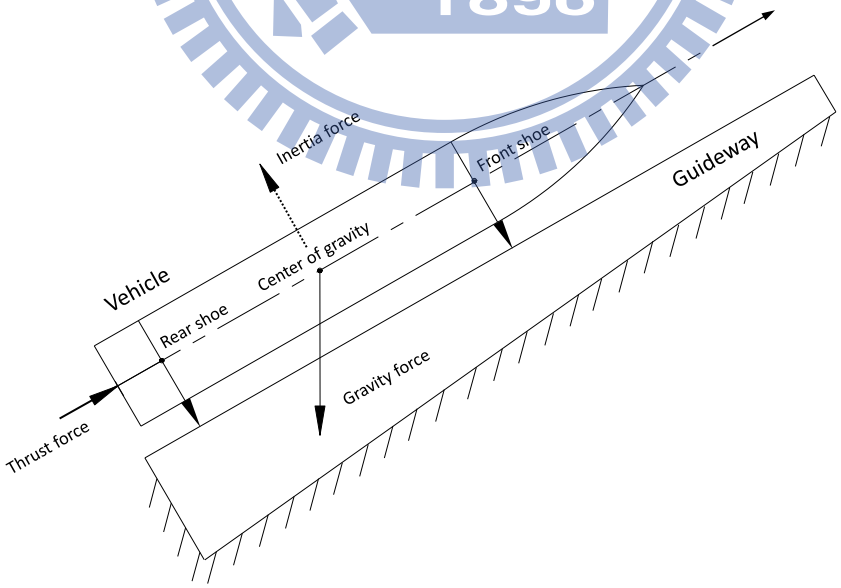

Figure 1.1: A typical vehicle launch system in a two-shoe contact phase.

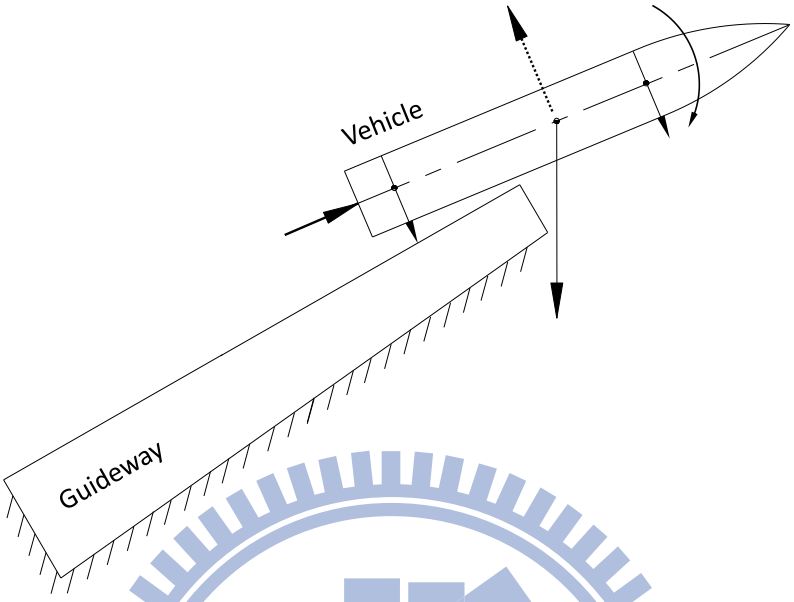

Figure 1.2: A typical vehicle launch system in a tip-off phase.

It is very important to accurately determine the behaviors of the vehicle When the vehicle excessively moves in the transverse direction during take-off, it is very possible that the vehicle collides with the guideway system. When the velocity of a vehicle is too low to develop the aerodynamic force for controlling its attitude or direction during the tip-off phase, its control fins can not function well, and the balance between the aerodynamic and other forces do not yet reach a stable state. Therefore, the control fins must be locked during the initial trajectory, and the initial flight conditions, which mainly result from the behaviors of the vehicle in the tip-off phase, must be accurately determined.

1.3 Literature Review

The dynamic responses of a beam subjected to a moving vehicle (or structure) have attracted the attention of researchers for a long time. An excellent state-of-the-art review

is given by the subcommittee on vibration problems associated with flexural member on transit systems [1]. The moving vehicle is often modeled as a moving force, a moving mass, a moving oscillator (also called a sprung mass model) or a moving beam. Modeling as a moving force is the simplest and oldest approach, which neglects the interaction between the vehicle and the beam [2–6]. Research work on this topic can be traced back to the 19^{th} century [2]. Timoshenko [3] derived numerous approximate solutions to the problem of a simply-supported beam under moving loads. Ayre *et al.* [4] studied the transverse vibrations of a two-span beam under a moving constant force. The moving force model is well known to apply only to the case in which the mass of the moving vehicle is much smaller than that of the beam, and only when the dynamic responses of the moving vehicle are not of interest. N. Sridharan *et al.* [5] presented a numerical analysis of vibration of beams subjected to moving loads. Numerical results obtained for the case of a constant force moving over a uniform simply supported beam have been compared with those obtained by using the analytical method. Hamada [5] has been presented a method , based on the double Laplace transformation, for dynamic analysis of a simply supported and damped Bernoulli-Euler uniform beam of finite length subjected to the action of a moving concentrated force. K. Henchi *et al.* [6] developed an exact dynamic stiffness element under the frame work of finite element approximation is presented to study the dynamic response of multi-span structures under a convoy of moving loads.

A moving mass model is a simple model that to some extent accounts for the interaction between the dynamic interaction between a moving structure and a beam [7–11]. The model was first proposed by Jeffcott [7] in 1929. Stanišić [8] employed the Fourier technique to investigate the responses of beams to an arbitrary number of concentrated moving masses. Akin and Mofid [9] presented a numerical solution by using the separation of variables technique to analyze the dynamic responses of an Euler-Bernoulli beam to a moving mass. Their solution scheme was very simple and can be used to determine the responses of beams under various boundary conditions.

Cifuentes [12] presents a combined finite element/finite difference technique to determine the response of a beam excited by a moving mass. The technique introduced herein is based on a Lagrange Multiplier formulation that allows one to represent the compatibility condition at the beam/mass interface using a set of auxiliary functions. This approach can be easily adapted to a standard finite element code. Michaltsos *et al.* [13] studied the linear dynamic response of a simply supported uniform beam under a moving load of constant magnitude and velocity by considering the effect of its mass. They highlighted the importance of considering the effect of the load mass. As the ratio M/ml (moving mass/mass of beam) increases, depending on the velocity, the ratio w_M/w_P (displacement of moving mass/displacement of load because of moving force) can increase considerably. Lee [14] studied the equation of motion in matrix form for an Euler beam acted upon by a concentrated mass moving at a constant speed is formulated by using the Lagrangian approach and the assumed mode method. Lee [15] also analysed extensively the transverse vibration of a Timoshenko beam acted on by an accelerating mass and compared with the corresponding behaviour of a Timoshenko beam subjected to an equivalent moving force neglecting the inertial effects of the mass. The effects of prescribed values of constant acceleration or deceleration of the moving mass on the deflection under the moving mass, as well as the contact forces, are investigated. Michaltsos [16] also studied the linear dynamic response of a simply supported elastic single-span beam under a moving load of constant magnitude and variable velocity, with an emphasis on the effect of acceleration or deceleration on the behaviour of the beam under a single load, or an actual vehicle model. Dehestani *et al.* [10] showed that it is necessary to consider the Coriolis acceleration associated with a mass moving along a vibrating beam. Wu [11] examined the effects of the inertial, Coriolis, and centrifugal forces induced by non-coupled moving masses on the dynamic responses of an inclined simply-supported beam. Further, Frýba [17] compiled a book containing descriptions of almost all studies on the vibration of solids and structures under a moving load.

A moving oscillator model includes mass, springs and dampers to capture the real dynamic characteristics of a moving vehicle. It is more complicated than a moving mass model [18–20]. Biggs [18] presented a semi-analytical solution to the problem of a sprung mass moving on a simply-supported beam. Using a series expansion technique, Pesterev *et al.* [19] examined the responses of an elastic continuum to multiple moving oscillators. Yang *et al.* [20] proposed a vehicle-bridge interaction element (VBI) to investigate the vibrations of simply-supported beams during the passage of high-speed trains.

The vehicle-bridge interaction dynamics has been also extensively studied for application to high-speed railways [21–28]. In particular, Yang *et al.* [21] investigated the vibration of simple beams during the passage of high-speed trains. Cojocaru *et al.* [27] studied the vibrations of an elastic bridge loaded by a second elastic beam moving with a constant speed. Zhang *et al.* [24] proposed a space model for train carriages and introduced a dynamic analysis for train-bridge interaction. Delgado and dos Santos [22] modeled the railway bridge-vehicle interaction on high-speed tracks.

Unlike a moving oscillator model, which treats a moving vehicle as a discrete system, a moving beam model considers a vehicle as a continuum and represents it as a beam. Cojocaru *et al.* [27] first studied the vibrations of an elastic bridge loaded by a second elastic beam that moved along the bridge at a constant speed. The vehicle was assumed to be connected to the bridge by means of a rigid interface. The quasi-static deformation of the bridge was obtained through the Laplace transform, while the dynamic responses of the bridge were determined via the Galerkin method. Delgado and dos Santos [22] modeled the railway bridge-vehicle interaction on high-speed tracks. The action of railway traffic on bridges is considered as a set of moving masses, being the effects of the moving forces and masses implied. Zhang *et al.* [29] investigated the dynamic responses of a simply-supported beam on which was moving an elastic beam at a constant speed using the modal superposition method. The model consisted of two Euler-Bernoulli beams that were connected by flexible springs at two points, so

that the interactive forces between the simply-supported beam and the moving beam were easily found from the relative deflection of the two points. A small rotation angle in rigid body motions was assumed. They developed a set of linear differential equations for the motions of two beams. Sreeram *et al.* [30] employ the Lagrangian multiplier technique to develop a h-p version finite element model for a certain class of dynamics problems. Variational principle is the basis of this formulation with essential conditions applied via Lagrangian multipliers. The example considered here is a problem of a beam moving over supports. Lagrangian multiplier implementation of the problem with finite element technique, is very effective compared to other global methods such as assumed mode technique. Kim [31] investigate the vibration and stability of an infinite Bernoulli-Euler beam resting on a Winkler-type elastic foundation when the system is subjected to a static axial force and a moving load with either constant or harmonic amplitude variations. Chen *et al.* [32] investigates dynamic stability in transverse parametric vibration of an axially accelerating viscoelastic tensioned beam. The beam is described by the Kelvin model, and the Galerkin method is applied to discretize the governing equation into a infinite set of ordinary-differential equations under the fixed-fixed boundary conditions. Fung *et al.* [33] studied a flexible beam slides in and out of the rigid wall. The equations of motion for a deploying beam with a tip mass are derived by using Hamilton's principle. Four dynamic models: Timoshenko, Euler, simple-flexible and rigid-body beam theories are used to describe the axially moving beam.

All of the aforementioned studies mainly focused on the dynamic responses of beams and were applicable to the design of railroad tracks, railroad bridges, and highway bridges. Relatively few studies focused on the dynamic behaviors of a vehicle, such as a missile, when the vehicle moves along the guideway, which can represent a launcher system (see Fig. 1.1). Analyses of various aspects of flexible vehicle behavior in free flight or with time-dependent constraints have appeared frequently in the literature. The interaction between the vehicle and its guideway differs considerably

between the two-shoe contact phase and the tip-off phase, and the vehicle displays very different behaviors. Consequently, the corresponding dynamic responses of the vehicle have to be modeled in these two phases.

1.4 Objectives, Approach and Research Coverage

Because the responses of the vehicle at take-off significantly affect the flight control of the vehicle, accurately determining the responses of the vehicle in the tip-off phase is crucial. This study applied the models of rigid vehicle and rigid guideway (R.R. model) [34], rigid vehicle and elastic guideway (R.E. model) [35], and elastic vehicle and elastic guideway (E.E. model) [36] for tip-off analysis of the vehicle at take-off.

In the R.E. model, the vehicle and the guideway are modeled as a rigid free-free beam and an inclined elastic simply-supported beam, respectively. The flexible guideway is assumed to be Euler-Bernoulli beam. The vehicle is connected to the guideway through two points of contact, which are considered to be rigid connections, so that their dynamic responses are the same during vehicle take-off. The equations of motion for the vehicle and its guideway, in terms of functions of the configuration coordinates and time, are established via the Newton's second law based on the free body diagram of the vehicle with appropriate displacement constraints.

In the E.E. model, the guideway is modeled as an inclined simply-supported uniform flexible beam, and the vehicle is treated as a flexible free-free beam under a pre-specified thrust force. Equations for governing the motions of the vehicle and the guideway are developed using the Lagrangian approach and the assumed mode method, on the basis of the Euler-Bernoulli beam theory. The governing equations take into account the inertia, Coriolis, and centrifugal forces that are induced by the vehicle as well as the dynamic interaction between the vehicle and its guideway. Table 1.1 summarizes the comparisons among the three models.

To solve for the governing equations in the R.E. model and E.E. model, a modal superposition technique is adopted to convert the governing equations, which are

nonlinear partial differential equations, into a set of nonlinear first-order differential equations with time as the independent variable. Then, the Petzold-Gear backward differentiation formula (BDF) numerical method [37] is employed to solve these first-order differential algebraic equations (DAEs). The proposed solutions are validated by comparing the results with published results obtained from models of a rigid vehicle on a rigid guideway. The effects of the length of the guideway, distance between the shoes of the vehicle, and mass and flexural rigidity ratios of the vehicle to the guideway upon tip-off of the vehicle are thoroughly studied. The results presented here provide valuable information for designing vehicle launch systems.

1.5 Dissertation Outline

The contents of the dissertation are organized as:

Chapter 1 describes the relevant literature review, the motivation and main purposes of the work.

Chapter 2 presents the R.R. model and re-develops solutions for the governing equations of the model. The equations of motion of the vehicle are derived by Newton's second law. The pitch angle and the pitch rate of the vehicle in this model were directly determined from the displacement and velocity of the vehicle at the points of two shoes.

Chapter 3 proposes the R.E. model and develops solutions for the governing equations of the model. Equations for governing the motion of the the guideway is derived by taking into account equations for the influences of the inertia force, Coriolis force, and centrifugal force induced by the vehicle as well as the dynamic interaction between the vehicle and its guideway, on the basis of the Euler-Bernoulli beam theory and the assumed mode method. Notably, the pitch angle and the pitch rate of the vehicle in this model were indirectly determined from the displacements and velocity of the guideway at the points of contact with the two shoes of the vehicle.

Chapter 4 proposes the E.E. model and develops solutions for the governing equa-

tions of the model. The equations of motion for the vehicle and the guideway are developed using the Lagrangian approach and the assumed mode method based on the Euler-Bernoulli hypothesis. Notably, the pitch angle and the pitch rate of the vehicle in this model were directly determined from the displacements and velocity of two shoes of the vehicle.

Chapter 5 shows the conclusions of the present study and suggestions for the future studies.

	Analytical Method	Calculation of Tip-off Response	Dynamical Interactions	Linearity of Differential Equation
R.R. Model 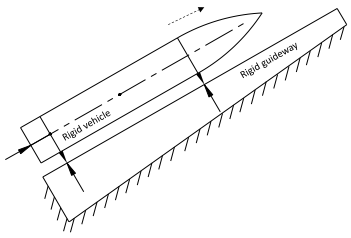	Newton's second law.	Direct calculation.	No.	Linear second order O.D.E.
R.E. Model 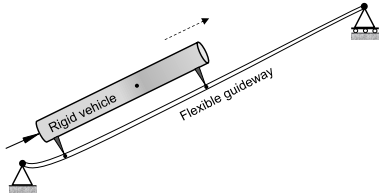	Newton's second law. Mode superposition. Displacement compatibility.	Indirect calculation.	Yes.	Nonlinear second order P.D.E.
E.E. Model 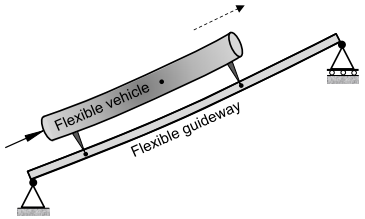	Newton's second law. Mode superposition. Lagrangian multiplier.	Direct calculation.	Yes.	Nonlinear second order P.D.E.

Table 1.1: Three types analytical models used for vehicle launch.

CHAPTER TWO

A rigid vehicle moving along an inclined rigid guideway

2.1 Theory and Formulation

Figure 2.1 schematically depicts a typical guideway for launching a vehicle. The guideway is considered as an inclined fixed rigid beam, while the vehicle is regarded as a rigid beam moving along the guideway under the action of a predetermined thrust force. This model is referred as R.R. model and the derivation of these formulas is based on Yao and Zhang [34].

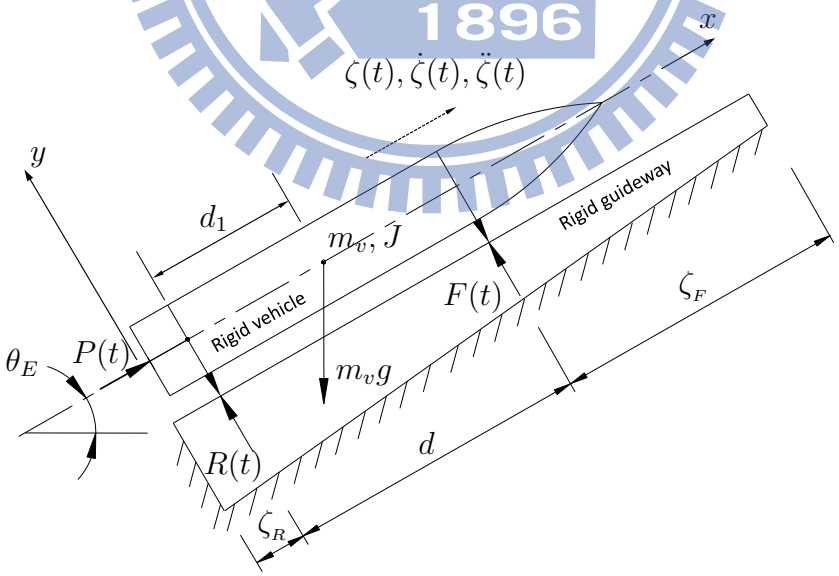

Figure 2.1: A typical rigid guideway used for rigid vehicle launch.

The vector of thrust is assumed to be along the vehicle's centerline (C.L.) and always coincides with the line joining the two contact points (see Fig. 2.1). While the vehicle moves, the two shoes of the vehicle are assumed to slide along the guideway by means of a rigid contact. The thrust force, $P(t)$ in Fig. 2.1, acting on a vehicle is predetermined in real applications. A typical real thrust-time curve is shown in Fig. 2.2. An ideal thrust-time curve in the design is obtained from full scale ground tests for a vehicle booster.

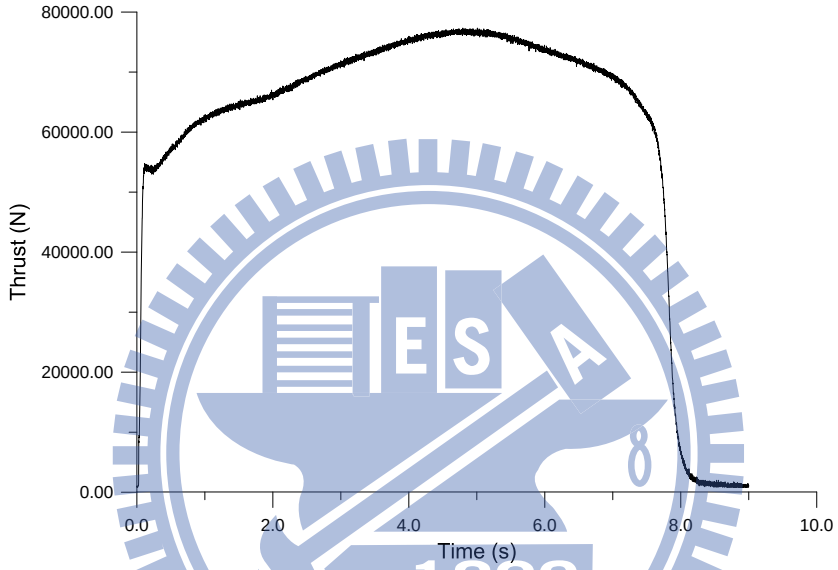

Figure 2.2: A typical real thrust-time curve.

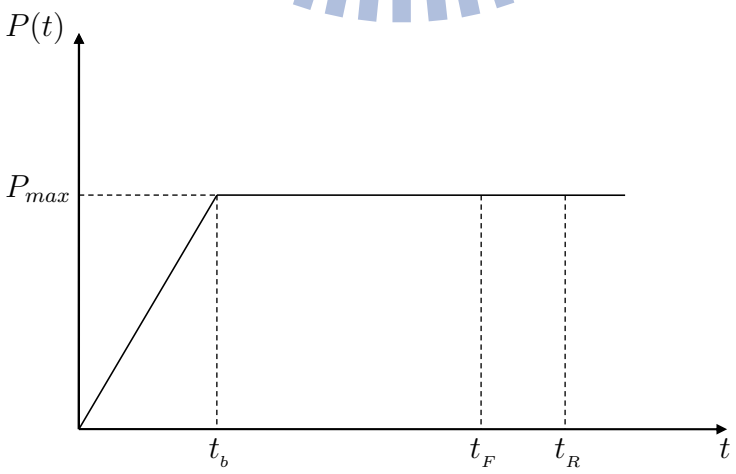

Figure 2.3: A typical thrust-time curve to simulate.

In order to simplify the analyses conducted in this work, we considered a simplified thrust-time curve given in Fig. 2.3, where t_b is the thrust build-up time. Normally, the time for the thrust force reaching a steady state is about 100 ms in real design. P_{max} is the value of $P(t)$ in the steady state; t_F and t_R are the times when the vehicle front shoe and rear shoe lose contact with the guideway, respectively. The term t_R is called the tip-off time. Between t_F and t_R, vehicle tip-off occurs.

When such a vehicle moves along a guideway, the vehicle is mainly subjected to the thrust, inertia, and gravity forces, and two different phases can be specified, namely, two-shoe contact phase and tip-off phase. In the two shoe contact phase (corresponding to $0 \leq t \leq t_{_F}$ in Fig. 2.3), the two shoes of the vehicle contact with the guideway, while in the tip-off phase (corresponding to $t_{_F} < t \leq t_{_R}$ in Fig. 2.3), only the rear shoe contact with the guideway.

From the typical thrust-time curve in Fig. 2.3 and the design parameters of a vehicle and its guideway, one can easily find the position $\zeta(t)$ and velocity $\dot{\zeta}(t)$ of the rear shoe (see Fig. 2.1), and t_F and t_R can be easily determined. Consequently, one is able to identify in which phase the vehicle is at a particular moment.

2.2 Two-shoe contact phase

- When $0 \leq t \leq t_{_b}$:

Based on the aforementioned assumptions and the relationship of geometry in Fig. 2.1, the equations of motion of the vehicle can be written as

$$m_v\ddot{\zeta}(t) = P(t) - m_v g \sin\theta_E \tag{2.1}$$

$$m_v\ddot{y}(t) = -R(t) - F(t) + m_v g \cos\theta_E \tag{2.2}$$

$$J\ddot{\theta} = F(t)\,(d - d_1) - R(t)d_1 \tag{2.3}$$

where m_v and J denote the mass and the mass moment of inertia of the vehicle; d denotes the distance between the front and rear shoes of the vehicle; d_1 is the distance between the rear shoe and the center of gravity of the vehicle; θ_E is the angle of inclination of the guideway; g is the gravitational acceleration; $F(t)$ and $R(t)$ represent the moving loads of the contact points at front shoe and rear shoe, respectively. Assume the system is initially at rest.

From the thrust-time curve in Fig. 2.3 and the design parameters of the vehicle and its guideway, integrating Eq. (2.1) yields $\zeta(t)$, $\dot{\zeta}(t)$ and $\ddot{\zeta}(t)$ as follows.

$$\ddot{\zeta}(t) = \frac{1}{m_v}\left(\frac{P_{max}}{t_b}t - m_v g \sin\theta_E\right) \tag{2.4}$$

$$\dot{\zeta}(t) = \frac{1}{m_v}\left(\frac{P_{max}}{2t_b}t^2 - m_v g \sin\theta_E \cdot t\right) + \dot{\zeta}(0) \tag{2.5}$$

$$\zeta(t) = \frac{1}{m_v}\left(\frac{P_{max}}{6t_b}t^3 - \frac{1}{2}m_v g \sin\theta_E \cdot t^2\right) + \dot{\zeta}(0)\cdot t + \zeta_R \tag{2.6}$$

$\dot{\zeta}(0)$ is the initial velocity of the vehicle and $\zeta(0)$ is the x coordinate from the rear shoe of vehicle to the left end of the guideway. When the system is initially at rest $\dot{\zeta}(0) = 0$ and $\zeta(0) = \zeta_R$.

When $t = t_b$, the thrust reaches steady state, and $\dot{\zeta}(t_b)$ and $\zeta(t_b)$ are given in Eqs. (2.7) and (2.8), which are obtained from Eqs. (2.5) and (2.6).

$$\dot{\zeta}(t_b) = \frac{t_b}{m_v}\left(\frac{P_{max}}{2} - m_v g \sin\theta_E\right) \tag{2.7}$$

$$\zeta(t_b) = \frac{t_b^2}{m_v}\left(\frac{P_{max}}{6} - \frac{1}{2}m_v g \sin\theta_E\right) + \zeta_R \tag{2.8}$$

These values are the initial values of the two-shoe contact phase when thrust force is in steady state.

Before the tip-off phase, the relative motion and rotation in y -direction and pitch direction are zero respectively. As a result, the reaction forces $F(t)$ and $R(t)$ between the vehicle and guideway can be obtained from Eqs. (2.2) and (2.3),

$$F(t) = \frac{d_1}{d} m_v g \cos\theta_E \tag{2.9}$$

$$R(t) = \left(\frac{d - d_1}{d}\right) m_v g \cos\theta_E \tag{2.10}$$

The reaction forces $F(t)$ and $R(t)$ are constant before the tip-off phase of vehicle.

- When $t_b < t \leq t_F$:

When the thrust reaches steady state, two shoes of the vehicle are still constrained by the guideway. The motion of vehicle is governed by,

$$\ddot{\zeta}(t) = \frac{1}{m_v}\left(P_{max} - m_v g \sin\theta_E\right) \tag{2.11}$$

Integrating Eq. (2.11) and employing $\dot{\zeta}(t_b)$ and $\zeta(t_b)$ as the initial conditions yields

$$\dot{\zeta}(t) = \frac{1}{m_v}\left(P_{max} - m_v g \sin\theta_E\right) \cdot (t - t_b) + \dot{\zeta}(t_b) \tag{2.12}$$

$$\zeta(t) = \frac{1}{2m_v}\left(P_{max} - m_v g \sin\theta_E\right) \cdot (t - t_b)^2 + \dot{\zeta}(t_b) \cdot (t - t_b) + \zeta(t_b) \tag{2.13}$$

When $t = t_F$, just before a vehicle moves into the tip-off phase, $\dot{\zeta}(t_F)$ and $\zeta(t_F)$ of the vehicle can be obtained from Eqs. (2.14) and (2.15) given in the following,

$$\dot{\zeta}(t_F) = \frac{1}{m_v}\left(P_{max} - m_v g \sin\theta_E\right) \cdot (t_F - t_b) + \dot{\zeta}(t_b) \tag{2.14}$$

$$\zeta(t_F) = \frac{1}{2m_v}\left(P_{max} - m_v g \sin\theta_E\right) \cdot (t_F - t_b)^2 + \dot{\zeta}(t_b) \cdot (t_F - t_b) + \zeta(t_b) \tag{2.15}$$

When $\zeta(t_F) = \zeta_F$, and the distance ζ_F between the front shoe of vehicle at $t = 0$ and the right end of guideway is predetermined in real application. Substituting $\zeta(t_F)$ into Eq. (2.15), one can determine t_F from Eq. (2.16) when the front shoe of vehicle loses contact. Then, substituting t_F into Eq. (2.14), one finds $\dot{\zeta}(t_F)$ of vehicle.

$$t_F = t_b + \frac{m_v}{\left(P_{max} - m_v g \sin\theta_E\right)} \cdot \left[\sqrt{\dot{\zeta}(t_b)^2 + \frac{2}{m_v}\left[\zeta_F - \zeta(t_b)\right]\left(P_{max} - m_v g \sin\theta_E\right)} - \dot{\zeta}(t_b)\right] \tag{2.16}$$

2.3 Tip-off phase

- When $t_F < t \leqslant t_R$:

Figure 2.4 presents the diagram of a vehicle and a guideway at $t_F < t \leqslant t_R$, when the rear shoe remains in contact with the guideway but the front shoe of the vehicle does not. Since the front shoe of the vehicle has lost contact with the guideway, the constraint on displacement, given in Eq. (2.9), vanishes.

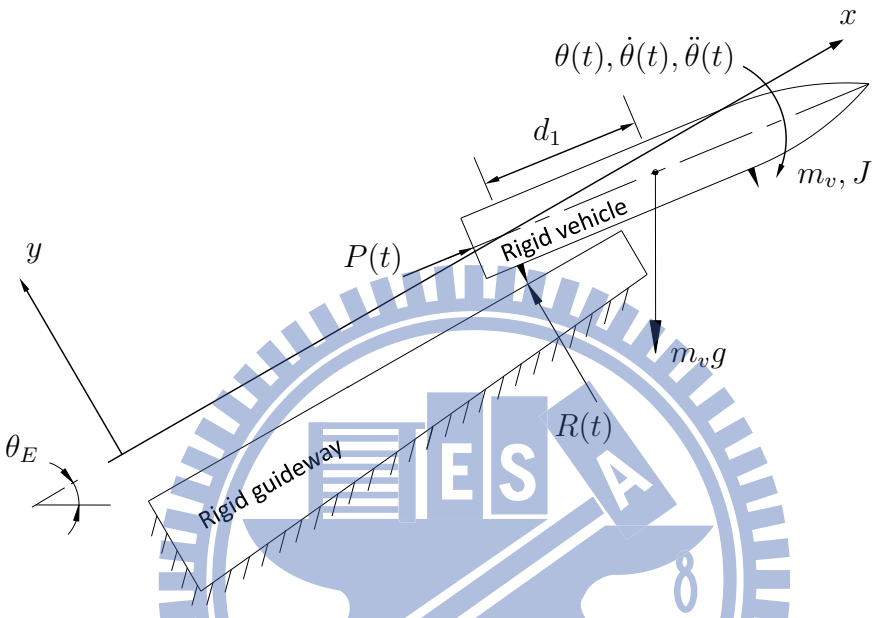

Figure 2.4: Motion of vehicle in tip-off phase.

When the vehicle is leaving the guideway at $t = t_R$, the velocity and position of vehicle are $\dot{\zeta}(t_R)$ and $\zeta(t_R)$ respectively. Using Eqs. (2.12) and (2.13) one finds

$$\dot{\zeta}(t_R) = \frac{1}{m_v}\left(P_{max} - m_v g \sin\theta_E\right) \cdot (t_R - t_b) + \dot{\zeta}(t_b) \tag{2.17}$$

$$\zeta(t_R) = \frac{1}{2m_v}\left(P_{max} - m_v g \sin\theta_E\right) \cdot (t_R - t_b)^2 + \dot{\zeta}(t_b) \cdot (t_R - t_b) + \zeta(t_b) \tag{2.18}$$

When $\zeta(t_R) = \zeta_F + d$ is predetermined in real application, one can find t_R from Eq. (2.19) by substituting $\zeta(t_R)$ into Eq. (2.18). Then, substituting t_R into Eq. (2.17) gives $\dot{\zeta}(t_R)$.

$$t_R = t_b + \frac{m_v}{(P_{max} - m_v g \sin\theta_E)} \cdot \left[\sqrt{\dot{\zeta}(t_b)^2 + \frac{2}{m_v}\left[\zeta_F - \zeta(t_b) + d\right](P_{max} - m_v g \sin\theta_E)} - \dot{\zeta}(t_b) \right] \tag{2.19}$$

When $t_F < t \leq t_R$, the motion of vehicle is governed by

$$m_v \ddot{\zeta}(t) = P_{max} - m_v g \sin\left[\theta_E + \bar{\theta}(t)\right] \tag{2.20}$$

$$m_v \ddot{y}(t) = P_{max} \sin\bar{\theta}(t) - m_v g \cos\left[\theta_E + \bar{\theta}(t)\right] + R(t) \tag{2.21}$$

$$J\ddot{\bar{\theta}}(t) = -R(t)d_1 \tag{2.22}$$

where

$\bar{\theta}(t)$: The pitch angle of vehicle.

$\ddot{\bar{\theta}}(t)$: The pitch acceleration of vehicle.

Since $\bar{\theta}(t)$ is very small, $\cos\left[\theta_E + \bar{\theta}(t)\right] \approx \cos\theta_E$ and $\sin\bar{\theta}(t) \approx \bar{\theta}(t)$. Because $y = d_1\bar{\theta}(t)$ and $\ddot{y} = d_1\ddot{\bar{\theta}}(t)$, Eqs. (2.21) and (2.22) can be simplified as

$$m_v d_1 \ddot{\bar{\theta}}(t) = P_{max}\bar{\theta}(t) - m_v g \cos\theta_E + R(t) \tag{2.23}$$

$$\begin{aligned} J\ddot{\bar{\theta}}(t) &= -R(t)d_1 \\ &= -\left[m_v d_1 \ddot{\bar{\theta}}(t) + m_v g \cos\theta_E - P_{max}\bar{\theta}(t)\right] d_1 \end{aligned} \tag{2.24}$$

Arranging Eqs. (2.23) and (2.24) one obtains the second order linear differential equation shown as follows,

$$\left(J + m_v d_1^2\right) \ddot{\bar{\theta}}(t) - P_{max} d_1 \bar{\theta}(t) = -m_v g d_1 \cos\theta_E \tag{2.25}$$

Denoting

$$A^2 = \frac{P_{max} d_1}{J + m_v d_1^2} \quad , \quad B = \frac{-m_v g d_1 \cos\theta_E}{J + m_v d_1^2}$$

and substituting A and B into Eq.(2.25) yield,

$$\ddot{\bar{\theta}}(t) - A^2 \bar{\theta}(t) = B \tag{2.26}$$

It is easy to find the general solution of Eq. (2.26)

$$\bar{\theta}(t) = C_1 \cdot e^{A(t-t_F)} + C_2 \cdot e^{-A(t-t_F)} - \frac{B}{A^2} \tag{2.27}$$

The constants of C_1 and C_2 can be determined from the initial conditions for the vehicle. One is able to determine $t = t_F$ from Eq. (2.16). Notably, the front shoe of vehicle loses contact with the guideway at $t = t_F$ and $\bar{\theta}(t_F) = 0$ and $\dot{\bar{\theta}}(t_F) = 0$. Then, $C_1 = C_2 = \frac{B}{2A^2}$ are obtained. Substituting C_1 and C_2 into Eq. (2.27), one obtains

$$\bar{\theta}(t) = \frac{B}{2A^2}\left[e^{A(t-t_F)} + e^{-A(t-t_F)} - 2\right] \tag{2.28}$$

$$\dot{\bar{\theta}}(t) = \frac{B}{2A}\left[e^{A(t-t_F)} - e^{-A(t-t_F)}\right] \tag{2.29}$$

Substituting the tip-off time of vehicle t_R determined from Eq. (2.19) into Eqs. (2.28) and (2.29), the pitch angle $\bar{\theta}(t_R)$ and the pitch rate $\dot{\bar{\theta}}(t_R)$ of vehicle are obtained, respectively. They are

$$\bar{\theta}(t_R) = \frac{B}{2A^2}\left[e^{A(t_R - t_F)} + e^{-A(t_R - t_F)} - 2\right] \tag{2.30}$$

$$\dot{\bar{\theta}}(t_R) = \frac{B}{2A}\left[e^{A(t_R - t_F)} - e^{-A(t_R - t_F)}\right] \tag{2.31}$$

2.4 Numerical examples and parametric study

The parameters of the vehicle launch system considered herein are listed in Table 2.1. Based on the formulations given in preceding sections, it is easy to determine $t_F = 0.5136$ s and $t_R = 0.6876$ s. Figures 2.5 and 2.6 depict the variations of pitch angle and pitch rate of the vehicle with time, respectively. The minimum pitch angle and pitch rate of the vehicle on the rigid guideway are $-2.0953°$ and $-24.794°/\text{s}$, respectively. The vehicle maintains a uniform rotational acceleration with respect to its rear shoe when the front shoe loses contact with the rigid guideway. The slope of the pitch rate with respect to time should be constant when the motion has a uniform rotational acceleration. Accordingly, one finds a nearly straight line in Fig. 2.6.

The responses of the vehicle at take-off significantly affect its flight control, and accurately determine the responses of the vehicle in the tip-off phase is crucial. Theoretically, a launch system should be designed to minimize the pitch angle and pitch rate of a vehicle at tip-off with consideration of space requirements in the launch system. In the following, we are going to investigate the effects of some parameters, such as inclination angle and length of guideway and the distance between two shoes of a vehicle, on the pitch angle and pitch rate of vehicle at tip-off time.

Table 2.1: Parameters of the vehicle launch system.

Parameters	Design value of launch system
θ_E	0.5 rad
m_v	1.6 $\times 10^3$ kg
J	4.7 $\times 10^3$ m^4
d	3.7 m
d_1	2.5 m
ζ_R	0.1 m
ζ_F	4.2 m
t_b	0.1 s
$P_{\max}$	7.0 $\times 10^4$ N
$\dot{\zeta}(0)$	0.0 m/s
Δt	0.0001 s

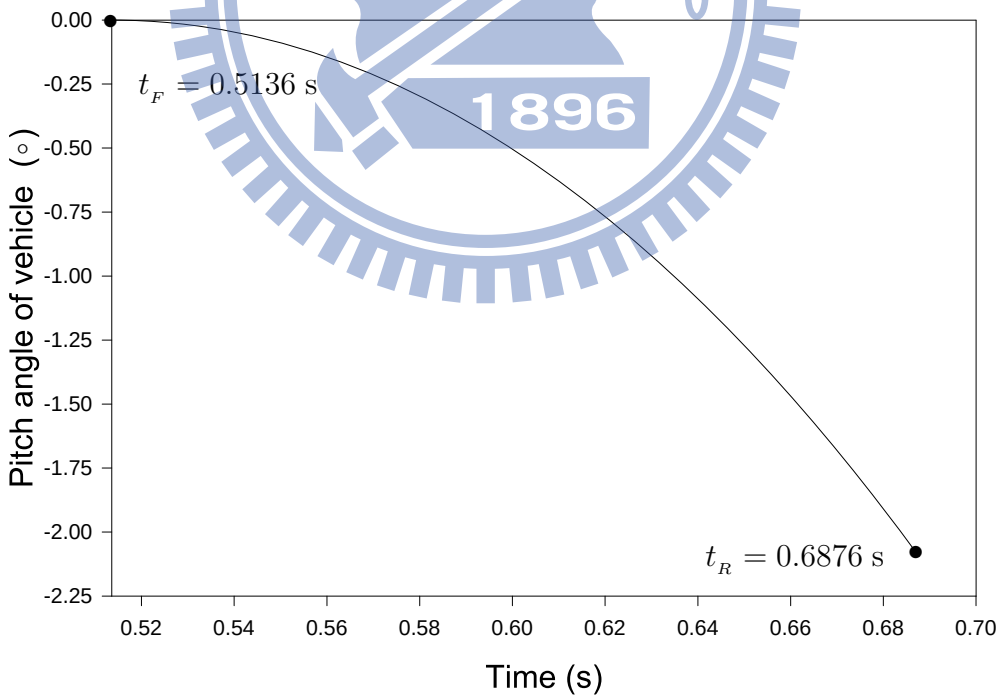

Figure 2.5: Pitch angle $\bar{\theta} - t$ of vehicle on rigid guideway.

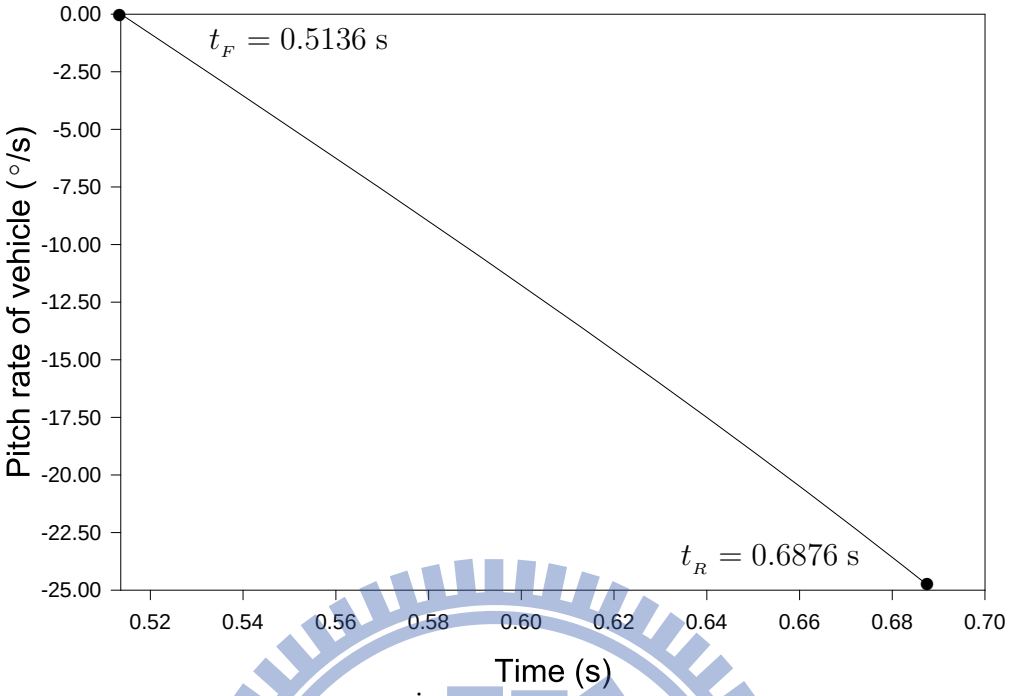

Figure 2.6: Pitch rate $\dot{\theta} - t$ of vehicle on rigid guideway.

2.4.1 Influence of angle of inclination of guideway

The force component in the transverse direction of the moving loads decreases when the angle of inclination θ_E of the guideway increases. Although an increase in θ_E decreases the tip-off of the vehicle, it also reduces the initial speed of the vehicle before take-off. The initial speed of the vehicle strongly affects the tolerance of a flight control system. Therefore, the angle of inclination of the guideway has to be carefully selected when one designs a launch system.

Using the parameters listed in Table 2.1 , we varied θ_E from 0.0 rad to 1.0 rad and computed the corresponding pitch angle and pitch rate at t_R (see Figs. 2.7 and 2.8). As mentioned before, the inclination angle of the guideway affects the vehicle speed and the transverse force acting on the vehicle before take-off. The larger the angle of inclination θ_E of the guideway is, the lower is longitudinal acceleration of vehicle before its take-off, and the smaller is the transverse force acting on the launched vehicle. When the longitudinal acceleration of vehicle decreases, the time interval $t_R - t_F$ increases,

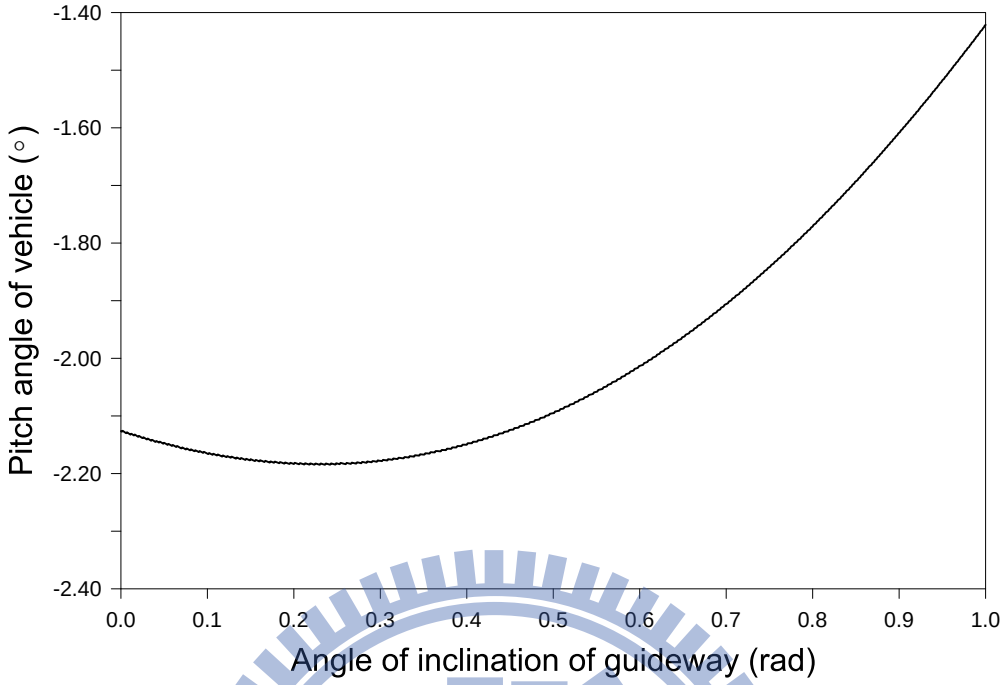

Figure 2.7: Effect of angle of inclination on pitch angle of vehicle ($\bar{\theta} - \theta_E$ diagram).

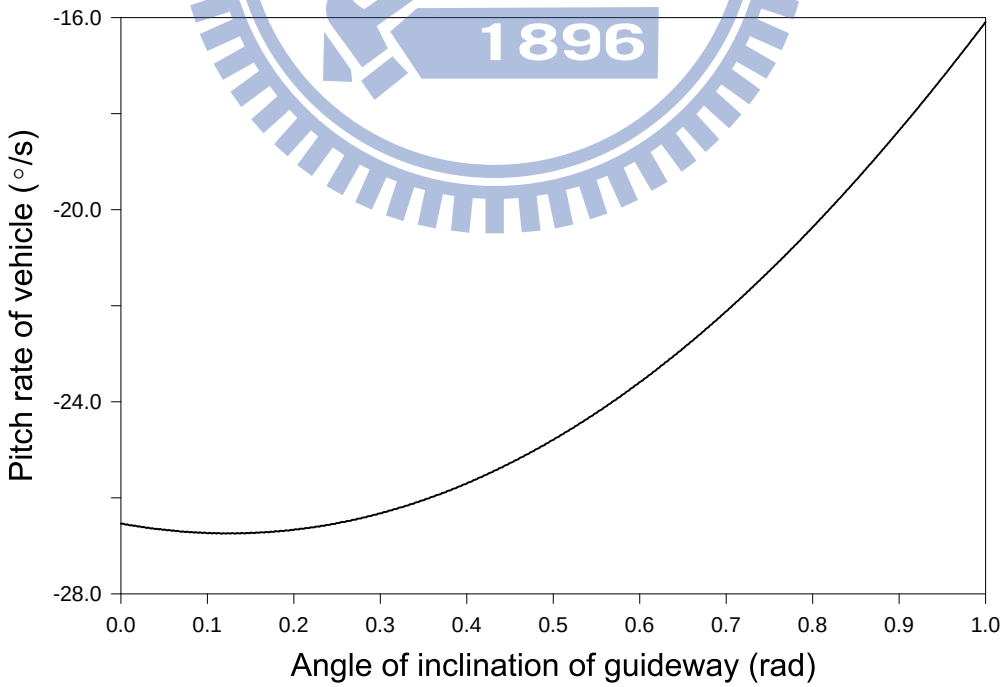

Figure 2.8: Effect of angle of inclination on pitch rate of vehicle ($\dot{\bar{\theta}} - \theta_E$ diagram).

this is disadvantageous because this increases the time of the vehicle tip-off phase. While, increasing the inclination angle of the guideway decreases the transverse force acting on the vehicle, which is desirable to reduce the tip-off response. Consequently, it is not easy to determine an appropriate inclination angle of the guideway.

2.4.2 Influence of length of guideway

An increase in the length of guideway raises the speed of vehicle during take-off and reduces the time interval $t_R - t_F$ in the tip-off phase. This is highly useful for decreasing the dynamic responses of a vehicle. To investigate the effect of the length of guideway on the pitch angle and pitch rate of a vehicle moving on the guideway, we changed L from $4.0\ \mathrm{m}$ to $12.0\ \mathrm{m}$ and used the other parameters listed in Table 2.1 to compute the corresponding pitch angle and pitch rate at t_R and the results are shown in Figs. 2.9 and 2.10. As expected, as the length of the guideway increases, the values of pitch angle and pitch rate of vehicle at tip-off time are gradually decreased.

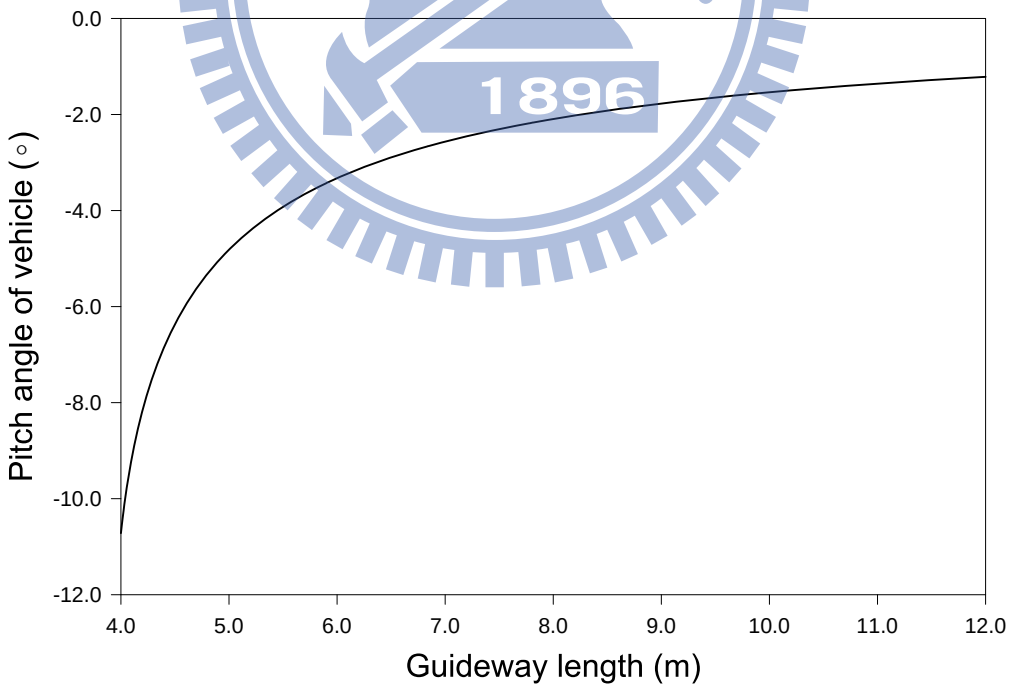

Figure 2.9: Effect of guideway length on pitch angle of vehicle ($\bar{\theta} - L$ diagram).

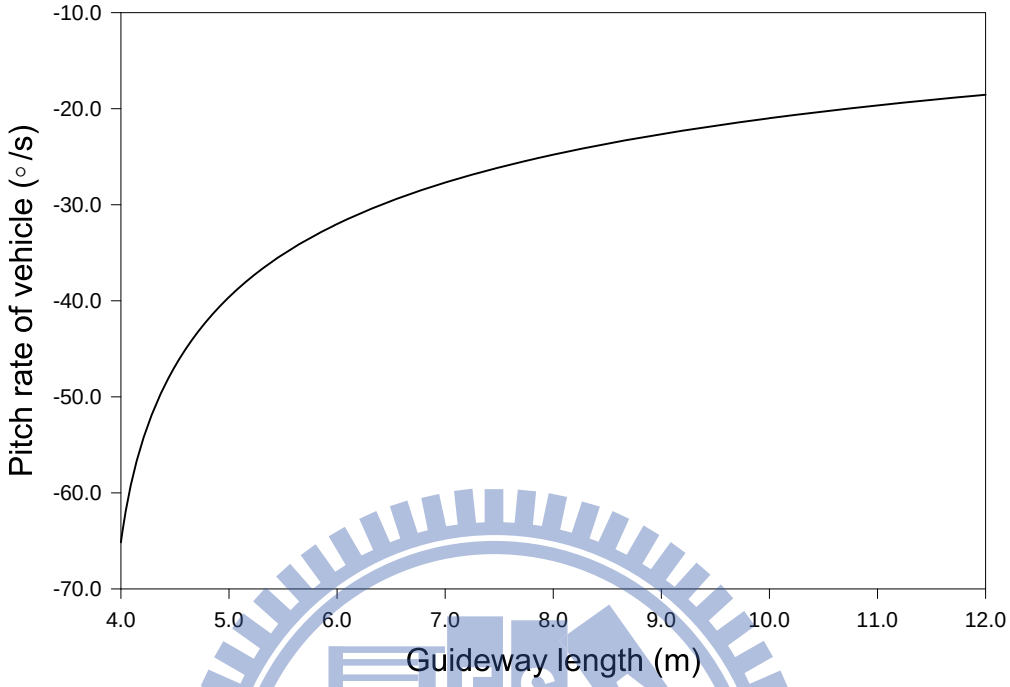

Figure 2.10: Effect of guideway length on pitch rate of vehicle ($\dot{\theta} - L$ diagram).

Although Figs. 2.9 and 2.10 indicate that the increase of the guideway length decreases of the tip-off pitch angle and pitch rate of vehicle, the guideway length has to be determined carefully not only by considering the wanted tip-off pitch angle and pitch rates of vehicle but also by fitting the space limits in launch systems. Normally, the length of a guideway is slightly greater than that of a vehicle.

2.4.3 Influence of distance between shoes of vehicle

Figures 2.11 and 2.12, respectively, depict the variations of the pitch angle and pitch rate of vehicle at the tip-off time with the distance between shoes of a vehicle. The range of the distance between shoes of a vehicle is between 2.6 m to 4.8 m. A decrease in the distance between the shoes of a vehicle leads to a decrease in the time interval of the tip-off phase. That is, the time interval $t_R - t_F$ corresponding to the two shoes losing contact with the guideway decreases. However, this situation could cause stress

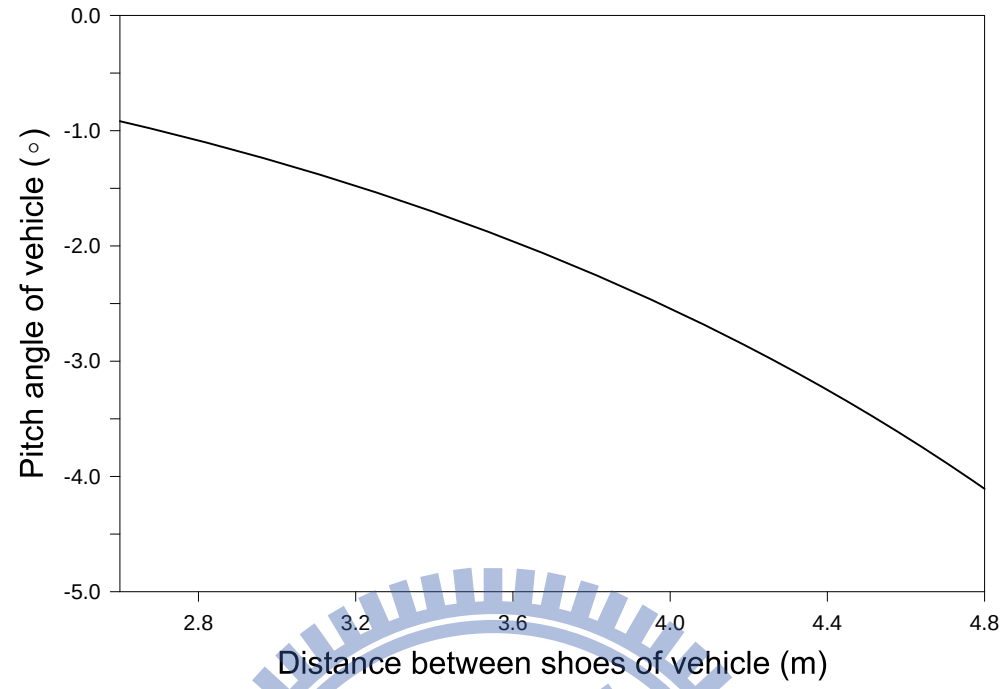

Figure 2.11: Effect of distance between the shoes of the vehicle on pitch angle of vehicle ($\bar{\theta} - d$ diagram).

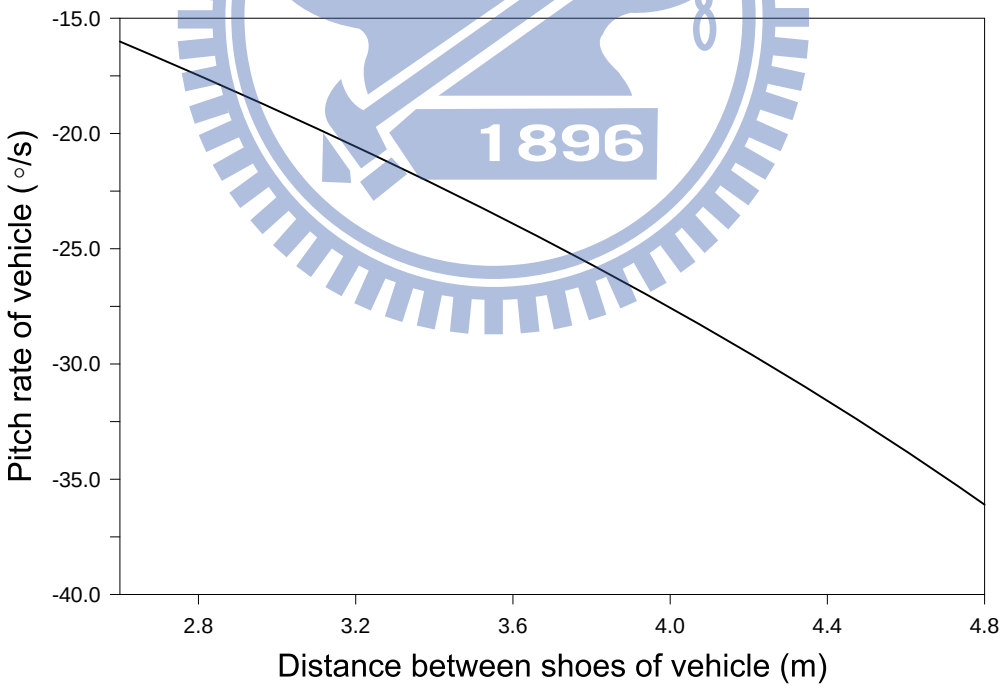

Figure 2.12: Effect of distance between the shoes of the vehicle on pitch rate of vehicle ($\dot{\bar{\theta}} - d$ diagram).

concentration in the guideway and unstable behaviors of the vehicle. Some other problems may also arise, and those are beyond the scope of this study.

CHAPTER THREE

A rigid vehicle moving along an inclined flexible guideway

3.1 Mathematical modeling behaviors of a guideway

Similar to Fig. 2.1, a schematic of a typical straight guideway used for a vehicle launch is shown in Fig. 3.1, in which the guideway is not assumed rigid. The launch system is considered as an inclined simply supported uniform elastic beam, whereas the vehicle is still regarded as a rigid beam. This model is referred as R.E. model.

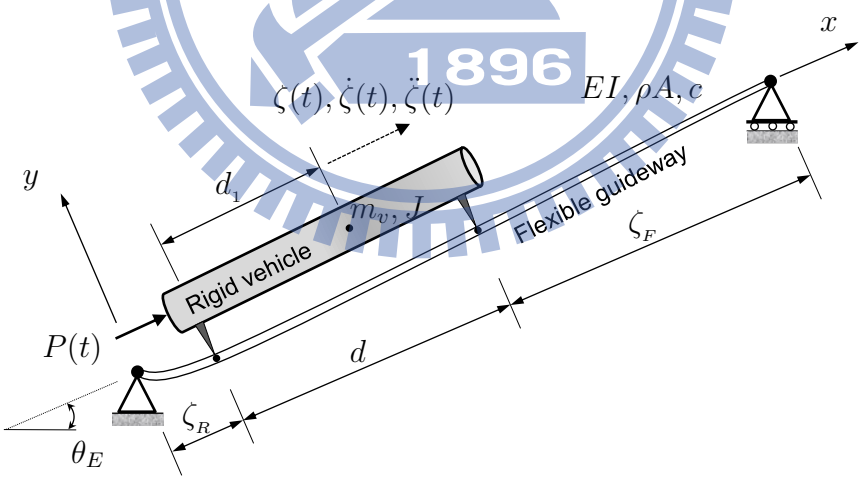

Figure 3.1: A typical flexible guideway used for rigid vehicle launch.

During the motion of the vehicle, the two shoes of the vehicle are assumed to slide along the guideway by means of a rigid contact. The thrust vector is assumed

to be along the vehicle's centerline (C.L.) and it always coincides with the line joining the two contact points. The vehicle and the guideway are considered to be two free bodies in Fig. 3.2. The typical displacement relationship between the vehicle and its guideway is shown in Fig. 3.3.

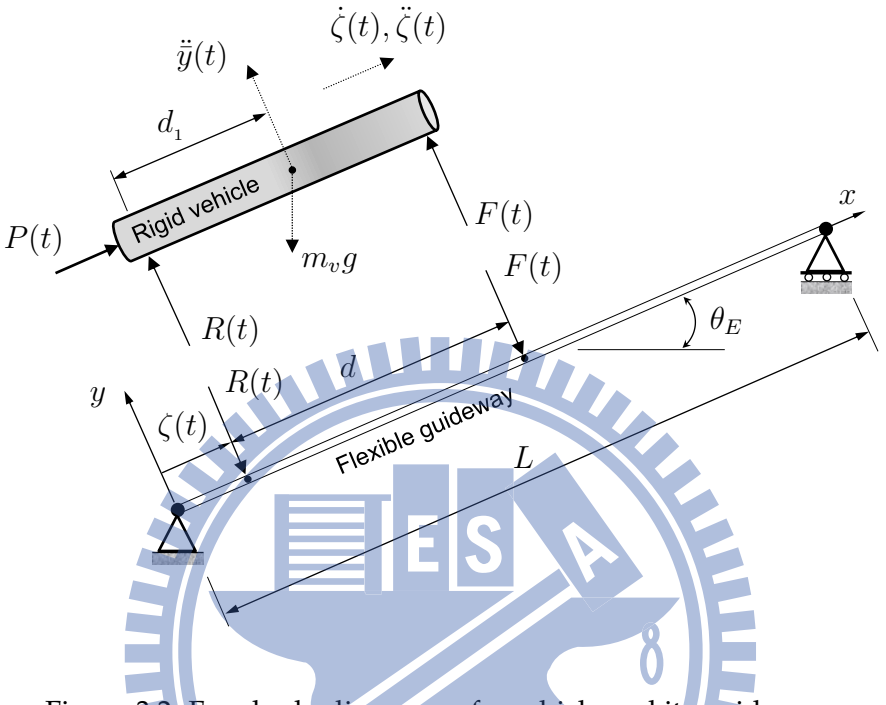

Figure 3.2: Free-body diagrams of a vehicle and its guideway.

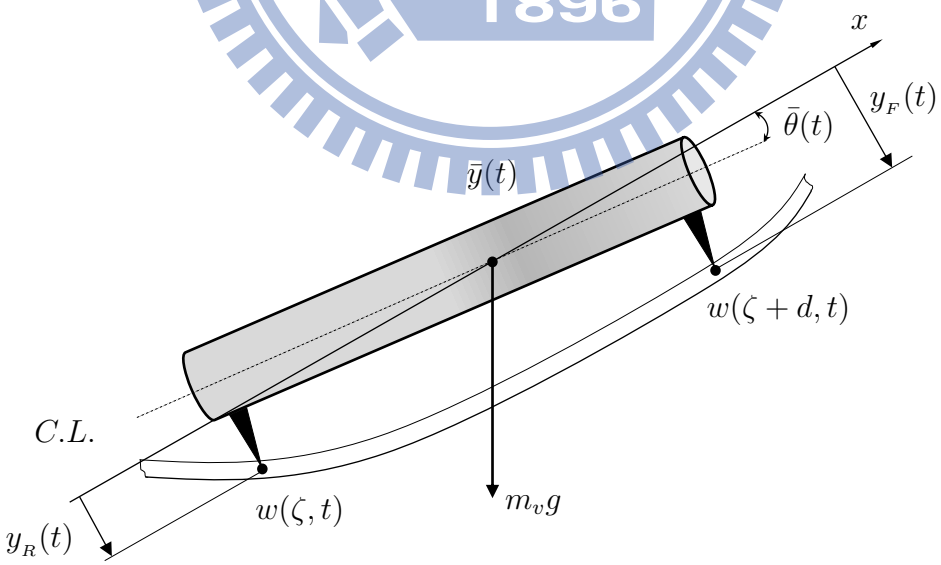

Figure 3.3: Typical displacements of vehicle and its guideway.

3.1.1 Position history of vehicle

As mentioned in Chapter 2, two phases exist with the vehicle during take-off, *i.e.*, the two-shoe contact phase and the tip-off phase. From the typical thrust-time curve shown in Fig. 2.3 and the design parameters of the vehicle and its guideway, one can easily find the position of the rear shoe, $\zeta(t)$ (see Fig. 3.2), $t_{_F}$ and $t_{_R}$ by using the formulas for $\zeta(t)$, $t_{_F}$ and $t_{_R}$ given in Chapter 2.

3.1.2 Two-shoe contact phase

The vibration of the guideway is modeled as a simply supported Euler-Bernoulli beam with viscous damping and is subjected to given initial conditions and specified boundary conditions. Let F and R denote the moving loads of the contact points (see Fig. 3.2). Assume small deformations for beams, and the governing equation of transverse vibrations can be given by the following partial differential equation:

$$EI\frac{\partial^4 w\left(x,t\right)}{\partial x^4}+\rho A\frac{\partial^2 w\left(x,t\right)}{\partial t^2}+c\frac{\partial w(x,t)}{\partial t}=R\delta\left(x,\zeta\right)+F\delta\left(x,\zeta+d\right) \tag{3.1}$$

where $w\left(x,t\right)$ is the transverse displacement of the guideway; EI, the constant flexural rigidity of the guideway; ρA, the mass per unit length of the guideway; c, the damping coefficient per unit length; $\delta\left(.\right)$, the Dirac delta function; and $R\delta\left(x,\zeta\right)+F\delta\left(x,\zeta+d\right)$, an external force acting on the guideway because of the motion of the vehicle in the two shoe contact phase.

Based on the aforementioned assumptions and the relationship of geometry in Fig. 3.3, the transverse displacement $\bar{y}$ of the vehicle can be expressed as

$$\bar{y}=\frac{d_{_1}}{d}y_{_F}+\frac{\left(d-d_{_1}\right)}{d}y_{_R} \tag{3.2}$$

where d denotes the distance between the shoes of the vehicle; $d_{_1}$ is the distance between the rear shoe and the center of gravity of the vehicle. For simplicity, $y_{_R}=w(\zeta,t)$

and $y_{_F} = w(\zeta + d, t)$ denote the displacements of the two shoe contact points in the y-direction, respectively, when the vehicle is moving along the deformed guideway.

The pitch angle $\bar{\theta}$ of vehicle can be obtained by

$$\bar{\theta} = \frac{y_{_F} - y_{_R}}{d} \tag{3.3}$$

Accordingly, the equations of motion of the vehicle can be written as

$$m_v \ddot{\bar{y}} = -R - F + m_v g \cos\theta_{_E} \tag{3.4}$$

$$J\ddot{\bar{\theta}} = d_{_1} R - (d - d_{_1}) F \tag{3.5}$$

where the overhead dot $(\cdot)$ denotes the differentiation with respect to time t; m_v denotes the mass of the vehicle; J is the mass moment of inertia of the vehicle; $\theta_{_E}$ presents the angle of inclination of the guideway; and g is the gravitational acceleration.

Differentiation Eqs. (3.2) and (3.3) twice with respect to time t yields

$$\ddot{\bar{y}} = \frac{d_{_1}}{d}\ddot{y}_{_F} + \frac{(d - d_{_1})}{d}\ddot{y}_{_R} \tag{3.6}$$

$$\ddot{\bar{\theta}} = \frac{\ddot{y}_{_F} - \ddot{y}_{_R}}{d} \tag{3.7}$$

Substituting $\ddot{\bar{y}}$ from Eq. (3.6) into Eq. (3.4) results in

$$R + F = -m_v \left[\frac{d_{_1}}{d}\ddot{y}_{_F} + \frac{(d - d_{_1})}{d}\ddot{y}_{_R}\right] + m_v g \cos\theta_{_E} \tag{3.8}$$

Substituting $\ddot{\bar{\theta}}$ from Eq. (3.7) into Eq. (3.5) results in

$$R = \frac{1}{d_{_1}}\left[J\frac{(\ddot{y}_{_F} - \ddot{y}_{_R})}{d} + (d - d_{_1})F\right] \tag{3.9}$$

Substituting R from Eq. (3.9) into Eq. (3.8), we have

$$\frac{1}{d_1}\left[J\frac{(\ddot{y}_F-\ddot{y}_R)}{d}+(d-d_1)F\right]+F=-m_v\left[\frac{d_1}{d}\ddot{y}_F+\frac{(d-d_1)}{d}\ddot{y}_R\right]+m_v g\cos\theta_E \quad (3.10)$$

Solving for R and F in Eqs. (3.9) and (3.10), we obtain

$$F=m_v\left(\bar{g}r_1+J_1\ddot{y}_R-J_2\ddot{y}_F\right) \quad (3.11a)$$

$$R=m_v\left(\bar{g}r_2-J_3\ddot{y}_R+J_1\ddot{y}_F\right) \quad (3.11b)$$

where r_1, r_2, J_1, J_2, J_3, and $\bar{g}$ are constants defined as follows:

$$r_1=\frac{d_1}{d} \qquad r_2=\frac{d-d_1}{d} \qquad J_1=\frac{J}{m_v d^2}-r_1 r_2$$
$$J_2=\frac{J}{m_v d^2}+r_1^2 \qquad J_3=\frac{J}{m_v d^2}+r_2^2 \qquad \bar{g}=g\cos\theta_E \quad (3.12)$$

The expressions $(\ddot{y}_R,\ \ddot{y}_F)$, $(2\dot{y}'_R\dot{\zeta}, 2\dot{y}'_F\dot{\zeta})$, and $(y''_R\dot{\zeta}^2,\ y''_F\dot{\zeta}^2)$ denote the acceleration of the inertia force, Coriolis force, and centrifugal force, respectively, at the shoes, at the rear and front contact points; $\dot{\zeta}$ denotes the velocity of the moving vehicle in the local x-direction (see Fig. 3.2); the prime $(')$ denotes the differentiation with respect to coordinate x. Because $y_R=w(\zeta,t)$ and $y_F=w(\zeta+d,t)$, $\dot{y}'_R=\frac{\partial^2 w(\zeta,t)}{\partial x\partial t}$, $\dot{y}'_F=\frac{\partial^2 w(\zeta+d,t)}{\partial x\partial t}$, $y''_R=\frac{\partial^2 w(\zeta,t)}{\partial x^2}$ and $y''_F=\frac{\partial^2 w(\zeta+d,t)}{\partial x^2}$.

The equations of the contact load between the vehicle and its guideway are derived by taking into account the effects of the inertia force, Coriolis force, and centrifugal force of the moving vehicle. Equations (3.11a) and (3.11b) can be rewritten as follows:

$$R = m_v \left[\bar{g} r_2 - J_3 \left(\ddot{y}_R + 2\dot{y}'_R \dot{\zeta} + y''_R \dot{\zeta}^2 \right) + J_1 \left(\ddot{y}_F + 2\dot{y}'_F \dot{\zeta} + y''_F \dot{\zeta}^2 \right) \right] \tag{3.13a}$$

$$F = m_v \left[\bar{g} r_1 + J_1 \left(\ddot{y}_R + 2\dot{y}'_R \dot{\zeta} + y''_R \dot{\zeta}^2 \right) - J_2 \left(\ddot{y}_F + 2\dot{y}'_F \dot{\zeta} + y''_F \dot{\zeta}^2 \right) \right] \tag{3.13b}$$

In order to obtain the approximate solution of the coupled system of equations, the transverse displacement of the guideway, $w(x,t)$, can be expressed as the superposition of the normal mode, shown as follows:

$$w(x,t) = \sum_{i=1}^{N} \phi_i(x) Y_i(t) \quad ; \quad 0 \le t \le t_F \tag{3.14}$$

where $\phi_i(x)$ denotes the ith mode of the guideway, satisfying the boundary conditions, and $Y_i(t)$ is the generalized coordinate corresponding to the ith mode. The modes of natural vibrations of a simply supported homogeneous beam can be easily found and are given as follows:

$$\phi_i(x) = \sin(\beta_i x) \tag{3.15}$$

where $\beta_i^4 = \omega_i^2 \cdot \frac{\rho A}{EI}$, $\beta_i L = i\pi$; L is the length of the guideway; ω_i is circular frequency of the ith vibration of the guideway [38].

Substituting Eqs. (3.13), (3.14), and (3.15) into Eq. (3.1), multiplying both sides of the equation by $\phi_n(x)$, and integrating with respect to x from 0 to L, we obtain the following expression:

$$\begin{aligned} &\ddot{Y}_i(t) + 2\xi_i \omega_i \dot{Y}_i(t) + \omega_i^2 Y_i(t) \\ &= \frac{2m_v}{\rho A L} \left\{ \bar{g} r_2 \sin\left(\frac{i\pi\zeta}{L}\right) - \sum_{j=1}^{N} \Phi_{mij} \ddot{Y}_j(t) - \sum_{j=1}^{N} \Phi_{cij} \dot{Y}_j(t) \right. \\ &\qquad \left. - \sum_{j=1}^{N} \Phi_{kij} Y_j(t) + \bar{g} r_1 \sin\left[\frac{i\pi(\zeta + d)}{L}\right] \right\} \end{aligned} \tag{3.16}$$

Then, Eq. (3.16) can be rewritten as

$$\ddot{Y}_i(t) + \rho_M \sum_{j=1}^{N} \Phi_{mij} \ddot{Y}_j(t) + 2\xi_i \omega_i \dot{Y}_i(t) + \rho_M \sum_{j=1}^{N} \Phi_{cij} \dot{Y}_j(t) + \omega_i^2 Y_i(t) + \rho_M \sum_{j=1}^{N} \Phi_{kij} Y_j(t) = Q_i \tag{3.17}$$

where $\rho_M = \frac{2m_v}{\rho AL}$; $\rho_F = \frac{2m_v \bar{g}}{\rho AL}$; and Q_i, Φ_{mij}, Φ_{cij}, and Φ_{kij} are expressed as follows:

$$Q_i = \rho_F \left\{ r_2 \sin\left(\frac{i\pi\zeta}{L}\right) + r_1 \sin\left[\frac{i\pi(\zeta + d)}{L}\right] \right\} \tag{3.18}$$

$$\Phi_{mij} = \left\{ J_3 \sin\left(\frac{j\pi\zeta}{L}\right) - J_1 \sin\left[\frac{j\pi(\zeta + d)}{L}\right] \right\} \sin\left(\frac{i\pi\zeta}{L}\right) - \left\{ J_1 \sin\left(\frac{j\pi\zeta}{L}\right) - J_2 \sin\left[\frac{j\pi(\zeta + d)}{L}\right] \right\} \sin\left[\frac{i\pi(\zeta + d)}{L}\right] \tag{3.19a}$$

$$\Phi_{cij} = \frac{2j\pi\dot{\zeta}}{L} \left\{ J_3 \cos\left(\frac{j\pi\zeta}{L}\right) - J_1 \cos\left[\frac{j\pi(\zeta + d)}{L}\right] \right\} \sin\left(\frac{i\pi\zeta}{L}\right) - \frac{2j\pi\dot{\zeta}}{L} \left\{ J_1 \cos\left(\frac{j\pi\zeta}{L}\right) - J_2 \cos\left[\frac{j\pi(\zeta + d)}{L}\right] \right\} \sin\left[\frac{i\pi(\zeta + d)}{L}\right] \tag{3.19b}$$

$$\Phi_{kij} = \left(\frac{j\pi\dot{\zeta}}{L}\right)^2 \left\{ -J_3 \sin\left(\frac{j\pi\zeta}{L}\right) + J_1 \sin\left[\frac{j\pi(\zeta + d)}{L}\right] \right\} \sin\left(\frac{i\pi\zeta}{L}\right) + \left(\frac{j\pi\dot{\zeta}}{L}\right)^2 \left\{ J_1 \sin\left(\frac{j\pi\zeta}{L}\right) - J_2 \sin\left[\frac{j\pi(\zeta + d)}{L}\right] \right\} \sin\left[\frac{i\pi(\zeta + d)}{L}\right] \tag{3.19c}$$

where $i = 1, 2, ..., N$ *and* $j = 1, 2, ..., N$

Because the system is initially at rest, the guideway's initial velocity and acceleration are zero. Hence, the initial conditions are $\ddot{Y}_i(0) = 0$, $\dot{Y}_i(0) = 0$, $\dot{\zeta} = 0$, and $\Phi_{kij} = 0$. Application of these initial conditions leads to the initial displacement $Y_i(0)$ of the guideway because of the static load of the vehicle is

$$Y_i(0) = \frac{\rho_F}{\omega_i^2} \left\{ r_2 \sin\left(\frac{i\pi\zeta_R}{L}\right) + r_1 \sin\left[\frac{i\pi(\zeta_R + d)}{L}\right] \right\} \tag{3.20}$$

3.1.3 Tip-off phase

When the front shoe loses contact with the guideway, F reduces to zero in the tip-off phase. The vehicle and guideway can be considered as two free bodies shown in Fig. 3.4.

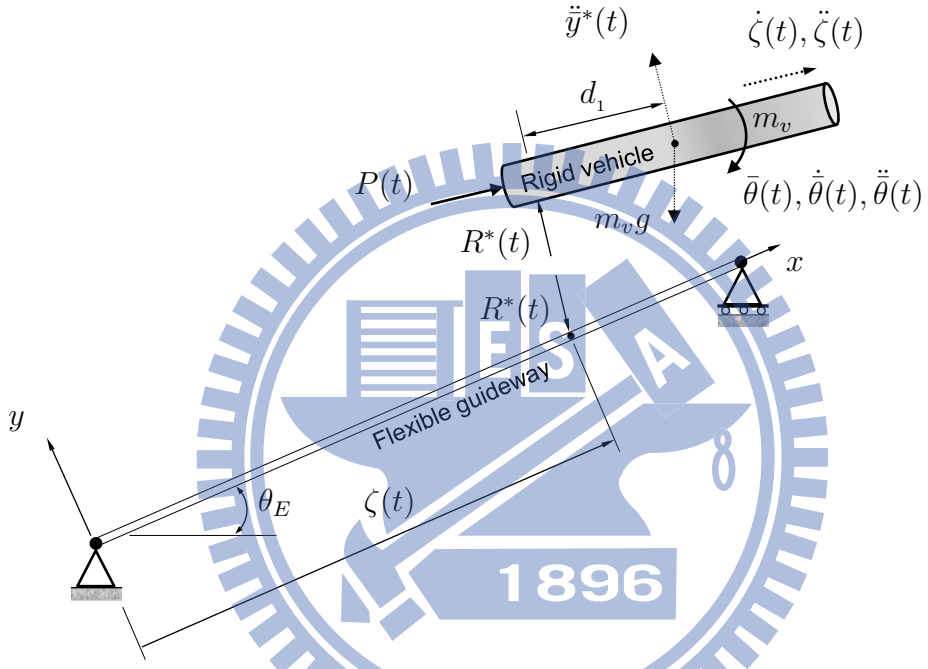

Figure 3.4: Free-body diagrams of vehicle in tip-off phase.

In the tip-off phase, Eq.(3.13b) equal to zero

$$F^* = m_v \left[\bar{g} r_1 + J_1 \left(\ddot{y}_R + 2\dot{y}'_R \dot{\zeta} + y''_R \dot{\zeta}^2 \right)^* - J_2 \left(\ddot{y}_F + 2\dot{y}'_F \dot{\zeta} + y''_F \dot{\zeta}^2 \right)^* \right] = 0 \tag{3.21}$$

Therefore,

$$\left(\ddot{y}_F + 2\dot{y}'_F \dot{\zeta} + y''_F \dot{\zeta}^2 \right)^* = \frac{1}{J_2} \left[\bar{g} r_1 + J_1 \left(\ddot{y}_R + 2\dot{y}'_R \dot{\zeta} + y''_R \dot{\zeta}^2 \right)^* \right] \tag{3.22}$$

Substituting $\left(\ddot{y}_F + 2\dot{y}'_F\dot{\zeta} + y''_F\dot{\zeta}^2\right)^*$ from Eq.(3.22) into Eq.(3.13a) results in

$$R^* = m_v\left(\frac{J_1 + r_1 r_2}{J_2}\right)\left[\bar{g} - \left(\ddot{y}_R + 2\dot{y}'_R\dot{\zeta} + y''_R\dot{\zeta}^2\right)^*\right] \tag{3.23}$$

The transverse vibrations in the guideway can be expressed as

$$EI\frac{\partial^4 w(x,t)}{\partial x^4} + \rho A\frac{\partial^2 w(x,t)}{\partial t^2} + c\frac{\partial w(x,t)}{\partial t} = R^*\delta(x,\zeta) \tag{3.24}$$

In the tip-off phase, we set

$$w(x,t) = \sum_{i=1}^{N}\phi_i(x)\,Y_i^*(t) \quad ; \quad t_F \le t \le t_R \tag{3.25}$$

Hence, by using a procedure similar to that described above, we obtain

$$\begin{aligned}&\ddot{Y}_i^*(t) + 2\xi_i\omega_i\dot{Y}_i^*(t) + \omega_i^2 Y_i^*(t)\\ &= \rho_M^*\left[\bar{g}\sin\left(\frac{i\pi\zeta}{L}\right) - \sum_{j=1}^{N}\Phi_{mij}^*\ddot{Y}_j^*(t) - \sum_{j=1}^{N}\Phi_{cij}^*\dot{Y}_j^*(t) - \sum_{j=1}^{N}\Phi_{kij}^*Y_j^*(t)\right]\end{aligned} \tag{3.26}$$

Then, Eq. (3.26) can be rewritten as

$$\begin{aligned}&\ddot{Y}_i^*(t) + \rho_M^*\sum_{j=1}^{N}\Phi_{mij}^*\ddot{Y}_j^*(t) + 2\xi_i\omega_i\dot{Y}_i^*(t)\\ &\quad + \rho_M^*\sum_{j=1}^{N}\Phi_{cij}^*\dot{Y}_j^*(t) + \omega_i^2 Y_i^*(t) + \rho_M^*\sum_{j=1}^{N}\Phi_{kij}^*Y_j^*(t) = \rho_F^*\sin\left(\frac{i\pi\zeta}{L}\right)\end{aligned} \tag{3.27}$$

where $\rho_F^* = \frac{2m_v\bar{g}\left(J_1 + r_1 r_2\right)}{\rho A L J_2}$; $\rho_M^* = \frac{2m_v\left(J_1 + r_1 r_2\right)}{\rho A L J_2}$; and Q_i^*, Φ_{mij}^*, Φ_{cij}^*, and Φ_{kij}^* are expressed as follows:

$$Q_i^* = \rho_F^*\sin\left(\frac{i\pi\zeta}{L}\right) \tag{3.28}$$

$$\Phi^*_{mij} = \sin\left(\frac{j\pi\zeta}{L}\right)\sin\left(\frac{i\pi\zeta}{L}\right) \tag{3.29a}$$

$$\Phi^*_{cij} = \frac{2j\pi\dot{\zeta}}{L}\cos\left(\frac{j\pi\zeta}{L}\right)\sin\left(\frac{i\pi\zeta}{L}\right) \tag{3.29b}$$

$$\Phi^*_{kij} = -\left(\frac{j\pi\dot{\zeta}}{L}\right)^2\sin\left(\frac{j\pi\zeta}{L}\right)\sin\left(\frac{i\pi\zeta}{L}\right) \tag{3.29c}$$

where $i = 1, 2, ..., N \quad and \quad j = 1, 2, ..., N$

These equations are subject to the continuity conditions $Y_i^*(0) = Y_i(t_F)$ and $\dot{Y}_i^*(0) = \dot{Y}_i(t_F)$, *i.e.*, the displacements and velocities of the guideway are continuous.

3.2 Calculation of dynamic response of guideway

It should be emphasized that Eqs. (3.17) and (3.27) represent a set of coupled second-order differential equations. Equations (3.17) and (3.27) can be rewritten in the form of a matrix, as follows:

$$\mathbf{M}\ddot{\mathbf{Y}} + \mathbf{C}\dot{\mathbf{Y}} + \mathbf{K}\mathbf{Y} = \mathbf{Q} \tag{3.30}$$

where

$$\mathbf{Y} = \left[Y_1, Y_2, ..., Y_i, ..., Y_N\right]^T$$
$$\dot{\mathbf{Y}} = \left[\dot{Y}_1, \dot{Y}_2, ..., \dot{Y}_i, ..., \dot{Y}_N\right]^T$$
$$\ddot{\mathbf{Y}} = \left[\ddot{Y}_1, \ddot{Y}_2, ..., \ddot{Y}_i, ..., \ddot{Y}_N\right]^T$$
$$\mathbf{Q} = \left[Q_1, Q_2, ..., Q_i, ..., Q_N\right]^T$$

Here, $\mathbf{Y}$ is a generalized coordinate; $\dot{\mathbf{Y}}$, a generalized velocity; $\ddot{\mathbf{Y}}$, a generalized acceleration; $\mathbf{Q}$, a generalized force; $\mathbf{M}$, a generalized mass matrix; $\mathbf{C}$, a generalized damping matrix; and $\mathbf{K}$, a generalized stiffness matrix.

In the two-shoe contact phase, expanding Eqs.(3.17), (3.18) and (3.19), yields the following M, C, and **K**

$$\mathbf{M} = \begin{bmatrix} 1+\rho_M\Phi_{m11} & \rho_M\Phi_{m12} & \cdots & \cdots & \cdots & \rho_M\Phi_{m1N} \\ \rho_M\Phi_{m21} & 1+\rho_M\Phi_{m22} & \cdots & \cdots & \cdots & \rho_M\Phi_{m2N} \\ \cdots & \cdots & \ddots & \cdots & \cdots & \cdots \\ \cdots & \cdots & \cdots & 1+\rho_M\Phi_{mij} & \cdots & \cdots \\ \cdots & \cdots & \cdots & \cdots & \ddots & \cdots \\ \rho_M\Phi_{mN1} & \rho_M\Phi_{mN2} & \cdots & \cdots & \cdots & 1+\rho_M\Phi_{mNN} \end{bmatrix}$$

$$\mathbf{C} = \begin{bmatrix} 2\xi_1\omega_1+\rho_M\Phi_{c11} & \rho_M\Phi_{c12} & \cdots & \cdots & \cdots & \rho_M\Phi_{c1N} \\ \rho_M\Phi_{c21} & 2\xi_2\omega_2+\rho_M\Phi_{c22} & \cdots & \cdots & \cdots & \rho_M\Phi_{c2N} \\ \cdots & \cdots & \ddots & \cdots & \cdots & \cdots \\ \cdots & \cdots & \cdots & 2\xi_i\omega_i+\rho_M\Phi_{cij} & \cdots & \cdots \\ \cdots & \cdots & \cdots & \cdots & \ddots & \cdots \\ \rho_M\Phi_{cN1} & \rho_M\Phi_{cN2} & \cdots & \cdots & \cdots & 2\xi_n\omega_n+\rho_M\Phi_{cNN} \end{bmatrix}$$

$$\mathbf{K} = \begin{bmatrix} \omega_1^2+\rho_M\Phi_{k11} & \rho_M\Phi_{k12} & \cdots & \cdots & \cdots & \rho_M\Phi_{k1N} \\ \rho_M\Phi_{k21} & \omega_2^2+\rho_M\Phi_{k22} & \cdots & \cdots & \cdots & \rho_M\Phi_{k2N} \\ \cdots & \cdots & \ddots & \cdots & \cdots & \cdots \\ \cdots & \cdots & \cdots & \omega_i^2+\rho_M\Phi_{kij} & \cdots & \cdots \\ \cdots & \cdots & \cdots & \cdots & \ddots & \cdots \\ \rho_M\Phi_{kN1} & \rho_M\Phi_{kN2} & \cdots & \cdots & \cdots & \omega_N^2+\rho_M\Phi_{kNN} \end{bmatrix}$$

In the tip-off phase, expanding Eqs.(3.27), (3.28) and (3.29), one obtains the following $\mathbf{M}^*$, $\mathbf{C}^*$, and $\mathbf{K}^*$

$$\mathbf{M}^* = \begin{bmatrix} 1+\rho_M^*\Phi_{11}^* & \rho_M^*\Phi_{12}^* & \cdots & \cdots & \cdots & \rho_M^*\Phi_{1N}^* \\ \rho_M^*\Phi_{21}^* & 1+\rho_M^*\Phi_{22}^* & \cdots & \cdots & \cdots & \rho_M^*\Phi_{2N}^* \\ \cdots & \cdots & \ddots & \cdots & \cdots & \cdots \\ \cdots & \cdots & \cdots & 1+\rho_M^*\Phi_{ij}^* & \cdots & \cdots \\ \cdots & \cdots & \cdots & \cdots & \ddots & \cdots \\ \rho_M^*\Phi_{N1}^* & \rho_M^*\Phi_{N2}^* & \cdots & \cdots & \cdots & 1+\rho_M^*\Phi_{NN}^* \end{bmatrix}$$

$$\mathbf{C}^* = \begin{bmatrix} 2\xi_1\omega_1+\rho_M\Phi_{c11}^* & \rho_M\Phi_{c12}^* & \cdots & \cdots & \cdots & \rho_M\Phi_{c1N}^* \\ \rho_M\Phi_{c21}^* & 2\xi_2\omega_2+\rho_M\Phi_{c22}^* & \cdots & \cdots & \cdots & \rho_M\Phi_{c2N}^* \\ \cdots & \cdots & \ddots & \cdots & \cdots & \cdots \\ \cdots & \cdots & \cdots & 2\xi_i\omega_i+\rho_M\Phi_{cij}^* & \cdots & \cdots \\ \cdots & \cdots & \cdots & \cdots & \ddots & \cdots \\ \rho_M\Phi_{cN1}^* & \rho_M\Phi_{cN2}^* & \cdots & \cdots & \cdots & 2\xi_n\omega_n+\rho_M\Phi_{cNN}^* \end{bmatrix}$$

$$\mathbf{K}^* = \begin{bmatrix} \omega_1^2+\rho_M\Phi_{k11}^* & \rho_M\Phi_{k12}^* & \cdots & \cdots & \cdots & \rho_M\Phi_{k1N}^* \\ \rho_M\Phi_{k21}^* & \omega_2^2+\rho_M\Phi_{k22}^* & \cdots & \cdots & \cdots & \rho_M\Phi_{k2N}^* \\ \cdots & \cdots & \ddots & \cdots & \cdots & \cdots \\ \cdots & \cdots & \cdots & \omega_i^2+\rho_M\Phi_{kij}^* & \cdots & \cdots \\ \cdots & \cdots & \cdots & \cdots & \ddots & \cdots \\ \rho_M\Phi_{kN1}^* & \rho_M\Phi_{kN2}^* & \cdots & \cdots & \cdots & \omega_N^2+\rho_M\Phi_{kNN}^* \end{bmatrix}$$

The differential-algebraic system technique was used to obtain numerical solutions of these equations. Eq. (3.30) was transformed into a system of first-order differential equations in the state space form by taking time as an additional variable. The procedure of the same is described below.

Suppose that at time t, the generalized coordinate is $\mathbf{Y} = [Y_1, Y_2, ..., Y_N]^T$. We set a group of functions $\mathbf{Z} = [Z_1, ..., Z_N \mid Z_{N+1}, ..., Z_{2N}]^T = [\mathbf{Z}_u \mid \mathbf{Z}_d]^T$ with time-dependent variables and assume that they have the following relationships:

$$\mathbf{Y} = \mathbf{Z}_u \tag{3.31a}$$

$$\dot{\mathbf{Y}} = \mathbf{Z}_d \tag{3.31b}$$

Hence,

$$\dot{\mathbf{Z}}_u = \mathbf{Z}_d \tag{3.32}$$

At the same time, we define a set of function $\mathbf{G} = [G_1, ..., G_N \mid G_{N+1}, ..., G_{2N}]^T = [\mathbf{G}_u \mid \mathbf{G}_d]^T$ related to time t as follows:

$$\mathbf{G}_u = \dot{\mathbf{Z}}_u - \mathbf{Z}_d \tag{3.33}$$

Equation (3.30) is expanded to N independent equations, and they can be transformed into a system of first-order differential equations as follows:

$$\mathbf{G}_d = \mathbf{M}\dot{\mathbf{Z}}_d + \mathbf{C}\mathbf{Z}_d + \mathbf{K}\mathbf{Z}_u - \mathbf{Q} \tag{3.34}$$

Hence, Eqs. (3.33) and (3.34) can be rewritten as

$$
\begin{aligned}
&[\mathbf{G}]^T_{2N\times 1} \\
&= \begin{bmatrix} \mathbf{I} & \mathbf{O}_1 \\ \mathbf{O}_1 & \mathbf{M} \end{bmatrix}_{2N\times 2N} \left[\dot{\mathbf{Z}}\right]^T_{2N\times 1} \\
&\quad + \begin{bmatrix} \mathbf{O}_1 & -\mathbf{I} \\ \mathbf{K} & \mathbf{C} \end{bmatrix}_{2N\times 2N} \left[\mathbf{Z}\right]^T_{2N\times 1} - \begin{bmatrix} \mathbf{O}_2 \\ \mathbf{Q} \end{bmatrix}^T_{2N\times 1}
\end{aligned} \tag{3.35}
$$

where $\mathbf{O}_1$ is an $N \times N$ zero matrix, $\mathbf{O}_2$ is an $N \times 1$ zero matrix, and $\mathbf{I}$ is an $N \times N$ unit matrix.

Then, solves a first order differential-algebraic system of equations, $\mathbf{G}(t, \mathbf{Z}, \dot{\mathbf{Z}}) = \mathbf{0}$, using the Petzold-Gear BDF method.

3.3 Modelling the dynamic responses of vehicle at tip-off

If the dynamic responses of the guideway, $w(x,t)$, $w(x+d,t)$, $\dot{w}(x,t)$, and $\dot{w}(x+d,t)$, at any time t corresponding to the two phases are determined, the dynamic responses of the guideway at any position x can be obtained. Using these results, we can formulate the tip-off dynamic responses of the vehicle. The needed equations are summarized as follows:

• For $t = 0$: The system is initially at rest.

The position displacement of the guideway, $w(x,0)$ is given by

$$
w(x,0) = \sum_{i=1}^{N} \sin\left(\frac{i\pi x}{L}\right) \frac{2m_v\bar{g}}{\rho AL\omega_i^2} \left\{ r_2 \sin\left(\frac{i\pi\zeta_R}{L}\right) + r_1 \sin\left[\frac{i\pi(\zeta_R + d)}{L}\right] \right\} \tag{3.36}
$$

The displacement of the vehicle's center of gravity, $\bar{y}(0)$ is given by

$$\begin{aligned}\bar{y}(0) &= r_1 w(\zeta_R + d, 0) + r_2 w(\zeta_R, 0) \\ &= \sum_{i=1}^{N} \frac{2m_v \bar{g}}{\rho A L \omega_i^2} \left\{ r_1 \sin\left[\frac{i\pi(\zeta_R + d)}{L}\right] + r_2 \sin\left(\frac{i\pi\zeta_R}{L}\right)\right\}^2 \end{aligned} \tag{3.37}$$

The pitch angle of the vehicle, $\bar{\theta}(0)$ is determined by

$$\begin{aligned}\bar{\theta}(0) &= \frac{1}{d}\left[w(\zeta_R + d, 0) - w(\zeta_R, 0)\right] \\ &= \sum_{i=1}^{N} \frac{2m_v \bar{g}}{\rho A L d \omega_i^2} \left\{\sin\left[\frac{i\pi(\zeta_R + d)}{L}\right] - \sin\left(\frac{i\pi\zeta_R}{L}\right)\right\} \\ &\quad \cdot \left\{ r_2 \sin\left(\frac{i\pi\zeta_R}{L}\right) + r_1 \sin\left[\frac{i\pi(\zeta_R + d)}{L}\right]\right\} \end{aligned} \tag{3.38}$$

- For $0 < t \le t_F$:

The position displacement of the guideway, $w(\zeta, t)$ is given by

$$\begin{aligned} w(\zeta, t) &= \sum_{i=1}^{N} \phi_i(\zeta) Y_i(t) \\ &= \sum_{i=1}^{N} \frac{2m_v \bar{g}}{\rho A L \omega_i^2} \left\{ r_2 \sin\left(\frac{i\pi\zeta}{L}\right) + r_1 \sin\left[\frac{i\pi(\zeta + d)}{L}\right]\right\} \sin\left(\frac{i\pi\zeta}{L}\right) \end{aligned} \tag{3.39}$$

The displacement of the vehicle's center of gravity, $\bar{y}(t)$, is

$$\begin{aligned}\bar{y}(t) &= \bar{y}(0) + r_1 w(\zeta + d, t) + r_2 w(\zeta, t) \\ &= \sum_{i=1}^{N} \frac{2m_v \bar{g}}{\rho A L \omega_i^2} \left\{ r_1 \sin\left[\frac{i\pi(\zeta_R + d)}{L}\right] + r_2 \sin\left(\frac{i\pi\zeta_R}{L}\right)\right\}^2 \\ &\quad + \sum_{i=1}^{N} \left\{ r_1 \sin\left[\frac{i\pi(\zeta + d)}{L}\right] + r_2 \sin\left(\frac{i\pi\zeta}{L}\right)\right\} Y_i(t) \end{aligned} \tag{3.40}$$

Then, the velocity of the vehicle's center of gravity, $\dot{\bar{y}}(t)$, is

$$\begin{aligned}\dot{\bar{y}}(t) &= r_1 \dot{w}(\zeta + d, t) + r_2 \dot{w}(\zeta, t) \\ &= \sum_{i=1}^{N} \left\{ r_1 \sin\left[\frac{i\pi(\zeta + d)}{L}\right] + r_2 \sin\left(\frac{i\pi\zeta}{L}\right) \right\} \dot{Y}_i(t)\end{aligned} \tag{3.41}$$

The pitch angle of the vehicle, $\bar{\theta}(t)$, is

$$\begin{aligned}\bar{\theta}(t) &= \bar{\theta}(0) + \frac{1}{d}\left[w(\zeta + d, t) - w(\zeta, t)\right] \\ &= \sum_{i=1}^{N} \frac{2m_v \bar{g}}{\rho A L d \omega_i^2} \left\{ \sin\left[\frac{i\pi(\zeta_R + d)}{L}\right] - \sin\left(\frac{i\pi\zeta_R}{L}\right) \right\} \\ &\quad \cdot \left\{ r_2 \sin\left(\frac{i\pi\zeta_R}{L}\right) + r_1 \sin\left[\frac{i\pi(\zeta_R + d)}{L}\right] \right\} \\ &\quad + \sum_{i=1}^{N} \frac{1}{d} \left\{ \sin\left[\frac{i\pi(\zeta + d)}{L}\right] - \sin\left(\frac{i\pi(\zeta)}{L}\right) \right\} Y_i(t)\end{aligned} \tag{3.42}$$

The pitch rate of the vehicle, $\dot{\bar{\theta}}(t)$, is

$$\begin{aligned}\dot{\bar{\theta}}(t) &= \frac{1}{d}\left[\dot{w}(\zeta + d, t) - \dot{w}(\zeta, t)\right] \\ &= \frac{1}{d} \sum_{i=1}^{N} \left\{ \sin\left[\frac{i\pi(\zeta + d)}{L}\right] - \sin\left(\frac{i\pi\zeta}{L}\right) \right\} \dot{Y}_i(t)\end{aligned} \tag{3.43}$$

• For $t_F < t \leq t_R$:

In the vehicle tip-off phase, the front shoe loses contact with the guideway, while the rear shoe of the vehicle remains to move along the guideway. The vehicle is subjected to the thrust force, inertia force, Coriolis force, and centrifugal force. The vehicle

rotates with respect to its rear shoe. The free-body diagram of the vehicle (see Fig. 3.4) shows that its center of gravity is subjected to the gravitational acceleration, and its rear shoe is subjected to the acceleration $\left(\ddot{y}_R + 2\dot{y}'_R\dot{\zeta} + y''_R\dot{\zeta}^2\right)^*$ in the y-direction. The equations of equilibrium for the vehicle body are

$$\sum F_y = m_v\left[\bar{g} - \left(\ddot{y}_R + 2\dot{y}'_R\dot{\zeta} + y''_R\dot{\zeta}^2\right)^*\right] = m_v a_y \tag{3.44a}$$

$$\sum M_o = I_o\ddot{\bar{\theta}}^* = d_1 m_v a_y \tag{3.44b}$$

Hence, the rotational acceleration of the vehicle with respect to its rear shoe is defined as follows:

$$\ddot{\bar{\theta}}^*(t) = \frac{r_1}{J_2 d}\left\{\bar{g} - \sum_{i=1}^{N}\left[\ddot{Y}_i^*(t)\sin\left(\frac{i\pi\zeta}{L}\right) + \frac{2i\pi\dot{\zeta}}{L}\cos\left(\frac{i\pi\zeta}{L}\right)\dot{Y}_i^*(t) - \left(\frac{i\pi\dot{\zeta}}{L}\right)^2\sin\left(\frac{i\pi\zeta}{L}\right)Y_i^*(t)\right]\right\} \tag{3.45}$$

From the continuity of the displacements and velocities of the guideway in the two phases, we can obtain the continuity conditions $Y_i^*(0) = Y_i(t_F)$ and $\dot{Y}_i^*(0) = \dot{Y}_i(t_F)$.

The pitch angle of the vehicle, $\bar{\theta}^*(t)$, is obtained by

$$\begin{aligned}\bar{\theta}^*(t) &= \bar{\theta}(t_F) + (t - t_F)\dot{\bar{\theta}}(t_F) + \frac{1}{2}\ddot{\bar{\theta}}^*(t)(t - t_F)^2 \\ &= \bar{\theta}(t_F) + (t - t_F)\dot{\bar{\theta}}(t_F) + \frac{r_1}{2J_2 d}\left\{\bar{g} - \sum_{i=1}^{N}\left[\ddot{Y}_i^*(t)\sin\left(\frac{i\pi\zeta}{L}\right)\right.\right. \\ &\quad \left.\left. + \frac{2i\pi\dot{\zeta}}{L}\cos\left(\frac{i\pi\zeta}{L}\right)\dot{Y}_i^*(t) - \left(\frac{i\pi\dot{\zeta}}{L}\right)^2\sin\left(\frac{i\pi\zeta}{L}\right)Y_i^*(t)\right]\right\}(t - t_F)^2\end{aligned} \tag{3.46}$$

Then, the pitch rate of the vehicle, $\dot{\bar{\theta}}^*(t)$, is

$$\begin{aligned}\dot{\bar{\theta}}^*(t) &= \dot{\bar{\theta}}(t_F) + \ddot{\bar{\theta}}^*(t)(t-t_F) \\ &= \dot{\bar{\theta}}(t_F) + \frac{r_1}{J_2 d}\left\{\bar{g} - \sum_{i=1}^{N}\left[\ddot{Y}_i^*(t)\sin\left(\frac{i\pi\zeta}{L}\right)\right.\right. \\ &\quad \left.\left. + \frac{2i\pi\dot{\zeta}}{L}\cos\left(\frac{i\pi\zeta}{L}\right)\dot{Y}_i^*(t) - \left(\frac{i\pi\dot{\zeta}}{L}\right)^2\sin\left(\frac{i\pi\zeta}{L}\right)Y_i^*(t)\right]\right\}(t-t_F)\end{aligned} \tag{3.47}$$

The rear shoe displacement of the vehicle, $y_R^*(t)$, is

$$y_R^*(t) = w(\zeta,t) = \sum_{i=1}^{N}\phi_i(\zeta)Y_i^*(t) \tag{3.48}$$

The displacement of the vehicle's center of gravity, $\bar{y}^*(t)$, is given by

$$\begin{aligned}\bar{y}^*(t) &= y_R^*(t) + d_1\bar{\theta}^*(t) \\ &= \sum_{i=1}^{N}\sin\left(\frac{i\pi\zeta}{L}\right)Y_i^*(t) + d_1\bar{\theta}(t_F) + d_1(t-t_F)\dot{\bar{\theta}}(t_F) \\ &\quad + \frac{r_1^2}{2J_2}\left\{\bar{g} - \sum_{i=1}^{N}\left[\ddot{Y}_i^*(t)\sin\left(\frac{i\pi\zeta}{L}\right) + \frac{2i\pi\dot{\zeta}}{L}\cos\left(\frac{i\pi\zeta}{L}\right)\dot{Y}_i^*(t)\right.\right. \\ &\quad \left.\left. - \left(\frac{i\pi\dot{\zeta}}{L}\right)^2\sin\left(\frac{i\pi\zeta}{L}\right)Y_i^*(t)\right]\right\}(t-t_F)^2\end{aligned} \tag{3.49}$$

The velocity of the vehicle's center of gravity, $\dot{\bar{y}}^*(t)$, is given by

$$\begin{aligned}\dot{\bar{y}}^*(t) &= \dot{y}_R^*(t) + d_1\dot{\bar{\theta}}^*(t) \\ &= \sum_{i=1}^{N}\sin\left(\frac{i\pi\zeta}{L}\right)\dot{Y}_i^*(t) + d_1\dot{\bar{\theta}}(t_F) + \frac{r_1^2}{J_2}\left\{\bar{g} - \sum_{i=1}^{N}\left[\ddot{Y}_i^*(t)\sin\left(\frac{i\pi\zeta}{L}\right)\right.\right. \\ &\quad \left.\left. + \frac{2i\pi\dot{\zeta}}{L}\cos\left(\frac{i\pi\zeta}{L}\right)\dot{Y}_i^*(t) - \left(\frac{i\pi\dot{\zeta}}{L}\right)^2\sin\left(\frac{i\pi\zeta}{L}\right)Y_i^*(t)\right]\right\}(t-t_F)\end{aligned} \tag{3.50}$$

3.4 Numerical validation and examples

3.4.1 Case 1: Displacement of contact points between vehicle and guideway

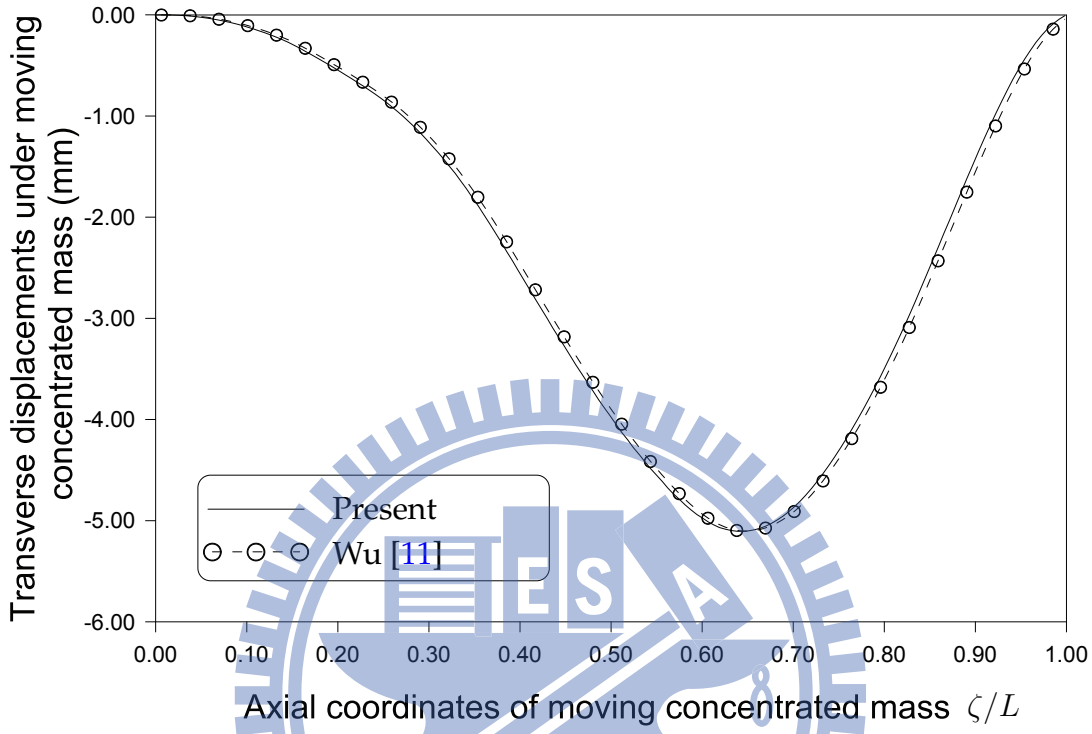

Figure 3.5: Time histories of transverse displacements under simulated moving concentrated mass.

We first considered a simply-supported horizontal undamped beam subjected to a moving concentrated mass, which was studied by Wu [11] using the moving mass element. The concentrated mass $m = 21.8\,\mathrm{kg}$ is assumed to move from the left end to the right end of the beam with a constant speed $V = 27.49\,\mathrm{m/s}$. The size and physical constants of the uniform undamped beam are as follows: a rectangular cross-section with width $b = 0.018113\,\mathrm{m}$ and thickness $h = 0.072322\,\mathrm{m}$; total length, $L = 4.352\,\mathrm{m}$; mass density, $\rho = 15267.1756\,\mathrm{kg/m^3}$; Young's modulus, $E = 2020.797216 \times 10^8\,\mathrm{N/m^2}$; $\Delta t = 0.001\,\mathrm{s}$; and $\xi = 0.005$. Although the solution proposed in this study is for the dynamic analysis of an inclined flexible guideway with a moving rigid vehicle, it can be used for a horizontal beam if the angle of inclination of the guideway is

considered to be close to zero. Furthermore, the distance between two contact points (two shoes of the vehicle) is set close to zero $(1 \times 10^{-15}\ \mathrm{m})$ to simulate the single moving mass problem. Figure 3.5 shows a comparison of the time histories of the transverse displacement of the contact point of the moving mass obtained by Wu [11] and those obtained in this study. The figure shows that the difference between the results is negligible.

3.4.2 Case 2: Comparison between tip-off results of rigid and pseudo-rigid guideways

We analyzed a rigid vehicle moving on a inclined rigid beam here. We assumed the flexural rigidity of the guideway to be $1.2 \times 10^{15}\ \mathrm{N \cdot m^2}$ to simulate a rigid guideway in the solutions given in this chapter; this value is equal to that of a pseudo-rigid guideway. The parameters listed in Table 3.1 were used. Figures 3.6 and 3.7 depict the pitch angle and pitch rate of vehicle in the tip-off phase, respectively. The figures also show the results by Yao and Zhang [34], who ignored both the Coriolis force and the centrifugal force in their analyses. For comparison, the results obtained from the present approach shown in Figs. 3.6 and 3.7 also neglected the Coriolis and the centrifugal forces. Some results at particular time are also listed in Tables 3.2 and 3.3. The present results are somewhat different from those of Yao and Zhang [34]. The results of Yao and Zhang [34] may not be accurate enough. The vehicle maintains its uniform rotational acceleration with respect to its rear shoe when the front shoe loses contact with the rigid guideway. Hence, the slope of the pitch rate with respect to time should be constant when the motion is a uniform rotational acceleration. A nearly straight line is obtained from the present approach, while the results of Yao and Zhang [34] clearly deviate from a straight line.

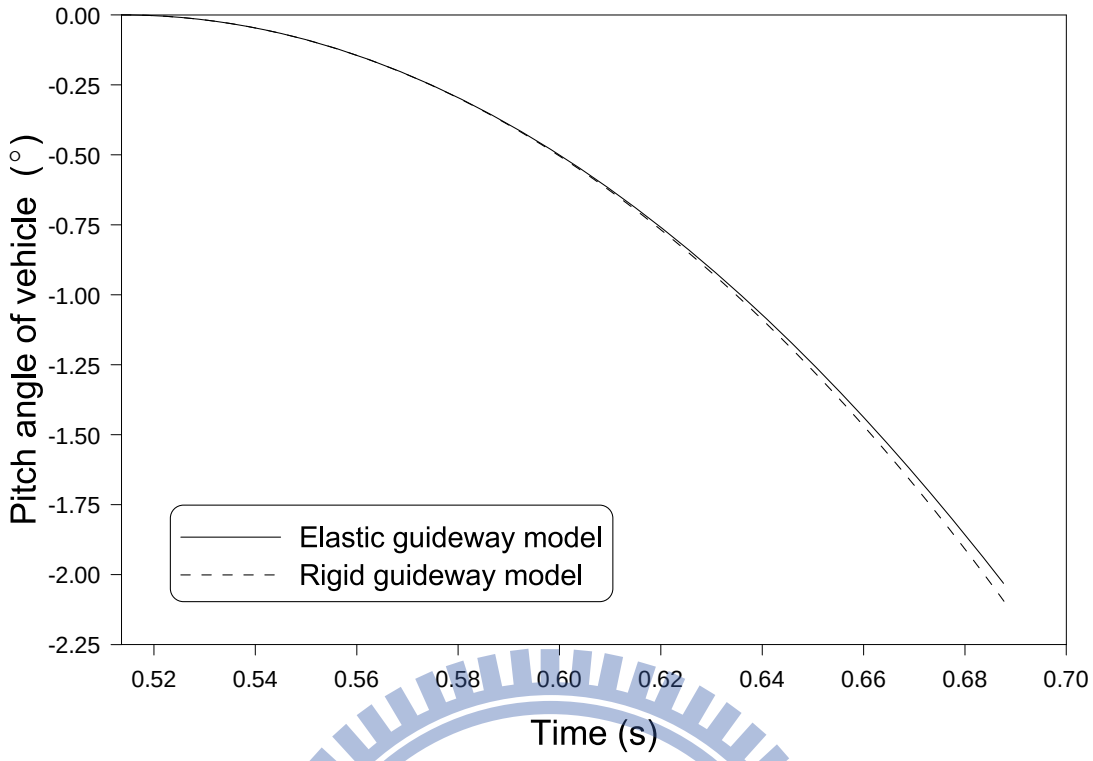

Figure 3.6: Comparison of pitch angles $\bar{\theta} - t$ of vehicle on pseudo-rigid (P.R.) guideway and rigid guideway.

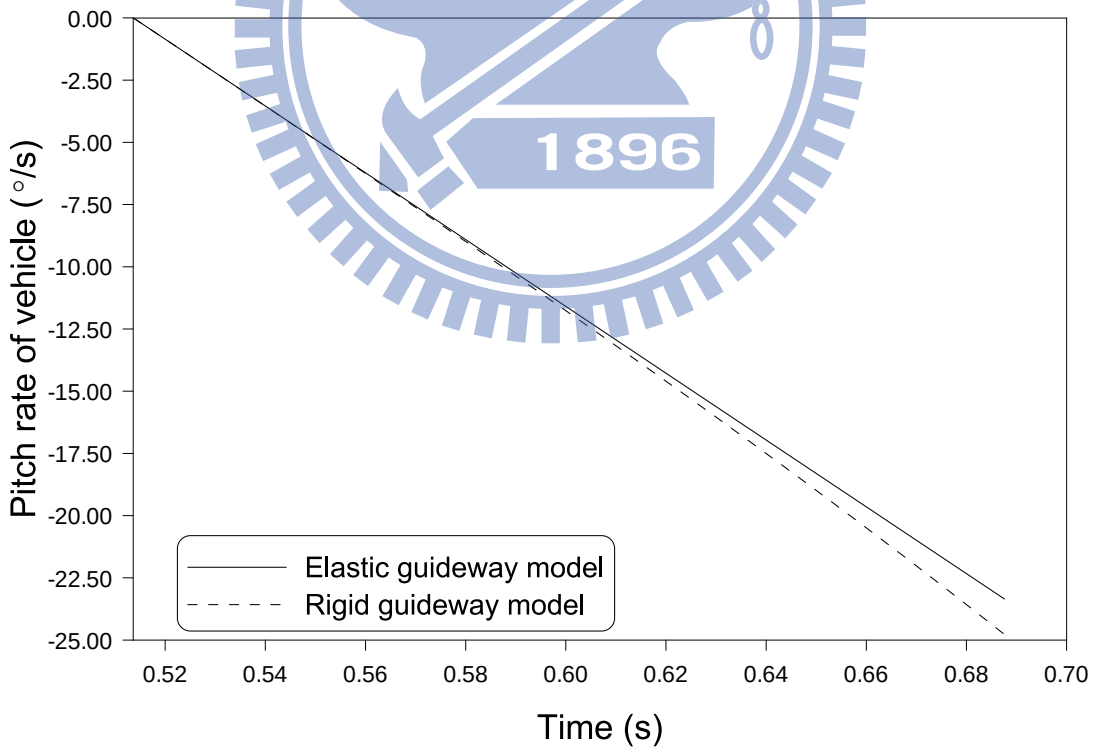

Figure 3.7: Comparison of pitch rates $\dot{\bar{\theta}} - t$ of vehicle on pseudo-rigid (P.R.) guideway and rigid guideway.

Table 3.1: Parameters of the vehicle launch system.

Parameters	Design value of launch system
EI	$1.2 \times 10^7\ \mathrm{N \cdot m^2}$
ρA	$1.5 \times 10^2\ \mathrm{kg/m}$
ξ	0.03
L	$8.0\ \mathrm{m}$
$\theta_{_E}$	$0.5\ \mathrm{rad}$
m_v	$1.6 \times 10^3\ \mathrm{kg}$
J	$4.7 \times 10^3\ \mathrm{m^4}$
d	$3.7\ \mathrm{m}$
$d_{_1}$	$2.5\ \mathrm{m}$
$\zeta_{_R}$	$0.1\ \mathrm{m}$
$\zeta_{_F}$	$4.2\ \mathrm{m}$
$t_{_b}$	$0.1\ \mathrm{s}$
$P_{\max}$	$7.0 \times 10^4\ \mathrm{N}$
$\dot{\zeta}(0)$	$0.0\ \mathrm{m/s}$
Δt	$0.0001\ \mathrm{s}$

Table 3.2: Comparison of pitch angles for pseudo-rigid guideway and rigid guideway.

	Pitch angle of vehicle (°)	
Time (s)	P.R.	Rigid
0.5136	$-7.6262E-08$	$-7.5517E-08$
0.5250	$-8.6705E-03$	$-8.6716E-03$
0.5500	$-8.8755E-02$	$-8.8872E-02$
0.5750	$-2.5273E-01$	$-2.5367E-01$
0.6000	$-5.0059E-01$	$-5.0431E-01$
0.6250	$-8.3234E-01$	$-8.4263E-01$
0.6500	$-1.2480E+00$	$-1.2712E+00$
0.6750	$-1.7475E+00$	$-1.7931E+00$
0.6876	$-2.0311E+00$	$-2.0928E+00$

Table 3.3: Comparison of pitch rates for pseudo-rigid guideway and rigid guideway.

	Pitch rate of vehicle ($^\circ/s$)	
Time (s)	P.R.	Rigid
0.5136	$4.5025E-03$	$4.5025E-03$
0.5250	$-1.5256E+00$	$-1.5260E+00$
0.5500	$-4.8812E+00$	$-4.8940E+00$
0.5750	$-8.2367E+00$	$-8.2984E+00$
0.6000	$-1.1592E+01$	$-1.1765E+01$
0.6250	$-1.4948E+01$	$-1.5318E+01$
0.6500	$-1.8303E+01$	$-1.8986E+01$
0.6750	$-2.1659E+01$	$-2.2795E+01$
0.6876	$-2.3350E+01$	$-2.4778E+01$

3.4.3 Case 3: Behavior of rigid vehicle on elastic guideway

After confirming the correctness of the present solutions, we further applied the solutions to study the behaviors of a rigid vehicle on a flexible beam. The parameters of the vehicle launch system used in this case are listed in Table 3.1.

In this test example, we obtained the time interval of the tip-off phase; this started at $t_{_F} = 0.5136$ s and ended at $t_{_R} = 0.6876$ s. Figure 3.8 shows the transverse displacement-time graph of the center of gravity of the vehicle. It shows that the position of the center of gravity of the vehicle tends to move upward before the tip-off phase. Figure 3.9 shows the transverse velocity-time graph of the center of gravity of the vehicle.

After the front shoe of the vehicle loses contact with the guideway, the constraint force acting on the shoe suddenly vanishes. Figure 3.9 shows an abrupt variation in the vertical velocity of the center of gravity of the vehicle in the initial tip-off phase. Although the transverse velocity of the center of gravity of the vehicle varied abruptly, the transverse displacements of the center of gravity of the vehicle were not obvious.

The pitch angles as well as the pitch rates for the two guideway models were com-

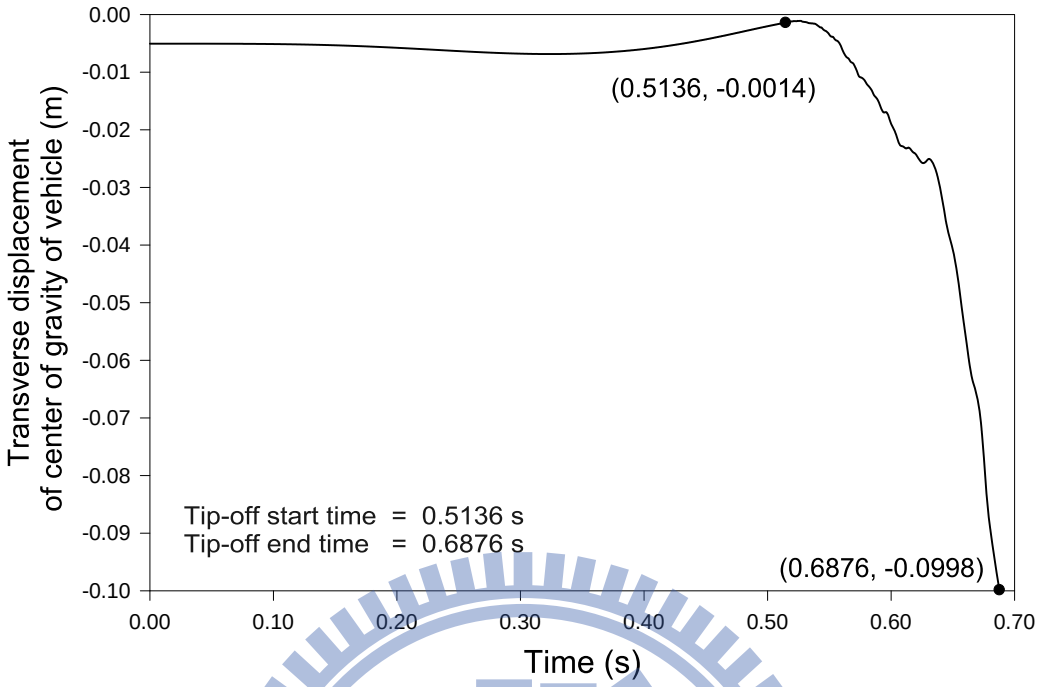

Figure 3.8: Transverse displacement of vehicle's center of gravity.

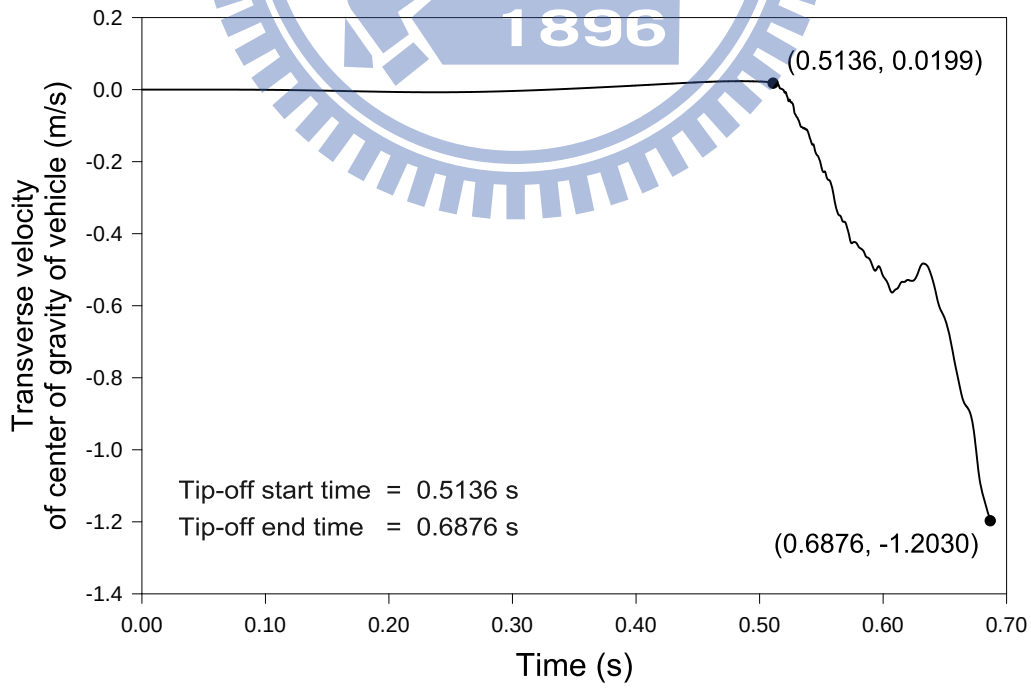

Figure 3.9: Transverse velocity of vehicle's center of gravity.

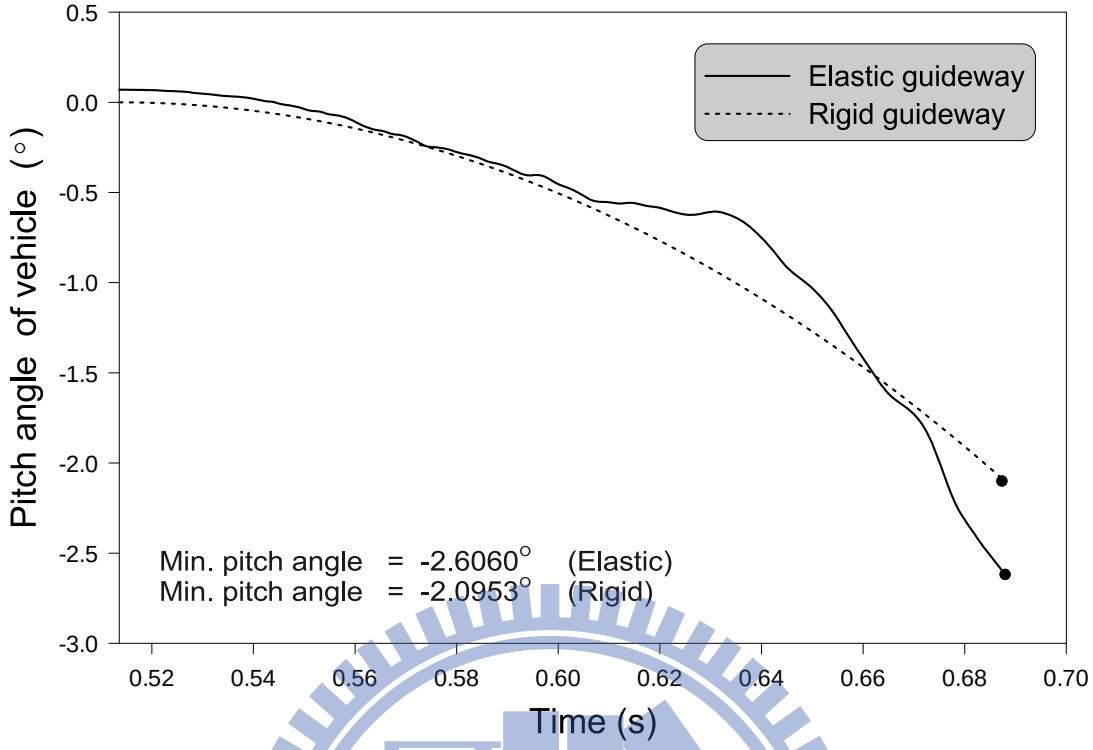

Figure 3.10: Comparison of pitch angles of vehicle on elastic guideway and rigid guideway.

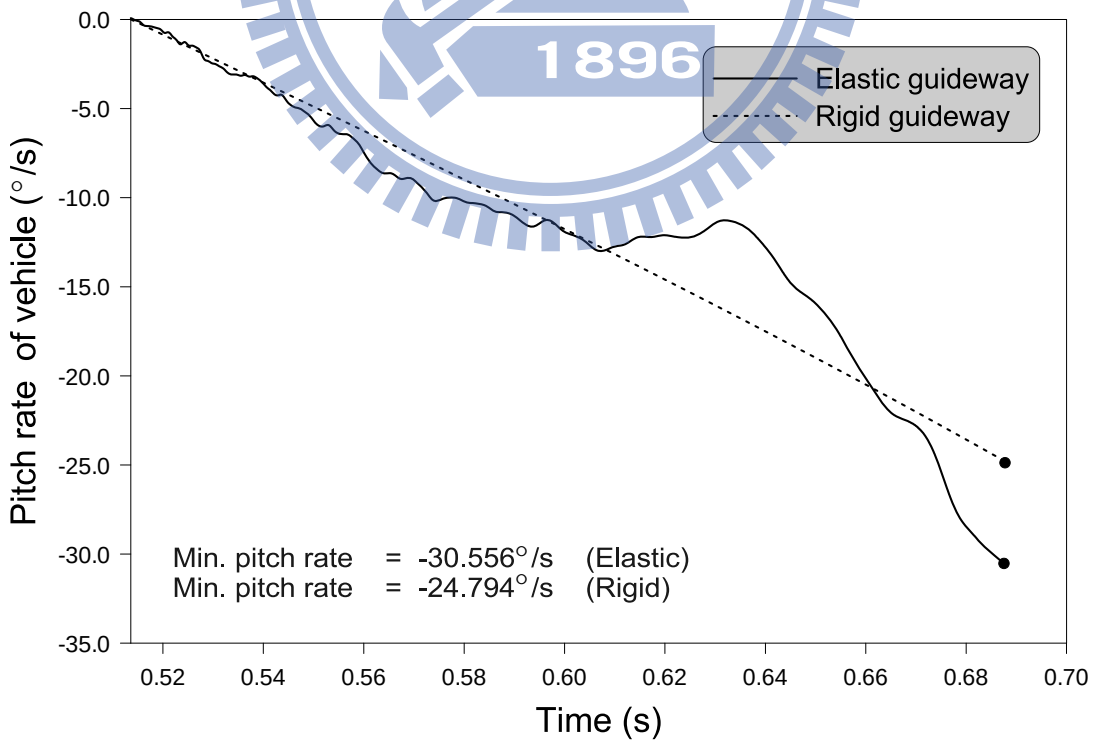

Figure 3.11: Comparison of pitch rates of vehicle on elastic guideway and rigid guideway.

pared with those obtained from the rigid guideway model in the previous section, as shown in Figs. 3.10 and 3.11. As shown in Figs. 3.10 and 3.11, the computed minimum pitch angles of the vehicle on the elastic guideway and rigid guideway are $-2.6060°$ and $-2.0953°$, respectively; the corresponding minimum pitch rates are $-30.556°/\mathrm{s}$ and $-24.794°/\mathrm{s}$.

The tip-off analysis results indicate that the vehicle vibrates excessively at approximately $0.6\ \mathrm{s}$ when the tip-off phase begins. This vibration is because of the dynamic interaction of the rear shoe of the vehicle and the elastic guideway when the front shoe of the vehicle loses contact with the guideway. In addition, the behavior of the dynamic interaction between the vehicle and the guideway cannot be observed and computed using the rigid guideway model. Therefore, the elastic guideway model has to be used for this purpose.

3.5 Parametric study

This study aims to investigate the motion of a vehicle on an elastic guideway before the take-off phase as well as the initial movement at the end of the phase. Therefore, in the parametric study, we focused on the effect of the dynamic interaction between a vehicle and its guideway on the tip-off analysis results of the vehicle. For this purpose, we determined the transverse displacement of the center of gravity, pitch angle, and pitch rate of the vehicle. For the parametric study, we used the nominal values of the parameters listed in Table 3.1. We estimated the values of parameters such as the damping ratio ξ, angle of inclination $\theta_{_E}$, length of guideway L, and distance between shoes of the vehicle d, and used L and d for the tip-off analysis. We performed a series of numerical simulations; the obtained results are shown in the graphs below.

3.5.1 Influence of damping ratio of guideway

The results obtained in this study clearly indicate that the damping ratio of the guideway ξ is sensitive to the analysis results, and the value of ξ is approximately less than 0.01. However, when ξ is greater than 0.01, the dynamic responses of the vehicle tend toward becoming linear.

According to the parameters listed in Table 3.1, we selected four different values for the damping ratio of the guideway, $\xi = 0.00$, 0.01, 0.03, and 0.05, in order to analyze the tip-off effect. Figures 3.12, 3.13, and 3.14 show the obtained results. We compared these results with those obtained for the rigid guideway model in the previous section. As indicated by the time history plots, with a larger damping ratio, the response to high-frequency variations reduces more sharply in the tip-off phase. Moreover, the dynamic response obtained for the elastic guideway model was 20% greater than that obtained for the rigid guideway model. The results of the simulation are listed in Table 3.4. For $\xi = 0.03$, the differences in the transverse displacement of the center of gravity, pitch angle, and pitch rate are 24.40%, 24.37%, and 23.24%, respectively.

We selected 1000 sets of ξ values ranging from 0.00 to 0.06 in this study. Figures 3.15, 3.16, and 3.17 show the dynamic responses of the vehicle with changes in the damping ratio. When ξ is greater than 0.01, the dynamic response of the vehicle tends toward becoming linear. Therefore, it would be preferable to select an appropriate guideway material or heavily damped guideways to minimize the dynamic response when designing launch systems.

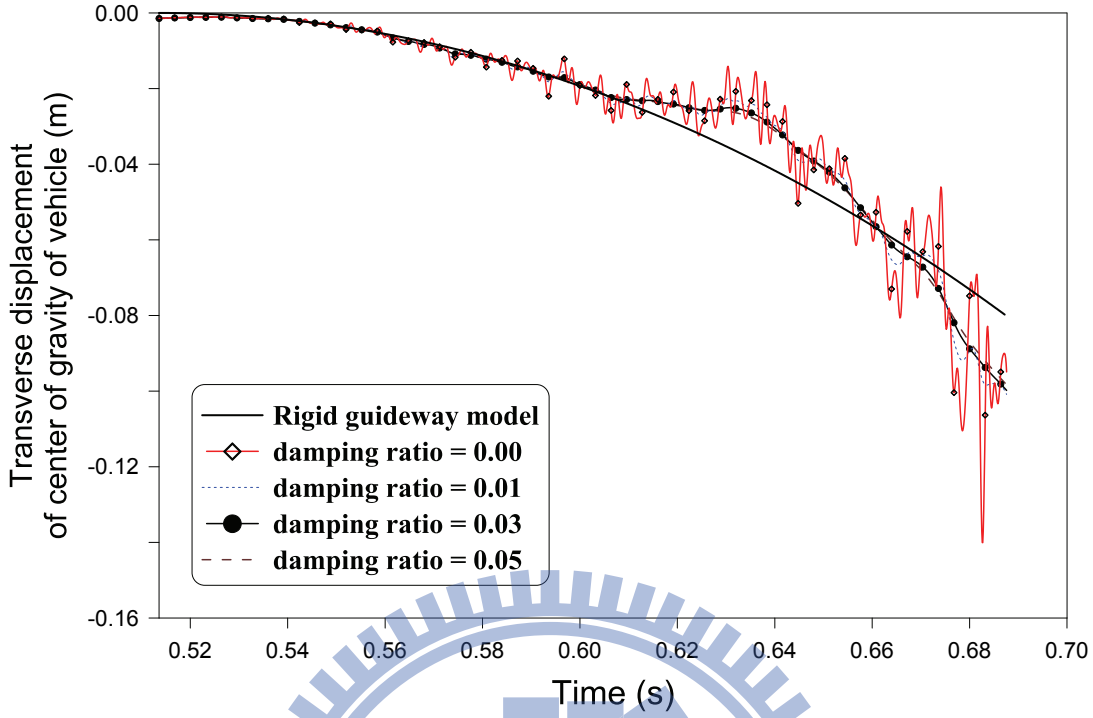

Figure 3.12: Effect of guideway damping on transverse displacement of vehicle's center of gravity ($\bar{y} - t$ diagram).

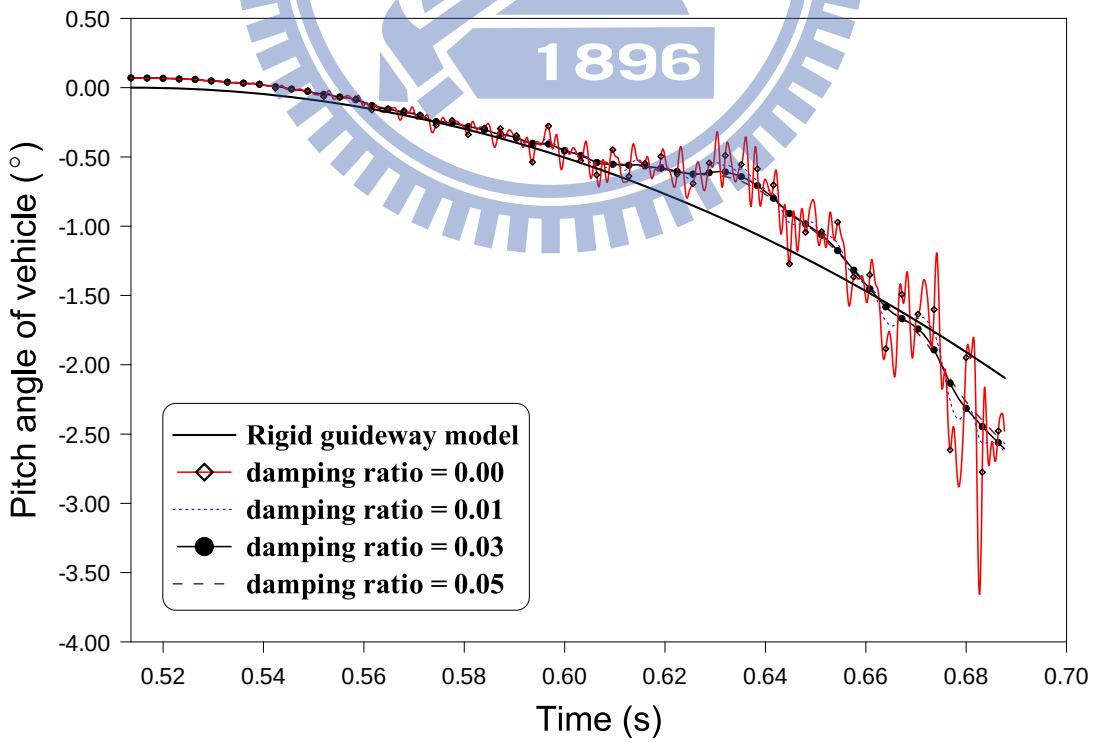

Figure 3.13: Effect of guideway damping on pitch angle of vehicle ($\bar{\theta} - t$ diagram).

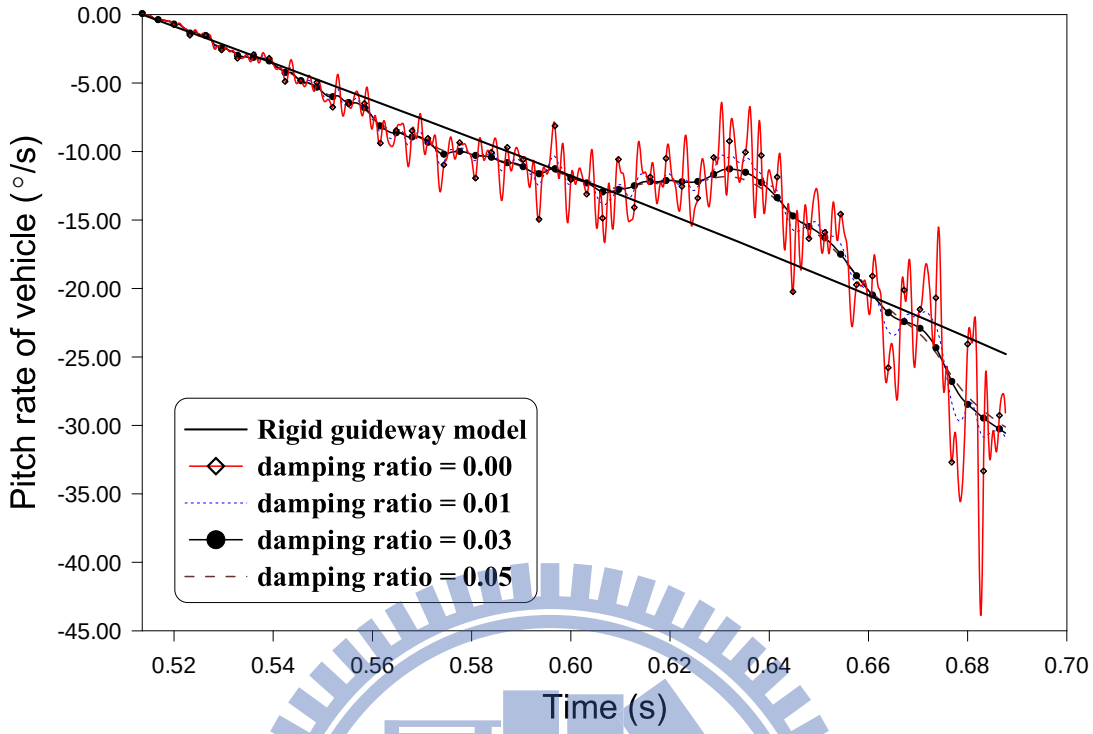

Figure 3.14: Effect of guideway damping on pitch rate of vehicle ($\dot{\bar{\theta}} - t$ diagram).

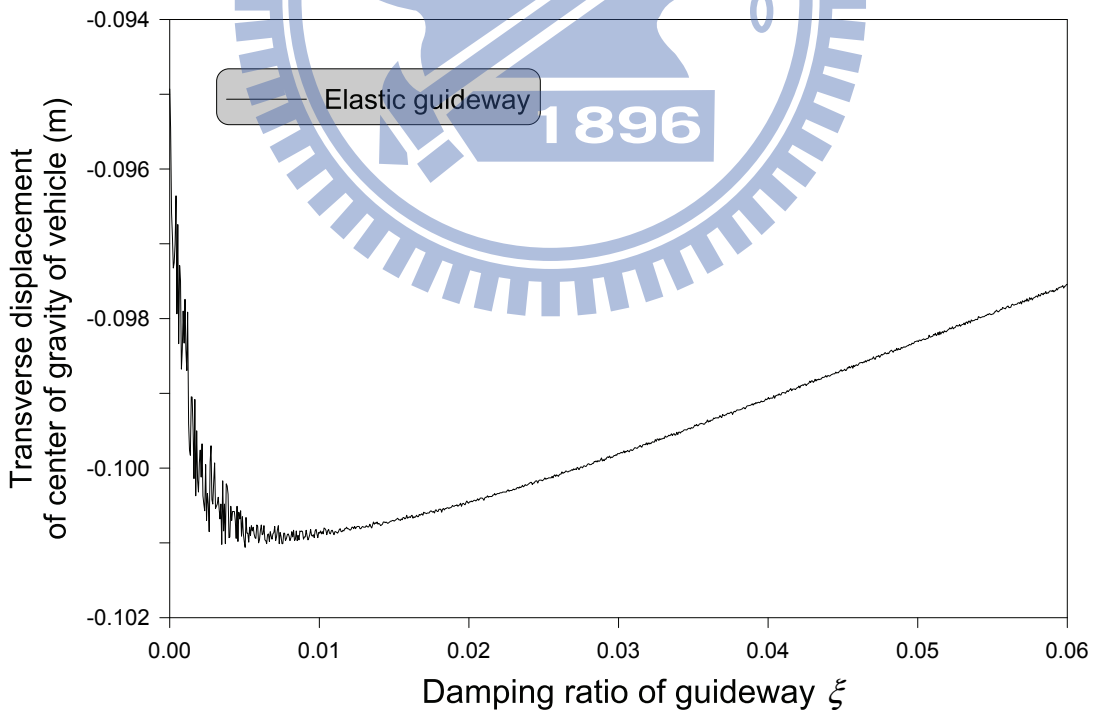

Figure 3.15: Effect of guideway damping on transverse displacement of vehicle's center of gravity ($\bar{y} - \xi$ diagram).

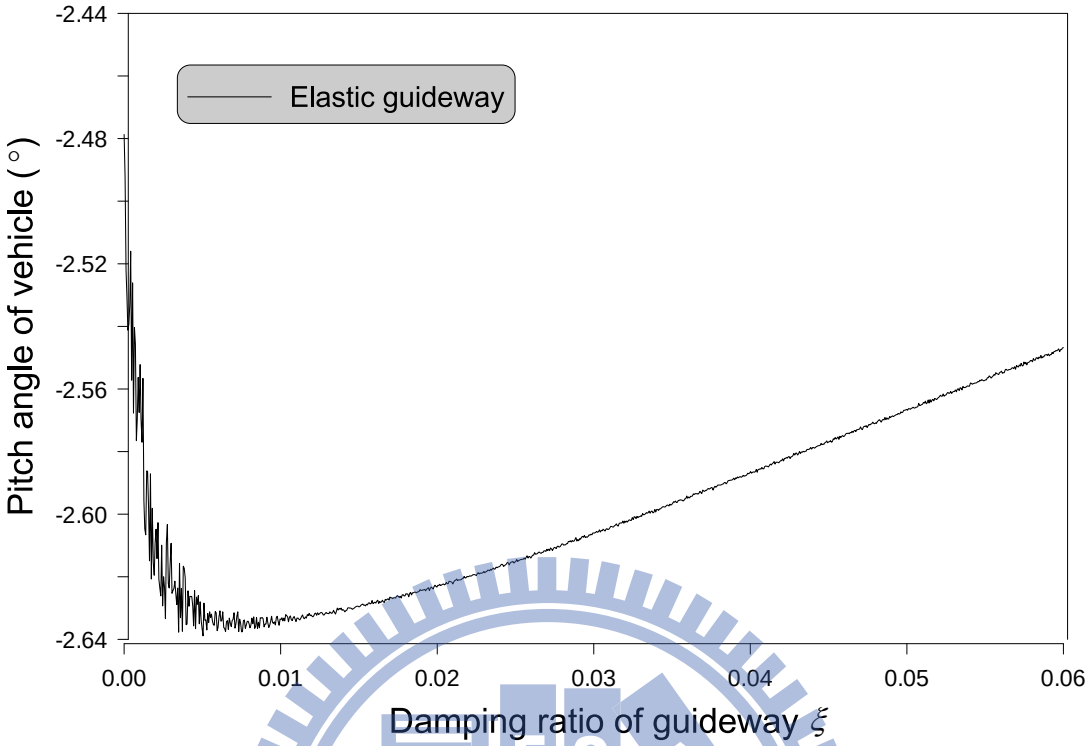

Figure 3.16: Effect of guideway damping on pitch angle of vehicle ($\bar{\theta} - \xi$ diagram).

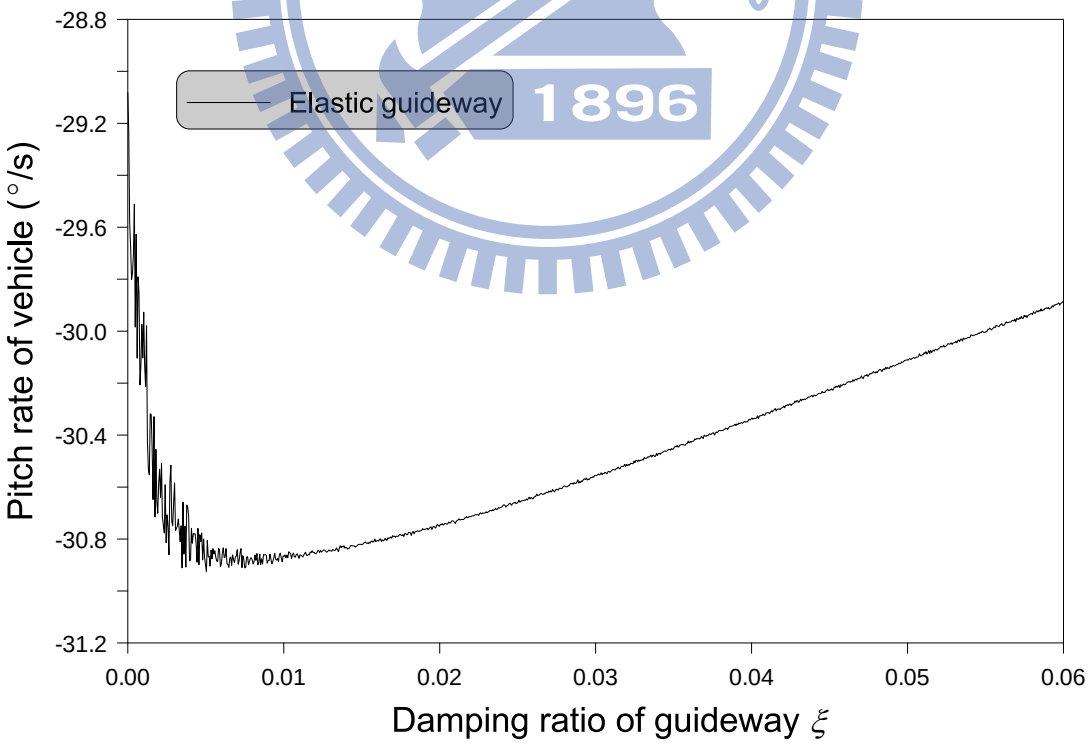

Figure 3.17: Effect of guideway damping on pitch rate of vehicle ($\dot{\bar{\theta}} - \xi$ diagram).

Table 3.4: Comparison of dynamic responses between elastic guideway model with different damping ratios and rigid guideway model.

Case.	$\bar{y}\ (m)$	%	$\bar{\theta}\ (^\circ)$	%	$\dot{\bar{\theta}}\ (^\circ/s)$	%
Rigid guideway	$-8.0231E-02$	–	$-2.0953E+00$	–	$-2.4794E+01$	–
$\xi = 0.00$	$-9.4929E-02$	18.32	$-2.4787E+00$	18.30	$-2.9082E+01$	17.29
$\xi = 0.01$	$-1.0086E-01$	25.71	$-2.6337E+00$	25.70	$-3.0867E+01$	24.49
$\xi = 0.03$	$-9.9806E-02$	24.40	$-2.6060E+00$	24.37	$-3.0556E+01$	23.24
$\xi = 0.05$	$-9.8314E-02$	22.54	$-2.5670E+00$	22.51	$-3.0114E+01$	21.46

3.5.2 Influence of angle of inclination of guideway

The force component induced in the transverse direction by the moving loads decreases when the angle of inclination $\theta_{_E}$ of the guideway increases. Although an increase in the value of $\theta_{_E}$ is advantageous in that it minimizes the dynamic responses of the launched vehicle, it also leads to a decrease in the initial speed of the vehicle before take-off. The initial speed of the vehicle will affect the tolerance of its flight control system. Therefore, the angle of inclination of the guideway has to be carefully selected when designing a launch system.

According to the parameters listed in Table 3.1, we selected 1000 sets of $\theta_{_E}$ values ranging from 0.0 rad to 1.0 rad in this study. Figures 3.18, 3.19, and 3.20 show the obtained results. We compared these results with those obtained for the rigid guideway model in Chapter two. As mentioned before, the angle of inclination of the guideway affects the vehicle speed and the transverse force acting on the launched vehicle before take-off. In other words, the larger the angle of inclination $\theta_{_E}$ of the guideway, the lower is the take-off speed and the smaller is the transverse force acting on the launched vehicle. When the take-off speed of the launched vehicle decreases, the time interval $t_{_R} - t_{_F}$ increases. This is disadvantageous because this decreases the vehicle tip-off effect. However, increasing the angle of inclination of the guideway may decrease the transverse force acting on the launched vehicle; this is advantageous in that

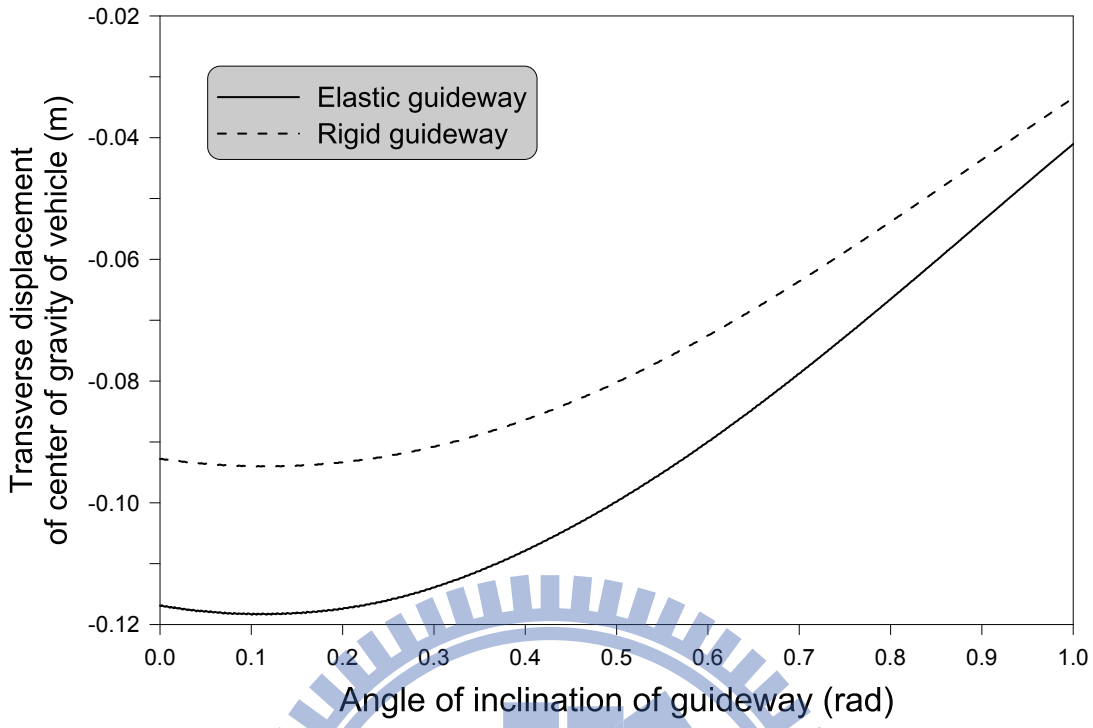

Figure 3.18: Effect of angle of inclination on transverse displacement of vehicle's center of gravity ($\bar{y} - \theta_E$ diagram).

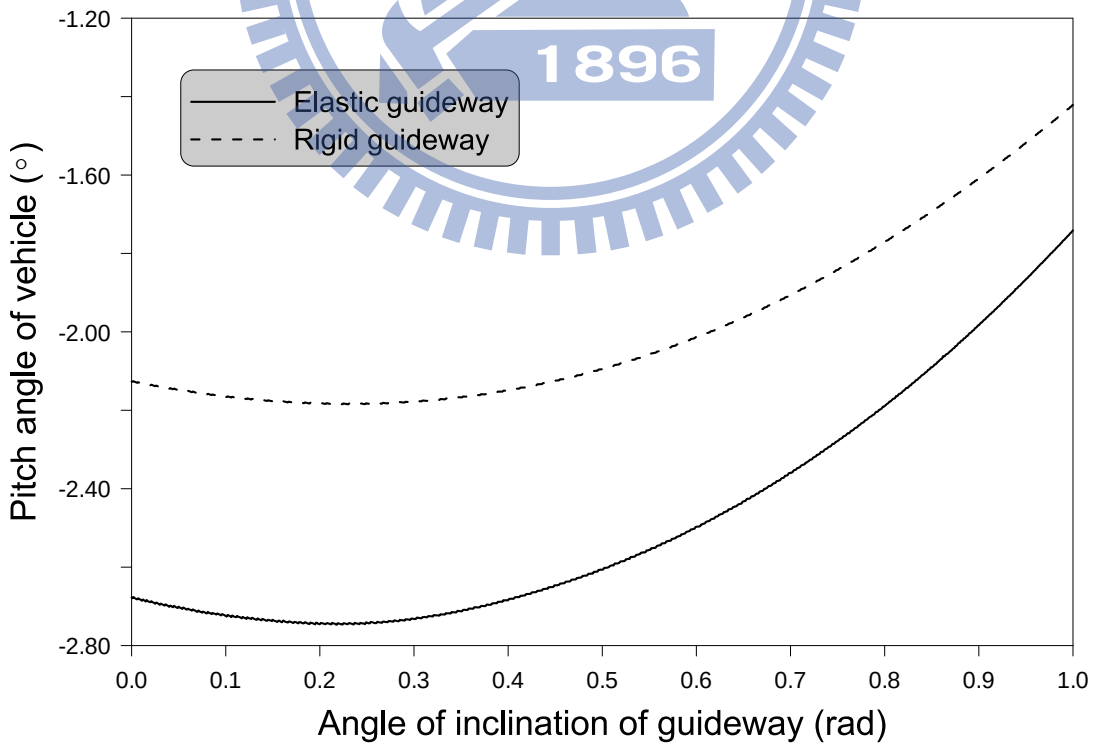

Figure 3.19: Effect of angle of inclination on pitch angle of vehicle ($\bar{\theta} - \theta_E$ diagram).

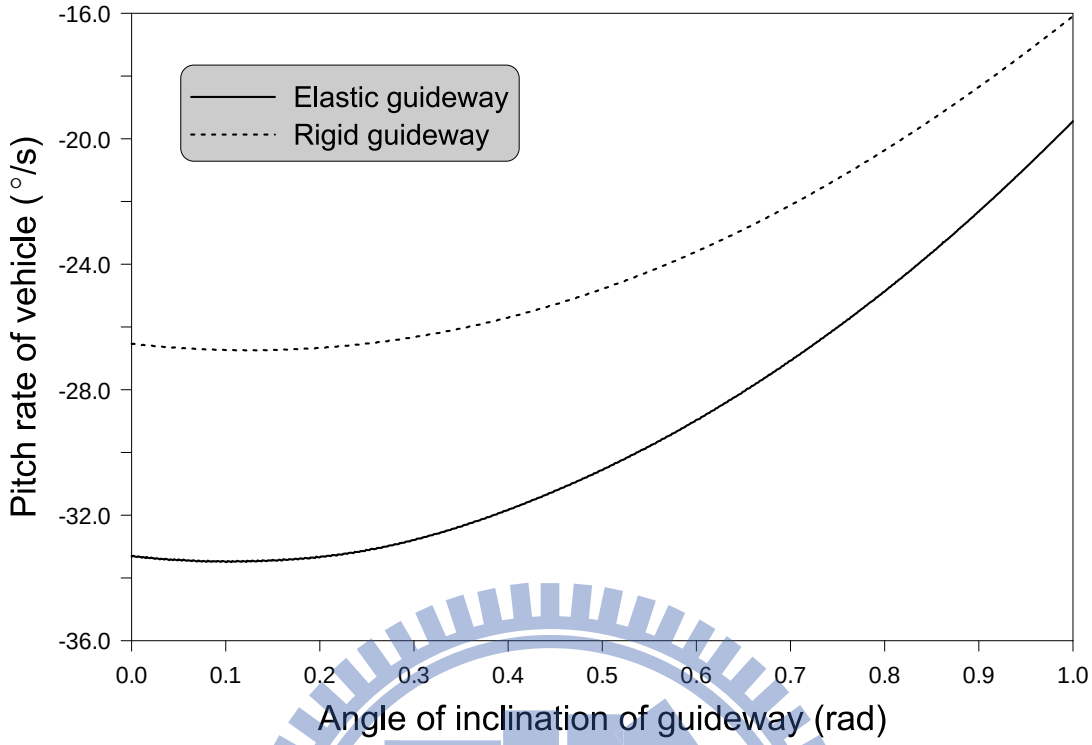

Figure 3.20: Effect of angle of inclination on pitch rate of vehicle ($\dot{\bar{\theta}} - \theta_E$ diagram).

it reduces the dynamic interactions between the vehicle and its guideway. The figures indicate that when the angle of inclination θ_E increases, the differences between the dynamic responses for the two models decrease. In other words, selecting the angle of inclination of the guideway is difficult.

3.5.3 Influence of length of guideway

An increase in the length of the guideway will help increase the speed of the vehicle during take off. Further, the time interval $t_R - t_F$ of the tip-off phase corresponding to the two shoes of the vehicle losing contact with the guideway will decrease. This is highly useful for decreasing the dynamic responses of the vehicle.

According to the parameters listed in Table 3.1, we selected 1000 sets of L values ranging from 4.0 m to 12.0 m to investigate the results of the variation of the tip-off effect. Figures 3.21, 3.22, and 3.23 show the obtained results. We compared these results with those obtained for the rigid guideway model in Chapter two. Obviously,

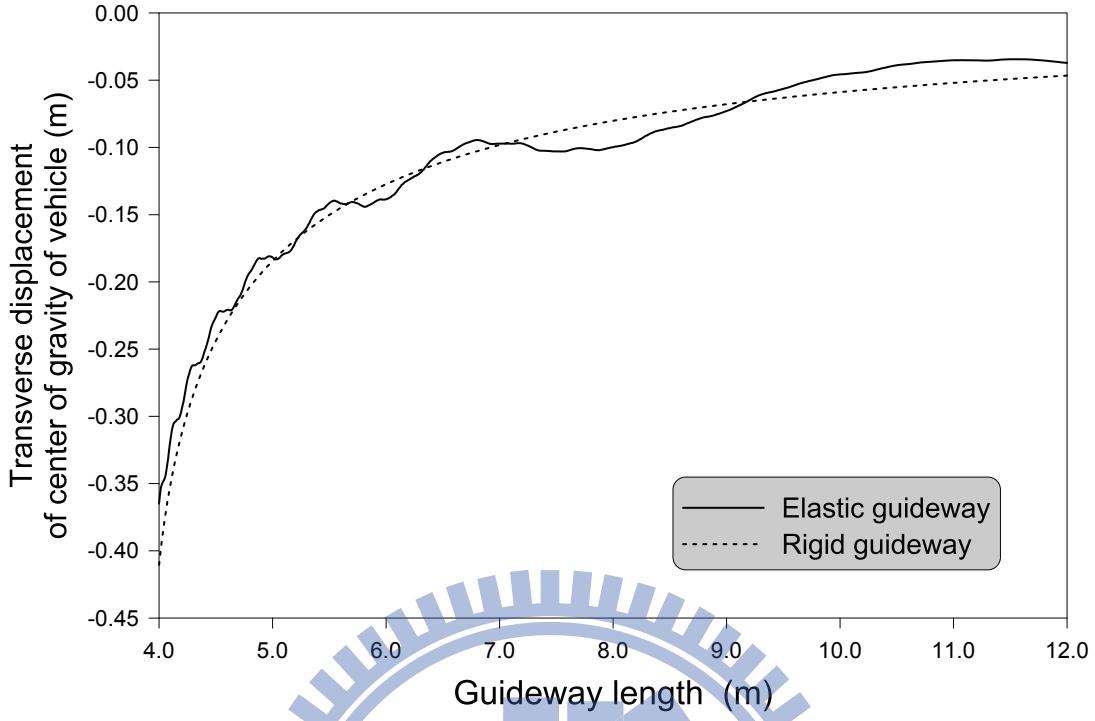

Figure 3.21: Effect of guideway length on transverse displacement of vehicle's center of gravity ($\bar{y} - L$ diagram).

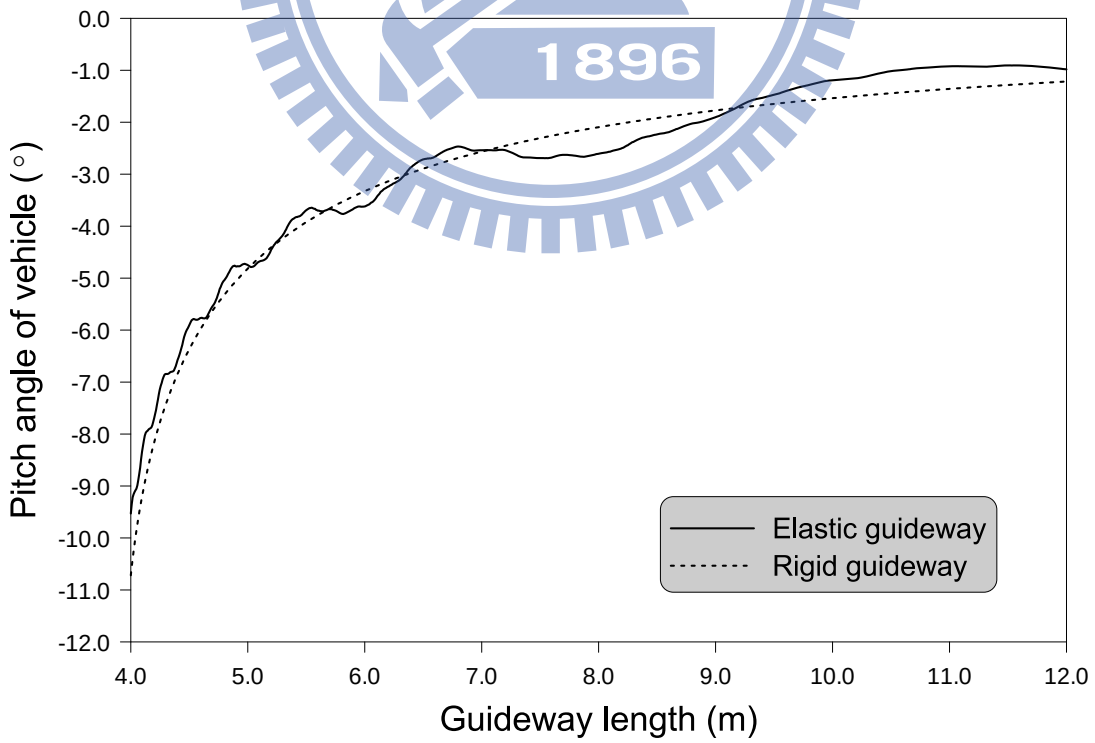

Figure 3.22: Effect of guideway length on pitch angle of vehicle ($\bar{\theta} - L$ diagram).

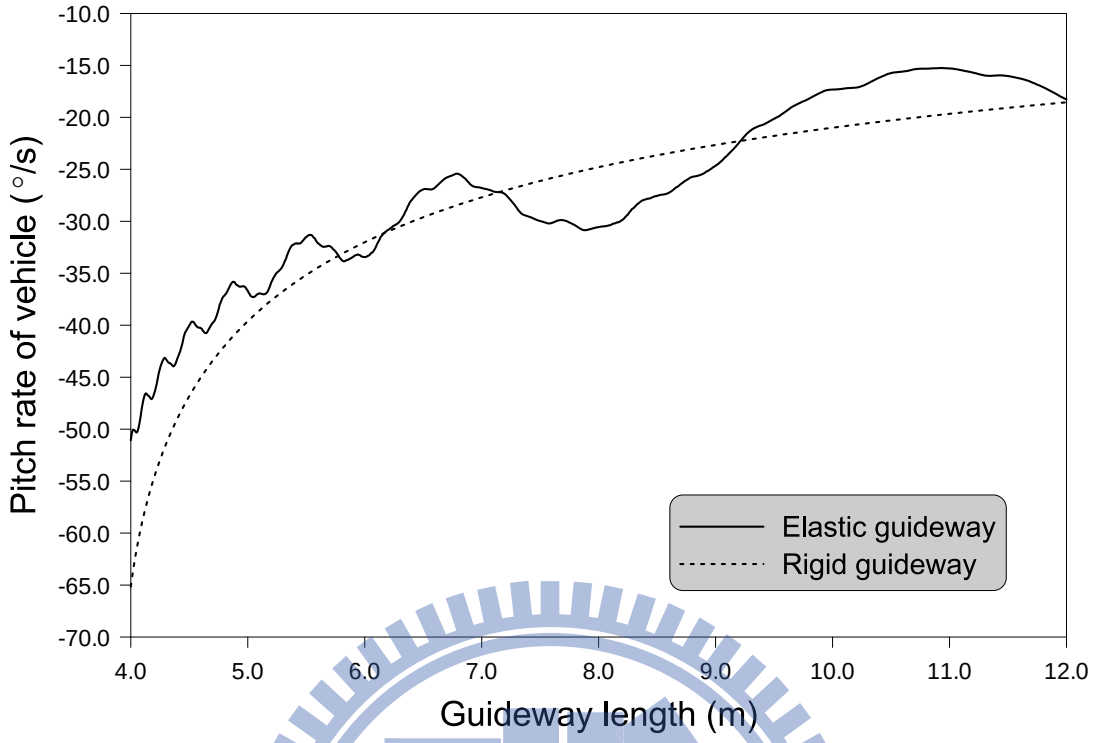

Figure 3.23: Effect of guideway length on pitch rate of vehicle ($\dot{\bar{\theta}} - L$ diagram).

as the length of the guideway increases, the results of the tip-off effect analysis of the rigid guideway model tend to decrease smoothly.

Although the analysis results of the elastic guideway model exhibit a similar behavior, they fluctuate along the curves of the rigid guideway model. The disturbance of this phenomenon is particularly evident in the analysis of the pitch rate. Although the results indicate that the increase in the guideway length decreases the dynamic interaction because of the tip-off effect, the guideway length has to be selected carefully considering the fluctuation in the results and the space limits of certain launch systems. In most cases, the length of the guideway must be limited to satisfy the space requirements of a launch system. Normally, the length of the guideway is slightly greater than that of the vehicle.

3.5.4 Influence of distance between shoes of vehicle

According to the parameters listed in Table 3.1, we selected 1000 sets of d values ranging from $2.6\ \mathrm{m}$ to $4.8\ \mathrm{m}$ to investigate the effect of d on the tip-off responses. Figures 3.24, 3.25, and 3.26 show the transverse displacement, pitch angle and pitch rate of vehicle varying with d, respectively. We compared the results with those obtained from the rigid guideway model described in Chapter 2. Obviously, the larger the distance, the more dynamic is the response in the tip-off phase of the vehicle. The dynamic response obtained from the elastic guideway model was 30% greater than that obtained from the rigid guideway model. The differences in the vertical displacement of the center of gravity, pitch angle, and pitch rate at $d = 2.8706\ \mathrm{m}$ are 30.96%, 30.82%, and 31.35%, as shown in Table 3.5. The influence of the distance between the shoes on the maximum difference of the vehicle's dynamic response are computed to be $3.0170\ \mathrm{cm}$ for the transverse displacement of the center of gravity, $0.7888°$ for the pitch angle, and $6.7160°/s$ for the pitch rate at $d \doteq 4.4\ \mathrm{m}$, as shown in Table 3.5.

A decrease in the distance between the shoes of the vehicle leads to a decrease in the time interval of the tip-off phase. That is, the time interval $t_R - t_F$ corresponding to the two shoes losing contact with the guideway decreases. However, this situation could cause stress concentration in the guideway and unstable behavior of the vehicle. More problems may arise, and these need to be investigated. However, this is beyond the scope of this study.

3.5.5 Influence of Coriolis force and centrifugal force

A launch system should be designed by considering two important factors: the mass of the vehicle and the length of the guideway. Generally, the time interval of the take-off phase of a heavy vehicle is less than $1\,s$, and the speed of the vehicle is around $30\,\mathrm{m/s}$ before take-off. When the vehicle is moving along a deformed guideway at

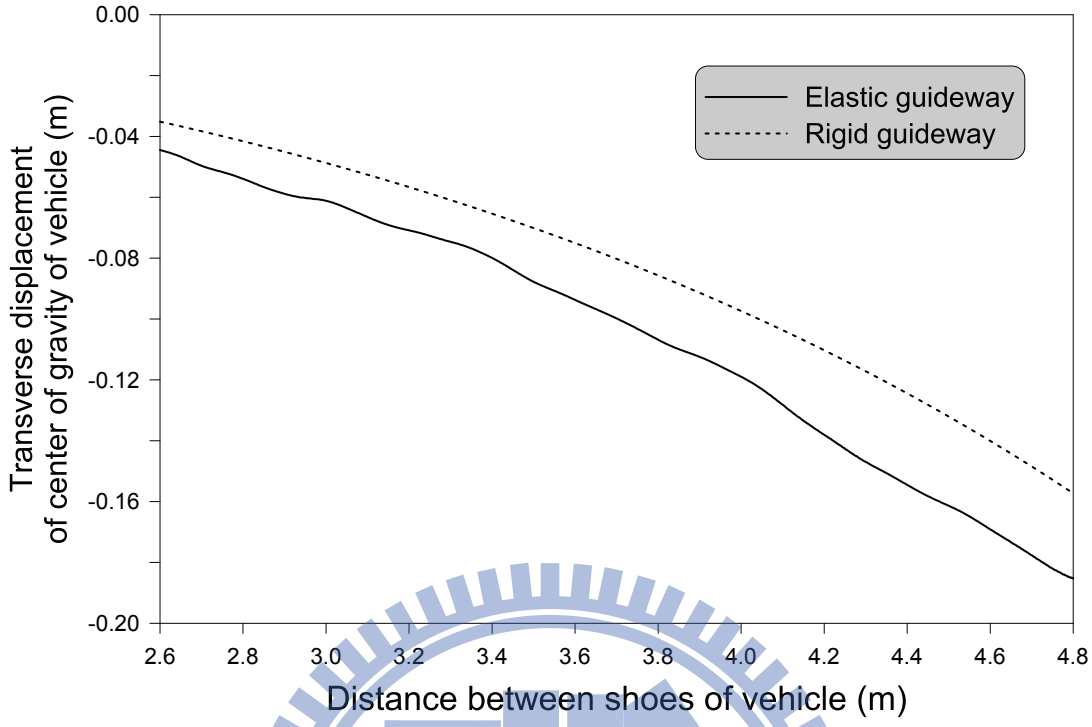

Figure 3.24: Effect of distance between the shoes of the vehicle on transverse displacement of vehicle's center of gravity ($\bar{y} - d$ diagram).

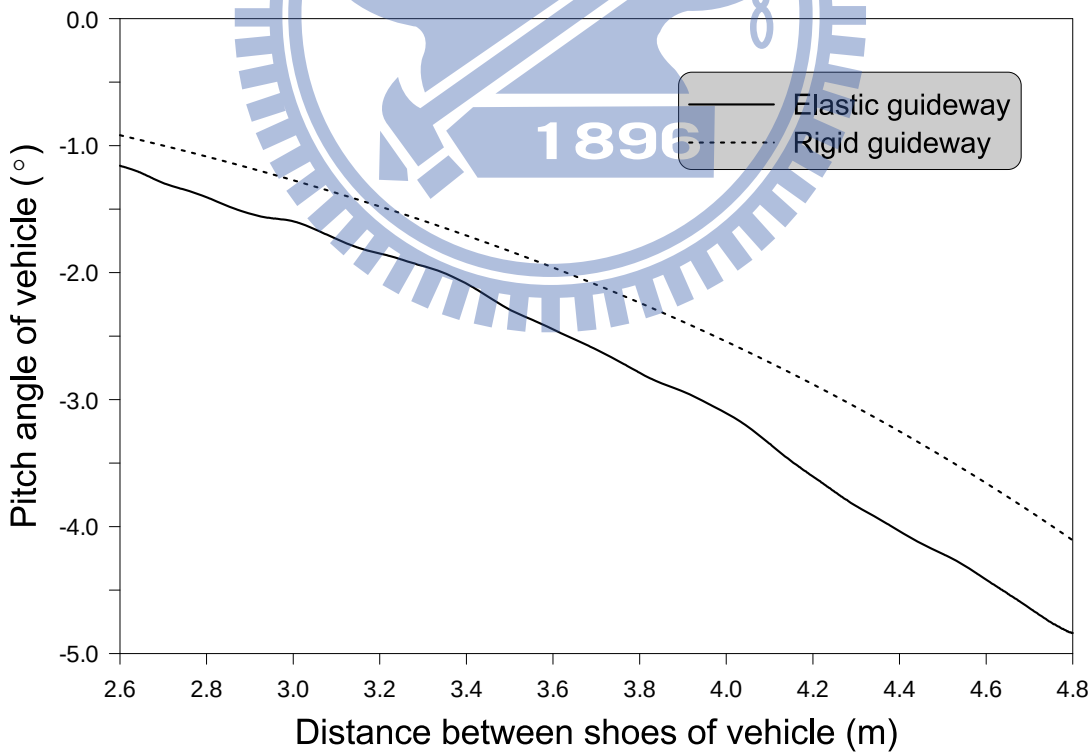

Figure 3.25: Effect of distance between the shoes of the vehicle on pitch angle of vehicle ($\bar{\theta} - d$ diagram).

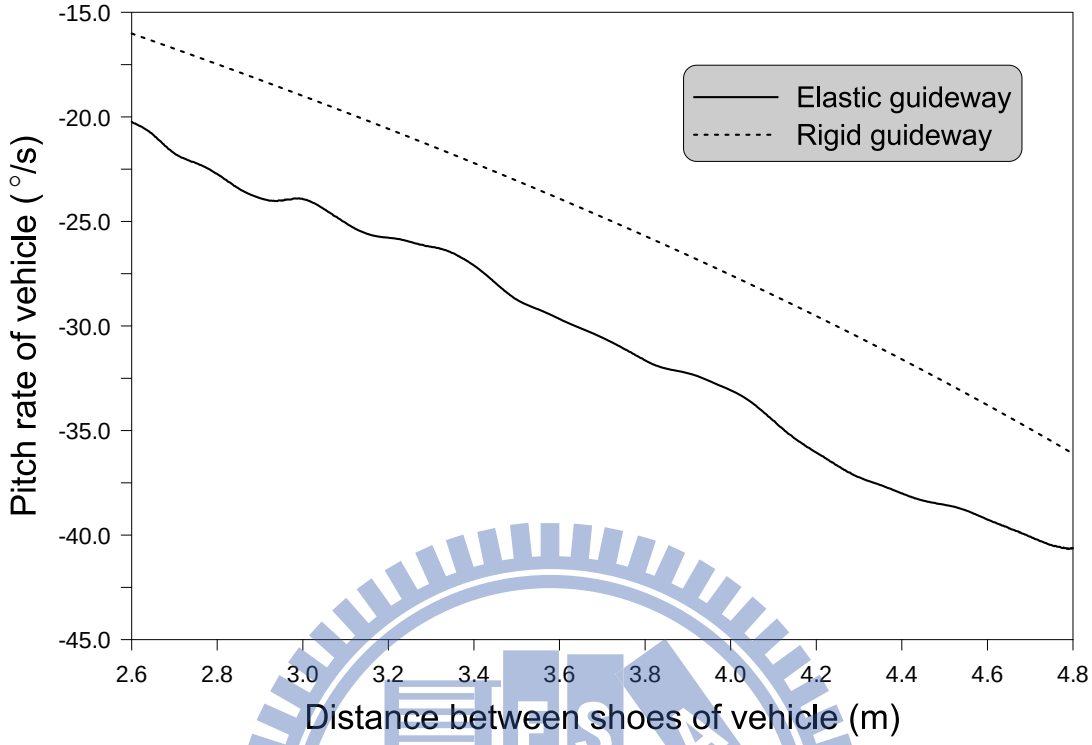

Figure 3.26: Effect of distance between the shoes of the vehicle on pitch rate of vehicle ($\dot{\bar{\theta}} - d$ diagram).

Table 3.5: Effect of distance between the shoes on maximum difference in dynamic response of vehicle.

$d\ (m)$	Guideway	$\bar{y}\ (m)$	%	$\bar{\theta}\ (^\circ)$	%	$\dot{\bar{\theta}}\ (^\circ/s)$	%
2.8706	Rigid	$-4.4018E-02$	–	$-1.1495E+00$	–	$-1.8009E+01$	–
	Elastic	$-5.7647E-02$	30.96	$-1.5038E+00$	30.82	$-2.3654E+01$	31.35
4.2830	Rigid	$-1.1597E-01$	–	$-3.0287E+00$	–	$-3.0368E+01$	–
	Elastic	$-1.4561E-01$	25.56	$-3.8032E+00$	25.57	$-3.7084E+01$	22.12
4.4238	Rigid	$-1.2621E-01$	–	$-3.2961E+00$	–	$-3.1846E+01$	–
	Elastic	$-1.5638E-01$	23.91	$-4.0845E+00$	23.92	$-3.8196E+01$	19.94
4.4304	Rigid	$-1.2671E-01$	–	$-3.3091E+00$	–	$-3.1916E+01$	–
	Elastic	$-1.5688E-01$	23.81	$-4.0979E+00$	23.84	$-3.8246E+01$	19.83

the abovementioned speed, the behavior of dynamic interactions should be studied by considering the effect of the Coriolis force and centrifugal force. According to the parameters listed in Table 3.1, we analyzed the tip-off effect of the vehicle under the action of the Coriolis force and centrifugal force. In this test example, the dynamic interaction was not significant. Figures 3.27, 3.28, and 3.29 show the results of the tip-off effect analysis. The figures indicate that the dynamic response under the action of the Coriolis force and centrifugal force is approximately 2.0% greater than that in the absence of these forces. The differences in the transverse displacement of the center of gravity, pitch angle, and pitch rate are 2.02%, 2.02%, and 1.95%, as shown in Table 3.6.

Dehestani *et al*. [10] and Wu [11] showed that it is important to consider the Coriolis force and centrifugal force associated with a high-speed vehicle moving along a vibrating guideway. Generally, in the interest of accuracy, the take-off attitude of a vehicle should be precisely computed. Therefore, if would be preferable to consider the effects of the Coriolis force and centrifugal force in the formulations.

Table 3.6: Effect of Coriolis and centrifugal forces on dynamic response of vehicle.

Case.	$\bar{y}\ (m)$	%	$\bar{\theta}\ (^\circ)$	%	$\dot{\bar{\theta}}\ (^\circ/s)$	%
C1	$-9.7830E-02$	–	$-2.5543E+00$	–	$-2.9971E+01$	–
C2	$-9.9806E-02$	2.02	$-2.6060E+00$	2.02	$-3.0556E+01$	1.95
C3	$-9.9016E-02$	1.21	$-2.5854E+00$	1.22	$-3.0305E+01$	1.11
C4	$-9.8453E-02$	0.64	$-2.5705E+00$	0.63	$-3.0174E+01$	0.68

3.5.6 Influence of guideway length and distance between the shoes

According to the parameters listed in Table 3.1, we selected d values ranging from 2.4 m to 5.0 m and L values ranging from 6.0 m to 10.0 m, to investigate their effects on the tip-off responses. Figures 3.30 and 3.31 show the results of the pitch angle and

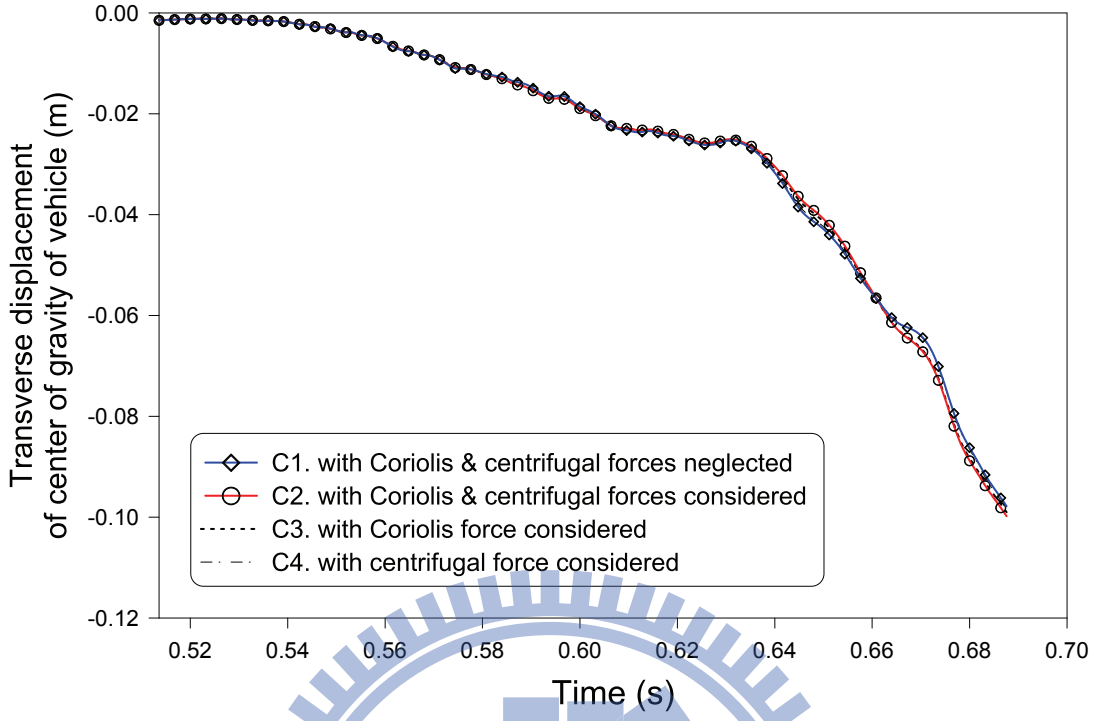

Figure 3.27: Effect of Coriolis and centrifugal forces on displacement of vehicle's center of gravity ($\bar{y} - t$ diagram).

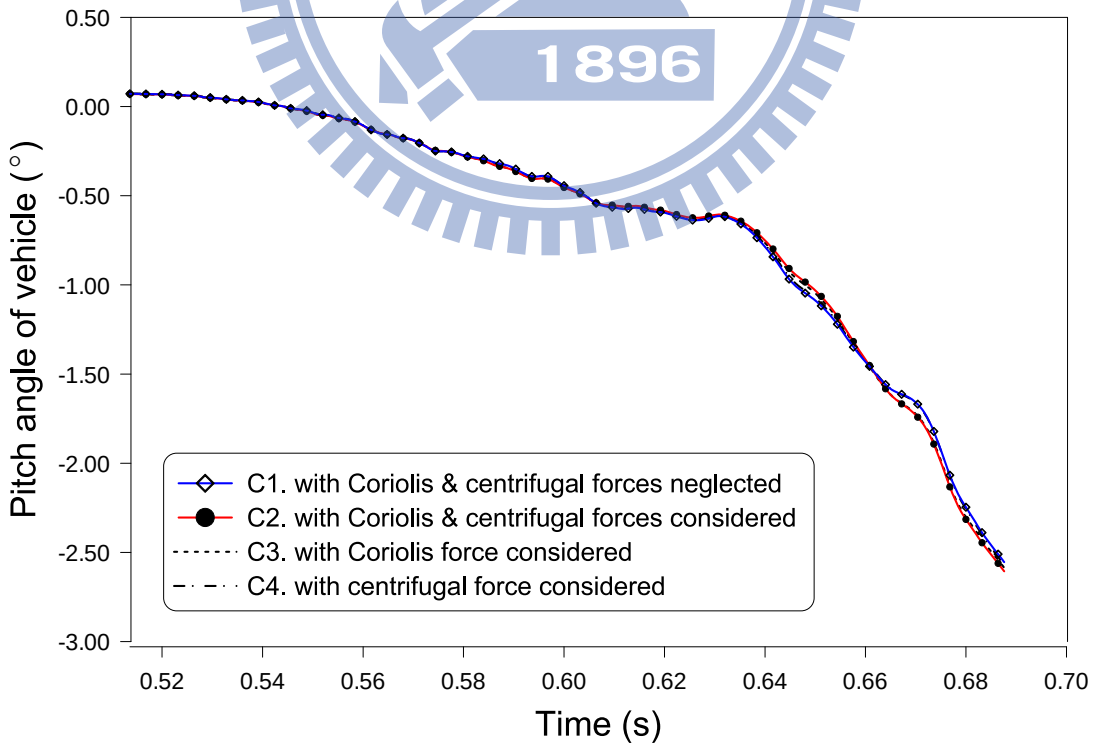

Figure 3.28: Effect of Coriolis and centrifugal forces on pitch angle of vehicle ($\bar{\theta} - t$ diagram).

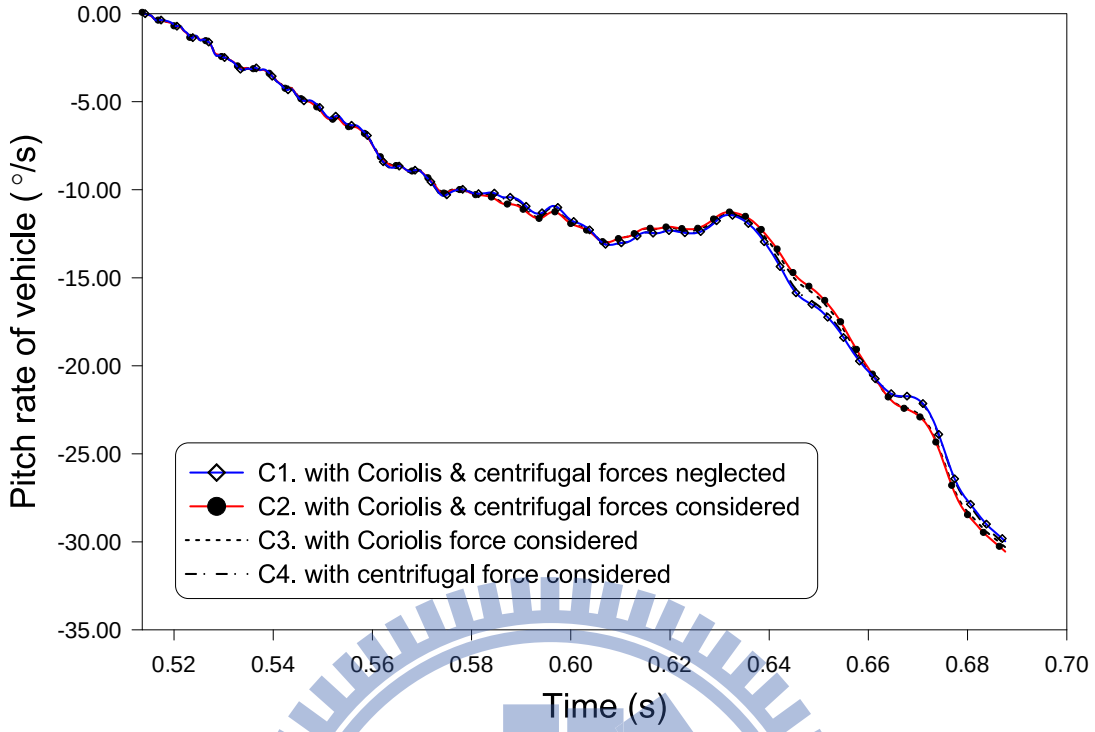

Figure 3.29: Effect of Coriolis and centrifugal forces on pitch rate of vehicle ($\dot{\bar{\theta}} - t$ diagram).

pitch rate analysis of the vehicle. From the contour lines, we can easily select a set of optimum parameters for designing launch systems.

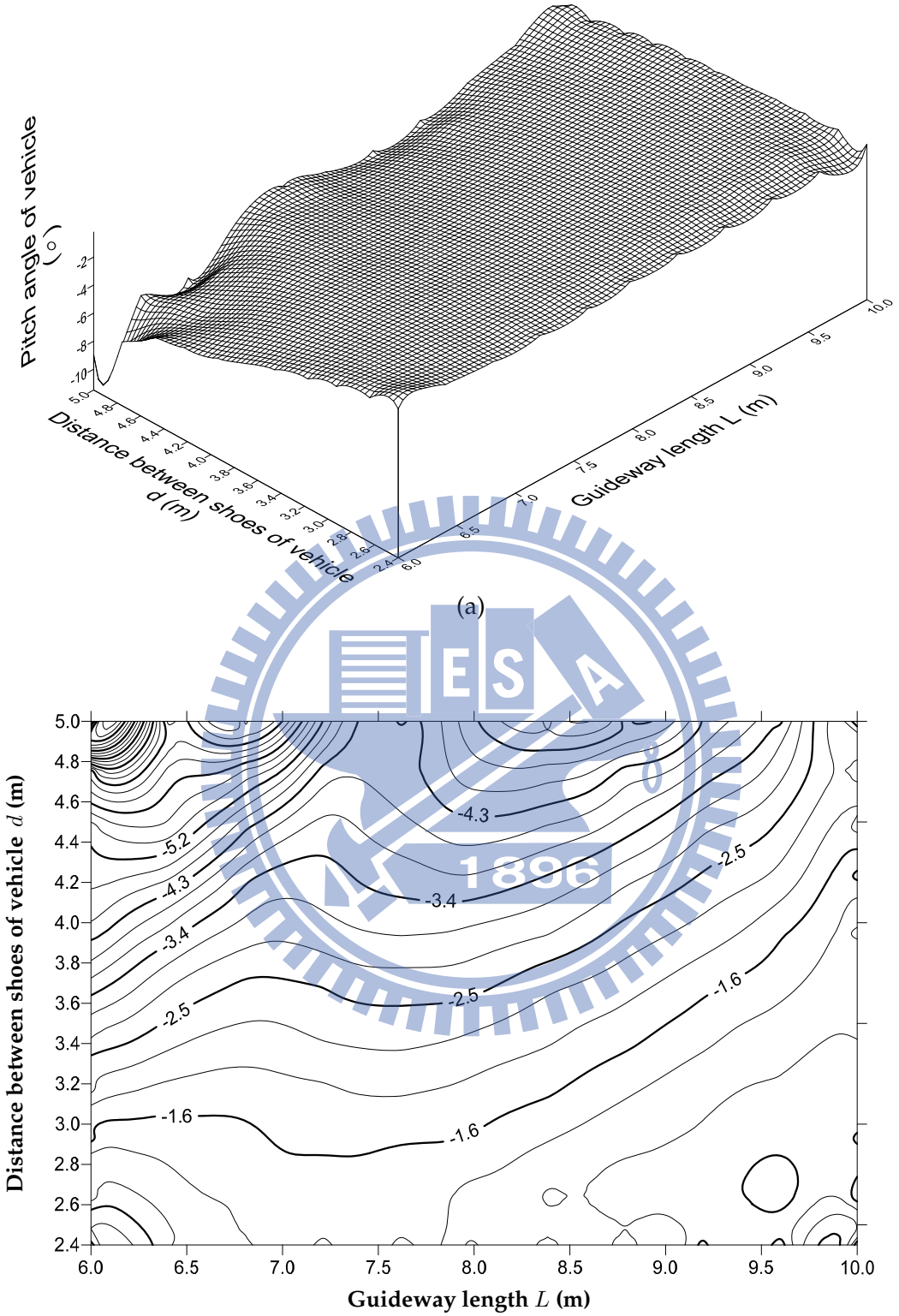

Figure 3.30: Effect of guideway length and distance between shoes on pitch angle of vehicle: (a) 3D plot (b) contour plot.

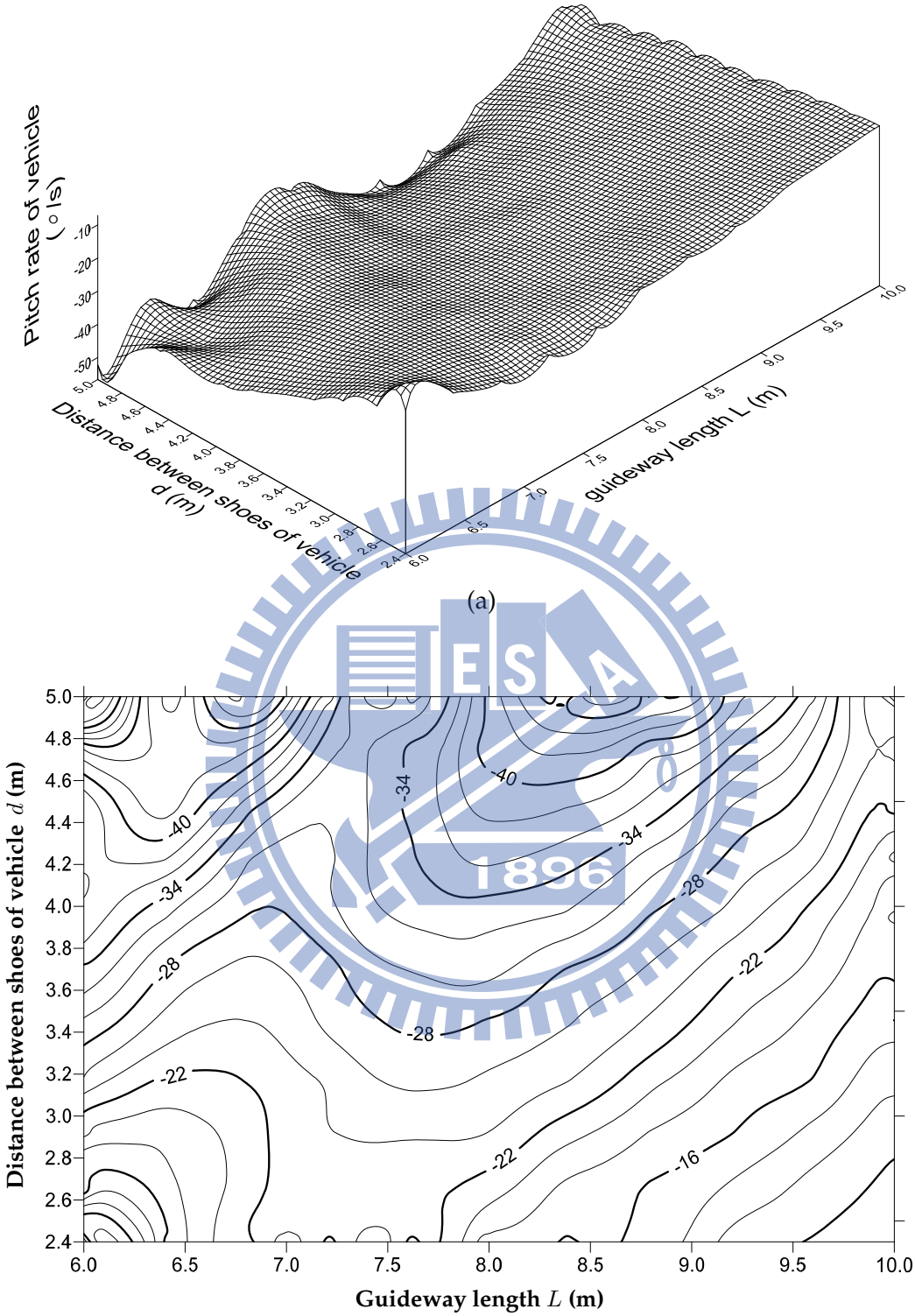

Figure 3.31: Effect of guideway length and distance between shoes on pitch rate of vehicle: (a) 3D plot (b) contour plot.

CHAPTER FOUR

A flexible vehicle moving along an inclined flexible guideway

4.1 Theory and Formulation

Similar to the development of solutions in Chapters two and three, Fig. 4.1 schematically depicts a typical straight flexible guideway that is used for launching a flexible vehicle. This model is referred as E.E. model. While the vehicle moves, the two shoes of the flexible vehicle are assumed to slide along the elastic guideway by means of a rigid contact. The vector of thrust is assumed to be along the vehicle's centerline (C.L.) and always coincides with the line joining the two contact points.

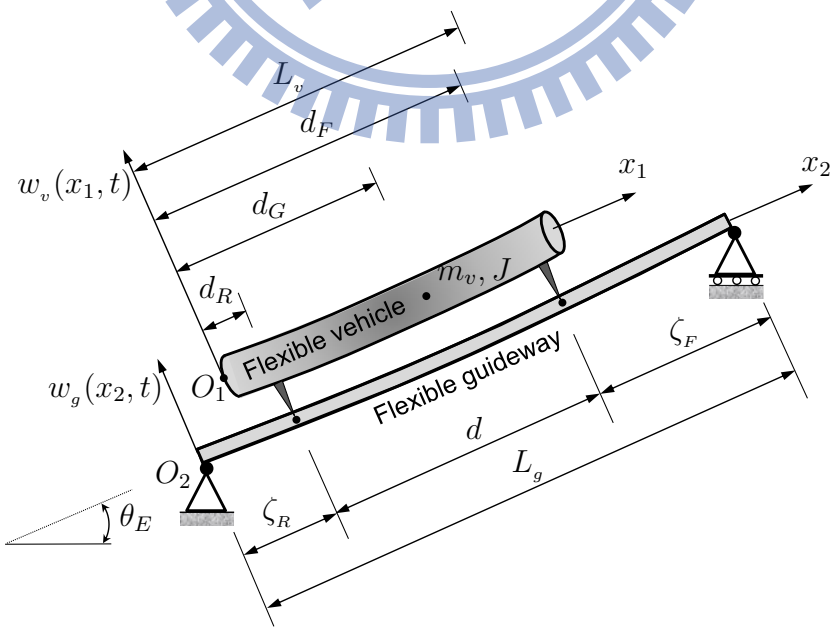

Figure 4.1: A typical flexible guideway used for flexible vehicle launch.

4.1.1 Position history of vehicle

As mentioned in Chapter 2, two phases exist when a vehicle moves along a guideway, *i.e.*, the two-shoe contact phase and the tip-off phase. From the typical thrust-time curve shown in Fig. 2.3 and the design parameters of the vehicle and its guideway, one can easily find the position of the rear shoe, $\zeta(t)$ (see Fig. 4.2), t_F and t_R can be easily determined to identify the particular phase with which the vehicle is associated at each instant. The formulas for $\zeta(t)$, t_F and t_R are given in Chapter 2.

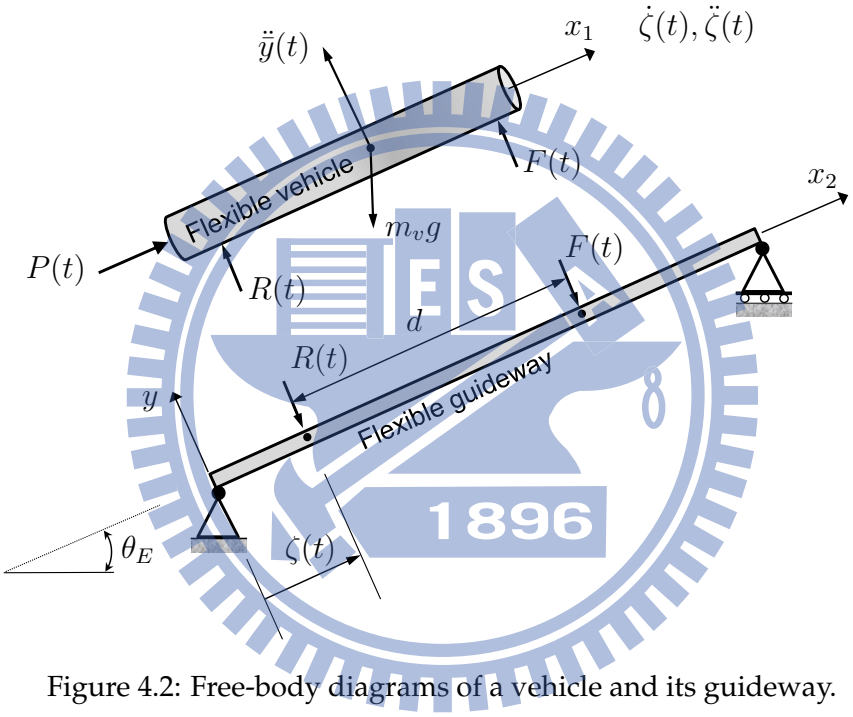

Figure 4.2: Free-body diagrams of a vehicle and its guideway.

4.1.2 Two-shoe contact phase

The dynamic response of the vehicle can be split into two parts, *i.e.*, the elastic deformation and rigid body motion, known to be completely uncoupled. The equations of motion and relevant boundary conditions can be derived using the Lagrangian approach. The kinetic energy and potential energy of the vehicle and the guideway are

$$K_v = \frac{1}{2}\int_0^{L_v} \rho_v A_v \left(\dot{w}_v + \dot{\zeta} w_v^{'}\right)^2 dx_1 + \frac{1}{2} m_v \left(\dot{\bar{x}}_r{}^2 + \dot{\bar{y}}_r{}^2\right) + \frac{1}{2} J \dot{\bar{\theta}}_r^2 \tag{4.1a}$$

$$K_g = \frac{1}{2}\int_0^{L_g} \rho_g A_g \dot{w}_g^2 dx_2 \tag{4.1b}$$

$$V_v = \frac{1}{2}\int_0^{L_v} \left(E_v I_v w_v^{''2} - P w_v^{'2}\right) dx_1 + \int_0^{L_v} \rho_v A_v g \cos\theta_E w_v dx_1 + \left(m_v g \sin\theta_E\right) \bar{x}_r + \left(m_v g \cos\theta_E\right) \bar{y}_r \tag{4.1c}$$

$$V_g = \frac{1}{2}\int_0^{L_g} E_g I_g w_g^{''2} dx_2 \tag{4.1d}$$

where subscripts $(_v)$ and $(_g)$ refer to the vehicle and the guideway, respectively; the overhead dot $(\cdot)$ and the prime $(')$ denote differentiation with respect to time t and coordinate x, respectively; K and V are the kinetic energy and the potential energy, respectively; EI is the constant flexural rigidity; ρA represents the mass per unit length; J is the mass moment of inertia of the vehicle; $\dot{\zeta}(t)$ denotes the velocity of the vehicle in the local x_2-direction; $\bar{x}_r(t)$ is the axial coordinate of the vehicle under rigid body motion in the fixed coordinate system $x_2 O_2 y_2$; $\bar{y}_r(t)$ is the transverse displacement of the vehicle under rigid body motion, and $\bar{\theta}_r(t)$ is the angle of rotation of the vehicle under rigid body motion. The transverse elastic displacements of the vehicle $w_v(x_1, t)$ and the guideway $w_g(x_2, t)$ are described as functions of the axial coordinates x_1 and x_2, respectively.

The two shoes of the vehicle are assumed to slide along the elastic guideway by means of a rigid contact. Hence, the corresponding constraint equations are

$$w(d_R, t) = w_g(\zeta, t) \tag{4.2a}$$

$$w(d_F, t) = w_g(\zeta + d, t) \tag{4.2b}$$

where d_R is the distance between the left end and the rear shoe of vehicle; d_F is the distance between the left end and the front shoe of vehicle, and $w(d_R, t)$ and $w(d_F, t)$

are the total transverse displacements at the rear shoe and the front shoe of the vehicle, respectively. These displacements $w(d_R, t)$ and $w(d_F, t)$ comprise a rigid part and an elastic part.

The transverse elastic displacements of the beams can be expressed in terms of their normal modes as,

$$w_v(x_1, t) = \sum_{j=1}^{N} \phi_j(x_1) Y_j^v(t) \tag{4.3a}$$

$$w_g(x_2, t) = \sum_{j=1}^{N} \psi_j(x_2) Y_j^g(t) \tag{4.3b}$$

where $Y_j^v(t)$ and $Y_j^g(t)$ are the generalized coordinates corresponding to the jth mode of the vehicle and guideway, respectively; $\phi_j(x_1)$ and $\psi_j(x_2)$ denote the jth mode shape functions of the vehicle and guideway, respectively.

The vehicle is modeled as a beam with two free ends, and its mode shape functions $\phi_j(x_1)$ are [38]

$$\phi_j(x_1) = \cos(\beta_{vj} x_1) + \cosh(\beta_{vj} x_1) - \Upsilon_j \left[\sin(\beta_{vj} x_1) + \sinh(\beta_{vj} x_1)\right] \tag{4.4}$$

where $j = 1, 2, ..., N$

$$\beta_{vj}^4 = \omega_{vj}^2 \cdot \frac{\rho_v A_v}{E_v I_v}, \quad \Upsilon_j = \frac{\cos(\beta_{vj} L_v) - \cosh(\beta_{vj} L_v)}{\sin(\beta_{vj} L_v) - \sinh(\beta_{vj} L_v)}, \quad \beta_{vj} L_v \approx \left(j + \frac{1}{2}\right)\pi \tag{4.5}$$

ω_{vj} is the circular frequency of the jth mode of the vehicle, L_v is the length of the vehicle.

The guideway is modeled as a simply-supported beam whose mode shape functions are

$$\psi_j(x_2) = \sin\left(\frac{j\pi x_2}{L_g}\right), \qquad j = 1, 2, ..., N \tag{4.6}$$

where L_g is the length of the guideway.

The motions of vehicle and guideway have to satisfy Lagrange's equations,

$$\frac{d}{dt}\left[\frac{\partial \mathcal{L}(\mathbf{q},\dot{\mathbf{q}},t)}{\partial \dot{q}_k}\right] - \frac{\partial \mathcal{L}(\mathbf{q},\dot{\mathbf{q}},t)}{\partial q_k} = 0, \qquad k = 1,2,...,N \tag{4.7}$$

where functional $\mathcal{L}$, which depends on the generalized coordinates q_k and velocities $\dot{q}_k$, represents the difference between the kinetic energy and the potential energy of a conservative dynamic system. To account for the displacement constraints equations in Eqs. (4.2) ($w(d_R,t) - w_g(\zeta,t) = 0$ and $w(d_F,t) - w_g(\zeta+d,t) = 0$), extra terms are added to functional $\mathcal{L}$ using the Lagrange multiplier method. Accordingly, the Lagrangian functional $\mathcal{L}$ with the Lagrange multipliers λ_1 and λ_2 is further expressed as,

$$\begin{aligned}
\mathcal{L} &= (K_v + K_g) - (V_v + V_g) + \lambda_1 \mathcal{G}_1 + \lambda_2 \mathcal{G}_2 \\
&= \frac{1}{2}\int_0^{L_v} \rho_v A_v \left[\sum_{j=1}^{N}\left(\phi_j \dot{Y}_j^v + \dot{\zeta}\phi_j' Y_j^v\right)\right]^2 dx_1 + \frac{1}{2} m_v \left(\dot{\bar{x}}_r^{\,2} + \dot{\bar{y}}_r^{\,2}\right) + \frac{1}{2} J \dot{\bar{\theta}}_r^{\,2} \\
&\quad + \frac{1}{2}\int_0^{L_g} \rho_g A_g \left(\sum_{j=1}^{N}\psi_j \dot{Y}_j^g\right)^2 dx_2 - \frac{1}{2}\int_0^{L_g} E_g I_g \left(\sum_{j=1}^{N}\psi_j'' Y_j^g\right)^2 dx_2 \\
&\quad - \frac{1}{2}\int_0^{L_v}\sum_{j=1}^{N}\left[E_v I_v\left(\phi_j'' Y_j^v\right)^2 - P\left(\phi_j' Y_j^v\right)^2\right] dx_1 \\
&\quad - \int_0^{L_v} \rho_v A_v g\cos\theta_E \sum_{j=1}^{N}\phi_j Y_j^v dx_1 - \left(m_v g \sin\theta_E\right)\bar{x}_r - \left(m_v g\cos\theta_E\right)\bar{y}_r \\
&\quad + \lambda_1\left[\sum_{j=1}^{N}\phi_j(d_R) Y_j^v + y(d_R,t) - \sum_{j=1}^{N}\psi_j(\zeta) Y_j^g\right] \\
&\quad + \lambda_2\left[\sum_{j=1}^{N}\phi_j(d_F) Y_j^v + y(d_F,t) - \sum_{j=1}^{N}\psi_j(\zeta+d) Y_j^g\right]
\end{aligned} \tag{4.8}$$

where

$$\bar{x}_r(t) = \zeta(t) + r_1 d\cos\bar{\theta}_r(t) \tag{4.9a}$$

$$y(d_R,t) = \bar{y}_r(t) - r_1 d\sin\bar{\theta}_r(t) \tag{4.9b}$$

$$y(d_F,t) = \bar{y}_r(t) + r_2 d\sin\bar{\theta}_r(t) \tag{4.9c}$$

$$\begin{aligned}\mathcal{G}_1 &= w(d_R,t) - w_g(\zeta,t)\\ &= \sum_{j=1}^{N}\phi_j(d_R)Y_j^v(t) - \sum_{j=1}^{N}\psi_j(\zeta)Y_j^g(t) + \bar{y}_r(t) - r_1 d\sin\bar{\theta}_r(t)\end{aligned} \tag{4.9d}$$

$$\begin{aligned}\mathcal{G}_2 &= w(d_F,t) - w_g(\zeta+d,t)\\ &= \sum_{j=1}^{N}\phi_j(d_F)Y_j^v(t) - \sum_{j=1}^{N}\psi_j(\zeta+d)Y_j^g(t) + \bar{y}_r(t) + r_2 d\sin\bar{\theta}_r(t)\end{aligned} \tag{4.9e}$$

$r_1 = (d_G - d_R)/d$; $r_2 = (d_F - d_G)/d$; $y(d_R,t)$ and $y(d_F,t)$ denote the transverse displacements of the vehicle's rigid body motion at the rear shoe and front shoe, respectively, and $\mathcal{G}_1$ and $\mathcal{G}_2$ are the displacement constraints. The two unknowns λ_1 and λ_2 can be obtained if Lagrange's equations are solved with the constrained equations. Notably, no damping is considered in the preceding formulations.

Substituting Eqs. (4.2), (4.3), (4.4) and (4.6) into Eq.(4.8), and substituting the resulting expression for $\mathcal{L}$ into Eq. (4.7) yield

$$m_v\ddot{\bar{x}}_r(t) + m_v g\sin\theta_E - P(t) = 0 \tag{4.10a}$$

$$m_v\ddot{\bar{y}}_r(t) + m_v g\cos\theta_E - \lambda_1 - \lambda_2 = 0 \tag{4.10b}$$

$$J\ddot{\bar{\theta}}_r(t) + (r_1\lambda_1 - r_2\lambda_2)\,d\cos\bar{\theta}_r(t) - m_v g r_1 d\sin\theta_E\sin\bar{\theta}_r(t) = 0 \tag{4.10c}$$

$$\begin{aligned}&\widetilde{H}_i^a\ddot{Y}_i^v(t) + 2\dot{\zeta}\widetilde{H}_i^b\dot{Y}_i^v(t) + \left(\omega_{vi}^2\widetilde{H}_i^a + L_v\ddot{\zeta}\widetilde{H}_i^c + \dot{\zeta}^2\widetilde{H}_i^c + \ddot{\zeta}\widetilde{H}_i^b\right)Y_i^v(t)\\ &- \frac{1}{\rho_v A_v}\left[\lambda_1\phi_i(d_R) + \lambda_2\phi_i(d_F)\right] + g\cos\theta_E\widetilde{H}_i^d = 0\end{aligned} \tag{4.10d}$$

$$\ddot{Y}_i^g(t) + \omega_{gi}^2 Y_i^g(t) + \frac{2}{m_g}\left[\lambda_1\psi_i(\zeta) + \lambda_2\psi_i(\zeta+d)\right] = 0 \tag{4.10e}$$

$$\sum_{j=1}^{N}\phi_j(d_R)Y_j^v(t) - \sum_{j=1}^{N}\psi_j(\zeta)Y_j^g(t) + \bar{y}_r(t) - r_1 d\sin\bar{\theta}_r(t) = 0 \tag{4.10f}$$

$$\sum_{j=1}^{N}\phi_j(d_F)Y_j^v(t) - \sum_{j=1}^{N}\psi_j(\zeta+d)Y_j^g(t) + \bar{y}_r(t) + r_2 d\sin\bar{\theta}_r(t) = 0 \tag{4.10g}$$

where, $i = 1, 2, ..., N$, $m_g = \rho_g A_g L_g$, ω_{gi} is the circular frequency of the ith mode of the guideway, $\beta_{gi}^4 = \omega_{gi}^2 \cdot \frac{\rho_g A_g}{E_g I_g}$, $\beta_{gi} L_g = i\pi$, and (see Appendix A.1)

$$\begin{aligned}
\widetilde{H}_i^a &= \int_0^{L_v} \phi_i(x_1)\phi_i(x_1)dx_1 \\
&= \frac{1}{2\beta_{vi}} \Big[\left(\Upsilon_i^2 + 1\right) \cosh\left(\beta_{vi}L_v\right) \sinh\left(\beta_{vi}L_v\right) - 2\Upsilon_i \cosh^2\left(\beta_{vi}L_v\right) \\
&\quad + 2\left(\Upsilon_i^2 + 1\right) \sin\left(\beta_{vi}L_v\right) \cosh\left(\beta_{vi}L_v\right) + 2\beta_{vi}L_v \\
&\quad -4\Upsilon_i \sin\left(\beta_{vi}L_v\right) \sinh\left(\beta_{vi}L_v\right) \Big] \qquad (4.11a) \\
\widetilde{H}_i^b &= \int_0^{L_v} \phi_i^{'}(x_1)\phi_i(x_1)dx_1 \\
&= \frac{1}{2}\left(\Upsilon_i^2 + 1\right) \cosh^2\left(\beta_{vi}L_v\right) - \Upsilon_i \cosh\left(\beta_{vi}L_v\right) \sin\left(\beta_{vi}L_v\right) - 2 \\
&\quad - \Upsilon_i \cosh\left(\beta_{vi}L_v\right) \sinh\left(\beta_{vi}L_v\right) + \Upsilon_i^2 \sin\left(\beta_{vi}L_v\right) \sinh\left(\beta_{vi}L_v\right) \qquad (4.11b) \\
\widetilde{H}_i^c &= \int_0^{L_v} \phi_i^{''}(x_1)\phi_i(x_1)dx_1 \\
&= \frac{1}{2}\beta_{vi} \Big[\left(\Upsilon_i^2 + 1\right) \cosh\left(\beta_{vi}L_v\right) \sinh\left(\beta_{vi}L_v\right) - 2\Upsilon_i \cosh^2\left(\beta_{vi}L_v\right) \\
&\quad +4\Upsilon_i - 2\beta_{vi}L_v\Upsilon_i^2 \Big] \qquad (4.11c) \\
\widetilde{H}_i^d &= \int_0^{L_v} \phi_i(x_1)dx_1 \\
&= \frac{1}{\beta_{vi}} \Big[\sin\left(\beta_{vi}L_v\right) + \sinh\left(\beta_{vi}L_v\right) - \Upsilon_i \cosh\left(\beta_{vi}L_v\right) \Big] \qquad (4.11d)
\end{aligned}$$

To include the effect of damping in the system of the vehicle and the guideway, an approach that is commonly used in structural dynamics (Clough and Penzien [39]) is adopted to add the distributed viscous damping term to Eqs. (4.10d) and (4.10e). These equations are thus modified as,

$$\begin{aligned}
&\widetilde{H}_i^a \ddot{Y}_i^v(t) + \left(2\dot{\zeta}\widetilde{H}_i^b + 2\xi_v\omega_{vi}\widetilde{H}_i^a\right) \dot{Y}_i^v(t) + \Big(\omega_{vi}^2\widetilde{H}_i^a + L_v\ddot{\zeta}\widetilde{H}_i^c \\
&+\dot{\zeta}^2\widetilde{H}_i^c + \ddot{\zeta}\widetilde{H}_i^b\Big) Y_i^v(t) - \frac{1}{\rho_v A_v}\Big[\lambda_1\phi_i(d_R) + \lambda_2\phi_i(d_F)\Big] + g\cos\theta_E\widetilde{H}_i^d = 0 \qquad (4.12a) \\
&\ddot{Y}_i^g(t) + 2\xi_g\omega_{gi}\dot{Y}_i^g(t) + \omega_{gi}^2 Y_i^g(t) + \frac{2}{m_g}\Big[\lambda_1\psi_i(\zeta) + \lambda_2\psi_i(\zeta + d)\Big] = 0 \qquad (4.12b)
\end{aligned}$$

where $2\xi_v\omega_{vi}$ and $2\xi_g\omega_{gi}$ are the added damping terms, and ξ_v and ξ_g are the damping ratios corresponding to the mode shapes $\phi_i(x_1)$ and $\psi_i(x_2)$, respectively.

Equations (4.10a-4.10c, 4.10f, 4.10g) and (4.12) form a set of nonlinear ordinary differential equations for describing the rigid body motions of the vehicle and elastic deformations of the vehicle and the guideway. Equation (4.10a) describes the rigid body motion of the vehicle in the x_1 direction (see Fig. 4.2). This equation can be easily derived from Newton's second law and the free body diagram of the vehicle in Fig. 4.2. This equation was utilized to find the solution for $\zeta(t)$ given in Eqs. (2.6) and (2.13) where $\zeta(t) = \bar{x}_r(t) - r_1 d$. Consequently, Eqs. (4.10b, 4.10c, 4.10f, 4.10g) and (4.12) can be employed to find the transverse displacements of the vehicle and the guideway. A total of $2N+4$ equations with $2N+4$ to-be-determined functions, $Y_i^v(t)$, $Y_i^g(t)$, $\bar{y}_r(t)$, $\bar{\theta}_r(t)$, $\lambda_1(t)$ and $\lambda_2(t)$, are thus obtained. To solve these equations efficiently, Eqs. (4.10f) and (4.10g) are differentiated twice with respect to time, and using Eqs. (4.12) yield

$$\begin{aligned}
&\lambda_1 \left\{ \sum_{j=1}^{N} \left[d_{2j}\psi_j(\zeta) - d_{1j}\phi_j(d_R) \right] + \frac{1}{m_v} + \frac{r_1^2 d^2 \cos^2\bar{\theta}_r}{J} \right\} \\
&+ \lambda_2 \left\{ \sum_{j=1}^{N} \left[e_{2j}\psi_j(\zeta) - e_{1j}\phi_j(d_R) \right] + \frac{1}{m_v} - \frac{r_1 r_2 d^2 \cos^2\bar{\theta}_r}{J} \right\} \\
&- \sum_{j=1}^{N} \left\{ \phi_j(d_R) \left(b_{1j}\dot{Y}_j^v + c_{1j}Y_j^v + f_{1j} \right) - \psi_j(\zeta) \left(b_{2j}\dot{Y}_j^g + c_{2j}Y_j^g \right) \right. \\
&\left. + 2\dot{\zeta}\psi_j'(\zeta)\dot{Y}_j^g + \left[\ddot{\zeta}\psi_j'(\zeta) + \dot{\zeta}^2\psi_j''(\zeta) \right] Y_j^g \right\} - \frac{m_v g r_1^2 d^2 \sin\theta_E \sin\bar{\theta}_r \cos\bar{\theta}_r}{J} \\
&+ r_1 d\ddot{\bar{\theta}}_r^2 \sin\bar{\theta}_r - g\cos\theta_E = 0
\end{aligned} \tag{4.13a}$$

$$\begin{aligned}
&\lambda_1 \left\{ \sum_{j=1}^{N} \left[d_{2j}\psi_j(\zeta+d) - d_{1j}\phi_j(d_F) \right] + \frac{1}{m_v} - \frac{r_1 r_2 d^2 \cos^2\bar{\theta}_r}{J} \right\} \\
&+ \lambda_2 \left\{ \sum_{j=1}^{N} \left[e_{2j}\psi_j(\zeta+d) - e_{1j}\phi_j(d_F) \right] + \frac{1}{m_v} + \frac{r_2^2 d^2 \cos^2\bar{\theta}_r}{J} \right\} \\
&- \sum_{j=1}^{N} \left\{ \phi_j(d_F) \left(b_{1j}\dot{Y}_j^v + c_{1j}Y_j^v + f_{1j} \right) - \psi_j(\zeta+d) \left(b_{2j}\dot{Y}_j^g + c_{2j}Y_j^g \right) \right. \\
&\left. + 2\dot{\zeta}\psi_j'(\zeta+d)\dot{Y}_j^g + \left[\ddot{\zeta}\psi_j'(\zeta+d) + \dot{\zeta}^2\psi_j''(\zeta+d) \right] Y_j^g \right\} \\
&+ \frac{m_v g r_1 r_2 d^2 \sin\theta_E \sin\bar{\theta}_r \cos\bar{\theta}_r}{J} - r_2 d\ddot{\bar{\theta}}_r^2 \sin\bar{\theta}_r - g\cos\theta_E = 0
\end{aligned} \tag{4.13b}$$

where,

$$b_{1j} = 2\xi_v\omega_{vj} + \frac{2\dot{\zeta}\widetilde{H}_j^b}{\widetilde{H}_j^a}, \quad c_{1j} = \omega_{vj}^2 + \frac{L_v\ddot{\zeta}\widetilde{H}_j^c + \dot{\zeta}^2\widetilde{H}_j^c + \ddot{\zeta}\widetilde{H}_j^b}{\widetilde{H}_j^a},$$
$$d_{1j} = -\frac{\phi_j(d_R)}{\rho_v A_v \widetilde{H}_j^a}, \quad e_{1j} = -\frac{\phi_j(d_F)}{\rho_v A_v \widetilde{H}_j^a}, \quad f_{1j} = \frac{g\cos\theta_E \widetilde{H}_j^d}{\widetilde{H}_j^a},$$
$$b_{2j} = 2\xi_g\omega_{gj}, \quad c_{2j} = \omega_{gj}^2 \quad , \quad d_{2j} = \frac{2\psi_j(\zeta)}{m_g}, \quad e_{2j} = \frac{2\psi_j(\zeta + d)}{m_g} \tag{4.14}$$

Consequently, Eqs. (4.10b, 4.10c), (4.12) and (4.13) are used to determine the transverse motions of the vehicle and the guideway when $0 < t \leq t_{_F}$, as discussed below.

To solve the above governing equations, the initial conditions are required. The system (vehicle and guideway) is initially at rest, and the initial velocity and acceleration of the vehicle and the guideway are zero. However, the vehicle and guideway are both deformed under the weight of the vehicle. The initial displacement of the system can be determined from Eqs. (4.10b, 4.10c, 4.10f, 4.10g) and (4.12) by setting $\ddot{Y}_i^g(0) = 0$, $\dot{Y}_i^g(0) = 0$, $\ddot{Y}_i^v(0) = 0$, $\dot{Y}_i^v(0) = 0$, $\ddot{\zeta}(0) = 0$ and $\dot{\zeta}(0) = 0$. The equations which contain $2N + 4$ unknowns are expressed as a system of nonlinear algebraic equations having a real general coefficient shown as,

$$m_v g\cos\theta_E - \lambda_1(0) - \lambda_2(0) = 0 \tag{4.15a}$$
$$\left[r_1\lambda_1(0) - r_2\lambda_2(0)\right] d\cos\bar{\theta}_r(0) - m_v g r_1 d\sin\theta_E \sin\bar{\theta}_r(0) = 0 \tag{4.15b}$$
$$\omega_{vi}^2\widetilde{H}_i^a Y_i^v(0) - \frac{1}{\rho_v A_v}\left[\lambda_1(0)\phi_i(d_R) + \lambda_2(0)\phi_i(d_F)\right] + g\cos\theta_E\widetilde{H}_i^d = 0 \tag{4.15c}$$
$$\omega_{gi}^2 Y_i^g(0) + \frac{2}{m_g}\left[\lambda_1(0)\psi_i(\zeta_{_R}) + \lambda_2(0)\psi_i(\zeta_{_R} + d)\right] = 0 \tag{4.15d}$$
$$\sum_{j=1}^{N}\phi_j(d_R)Y_j^v(0) - \sum_{j=1}^{N}\psi_j(\zeta_{_R})Y_j^g(0) + \bar{y}_r(0) - r_1 d\sin\bar{\theta}_r(0) = 0 \tag{4.15e}$$
$$\sum_{j=1}^{N}\phi_j(d_F)Y_j^v(0) - \sum_{j=1}^{N}\psi_j(\zeta_{_R} + d)Y_j^g(0) + \bar{y}_r(0) + r_2 d\sin\bar{\theta}_r(0) = 0 \tag{4.15f}$$

where $_{i\,=\,1,\,2,\,...,\,N}$

Then, the initial values of $Y_i^g(0)$, $Y_i^v(0)$, $\bar{y}_r(0)$, $\bar{\theta}_r(0)$, $\lambda_1(0)$ and $\lambda_2(0)$ can be easily determined.

4.1.3 Tip-off phase

Figure 4.3 presents the free body diagram of the vehicle and the guideway for $t_F < t \leqslant t_R$, when the front shoe of the vehicle has lost contact with the guideway while the rear shoe remains in contact with the guideway. Similar to that in the two-shoe contact phase, the Lagrangian functional $\mathcal{L}$ in the tip-off phase is,

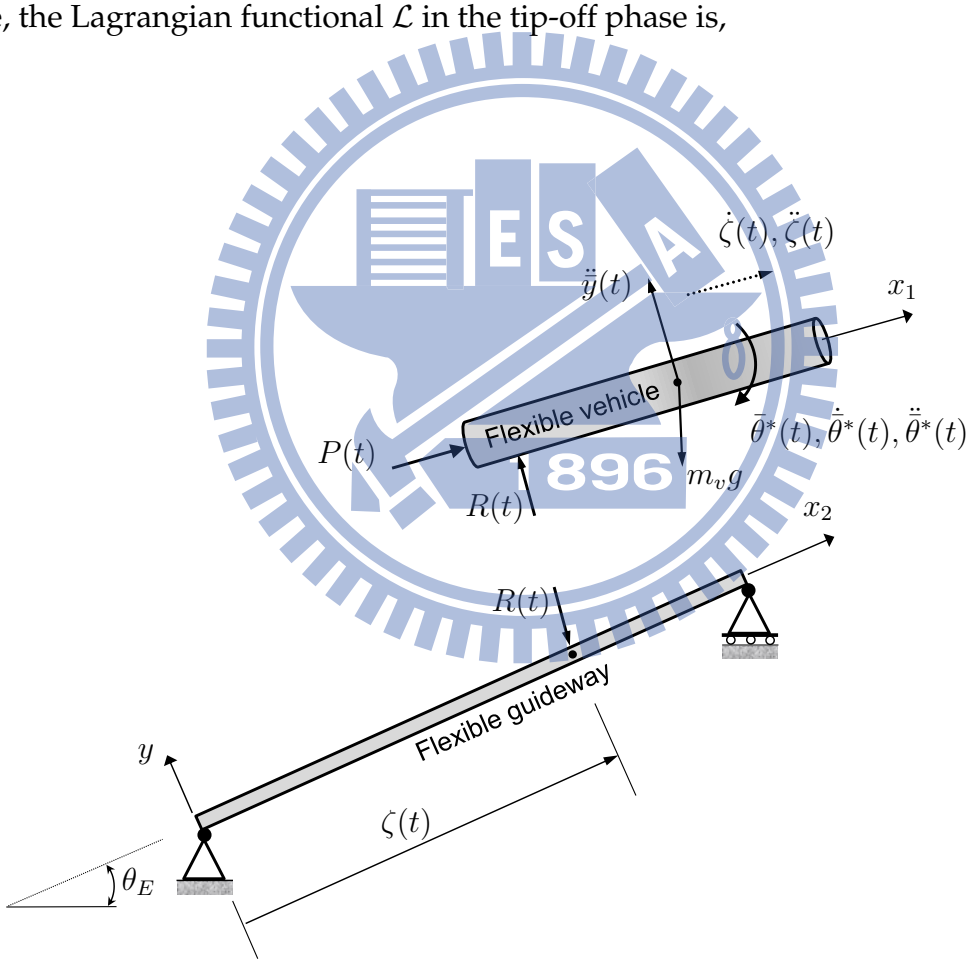

Figure 4.3: Free body diagrams of vehicle in tip-off phase.

$$
\begin{aligned}
\mathcal{L} &= \left(K_v^* + K_g^*\right) - \left(V_v^* + V_g^*\right) + \lambda_1^* \mathcal{G}_1^* \\
&= \frac{1}{2}\int_0^{L_v} \rho_v A_v \left[\sum_{j=1}^{N}\left(\phi_j \dot{Y}_j^{v*} + \dot{\zeta}\phi_j^{'} Y_j^{v*}\right)\right]^2 dx_1 + \frac{1}{2} m_v \left(\dot{\bar{x}}_r^{*2} + \dot{\bar{y}}_r^{*2}\right) + \frac{1}{2} J \dot{\bar{\theta}}_r^{*2} \\
&\quad + \frac{1}{2}\int_0^{L_g} \rho_g A_g \left(\sum_{j=1}^{N} \psi_j \dot{Y}_j^{g*}\right)^2 dx_2 - \frac{1}{2}\int_0^{L_g} E_g I_g \left(\sum_{j=1}^{N} \psi_j^{''} Y_j^{g*}\right)^2 dx_2 \\
&\quad - \frac{1}{2}\int_0^{L_v} \sum_{j=1}^{N}\left[E_v I_v \left(\phi_j^{''} Y_j^{v*}\right)^2 - P\left(\phi_j^{'} Y_j^{v*}\right)^2\right] dx_1 \\
&\quad - \int_0^{L_v} \rho_v A_v g \cos\theta_E \sum_{j=1}^{N} \phi_j Y_j^{v*} dx_1 - \left(m_v g \sin\theta_E\right) \bar{x}_r^* - \left(m_v g \cos\theta_E\right) \bar{y}_r^* \\
&\quad + \lambda_1^* \left[\sum_{j=1}^{N} \phi_j(d_R) Y_j^{v*} - \sum_{j=1}^{N} \psi_j(\zeta) Y_j^{g*} + \bar{y}_r^* - r_1 d \sin\bar{\theta}_r^*\right]
\end{aligned} \tag{4.16}
$$

where the superscript $(*)$ indicates that the physical quantities are in the tip-off phase. Since the front shoe of the vehicle has lost contact with the guideway, the constraint on displacement, given in Eq. (4.2b), vanishes. Following the procedure described in the preceding section, the following governing equations are obtained.

$$m_v \ddot{\bar{x}}_r^*(t) + m_v g \sin\theta_E - P(t) = 0 \tag{4.17a}$$

$$m_v \ddot{\bar{y}}_r^*(t) + m_v g \cos\theta_E - \lambda_1^* = 0 \tag{4.17b}$$

$$J\ddot{\bar{\theta}}_r^*(t) + \lambda_1^* r_1 d \cos\bar{\theta}_r^*(t) - m_v g r_1 d \sin\theta_E \sin\bar{\theta}_r^*(t) = 0 \tag{4.17c}$$

$$
\begin{aligned}
&\widetilde{H}_i^a \ddot{Y}_i^{v*}(t) + \left(2\xi_v \omega_{vi} \widetilde{H}_i^a + 2\dot{\zeta}\widetilde{H}_i^b\right)\dot{Y}_i^{v*}(t) + \left(\omega_{vi}^2 \widetilde{H}_i^a + L_v \ddot{\zeta}\widetilde{H}_i^c + \dot{\zeta}^2 \widetilde{H}_i^c\right. \\
&\quad \left. + \ddot{\zeta}\widetilde{H}_i^b\right) Y_i^{v*}(t) - \frac{\lambda_1^* \phi_i(d_R)}{\rho_v A_v} + g\cos\theta_E \widetilde{H}_i^d = 0
\end{aligned} \tag{4.17d}
$$

$$\ddot{Y}_i^{g*}(t) + 2\xi_g \omega_{gi} \dot{Y}_i^{g*}(t) + \omega_{gi}^2 Y_i^{g*}(t) + \frac{2\lambda_1^* \psi_i(\zeta)}{m_g} = 0 \tag{4.17e}$$

$$\sum_{j=1}^{N} \phi_j(d_R) Y_j^{v*}(t) - \sum_{j=1}^{N} \psi_j(\zeta) Y_j^{g*}(t) + \bar{y}_r^*(t) - r_1 d \sin\bar{\theta}_r^*(t) = 0 \tag{4.17f}$$

Again, Eq. (4.17a) is not needed for determining the transverse displacements of the vehicle and the guideway. Differentiating Eq. (4.17f) twice with respect to time

and applying Eqs. (4.17d) and (4.17e) yield

$$\lambda_1^*\left\{\sum_{j=1}^{N}\left[d_{2j}^*\psi_j(\zeta)-d_{1j}^*\phi_j(d_R)\right]+\frac{1}{m_v}+\frac{r_1^2d^2\cos^2\bar{\theta}_r^*}{J}\right\}$$
$$-\sum_{j=1}^{N}\left\{\phi_j(d_R)\left(b_{1j}^*\dot{Y}_j^{v*}+c_{1j}^*Y_j^{v*}+f_{1j}^*\right)-\psi_j(\zeta)\left(b_{2j}^*\dot{Y}_j^{g*}+c_{2j}^*Y_j^{g*}\right)\right.$$
$$\left.+2\dot{\zeta}\psi_j'(\zeta)\dot{Y}_j^{g*}+\left[\ddot{\zeta}\psi_j'(\zeta)+\dot{\zeta}^2\psi_j''(\zeta)\right]Y_j^{g*}\right\}-\frac{m_vgr_1^2d^2\sin\theta_E\sin\bar{\theta}_r^*\cos\bar{\theta}_r^*}{J}$$
$$+r_1d\dot{\bar{\theta}}_r^{*2}\sin\bar{\theta}_r^*-g\cos\theta_E=0 \tag{4.18}$$

where $d_{1j}^*=d_{1j}$, $e_{1j}^*=e_{1j}$, $f_{1j}^*=f_{1j}$, $b_{2j}^*=b_{2j}$, $c_{2j}^*=c_{2j}$, and

$$b_{1j}^*=2\xi_v\omega_{vj}+\frac{2\dot{\zeta}\widetilde{H}_j^b}{\widetilde{H}_j^a},\qquad c_{1j}^*=\omega_{vj}^2+\frac{L_v\ddot{\zeta}\widetilde{H}_j^c+\dot{\zeta}^2\widetilde{H}_j^c+\ddot{\zeta}\widetilde{H}_j^b}{\widetilde{H}_j^a},$$
$$d_{2j}^*=\frac{2\psi_j(\zeta)}{m_g},\qquad e_{2j}^*=\frac{2\psi_j(\zeta+d)}{m_g} \tag{4.19}$$

Equations (4.17b) to (4.17e) and Eq.(4.18) describe the transverse motions of the vehicle and the guideway in the tip-off phase; they form a set of $2N+3$ nonlinear equations. The initial conditions for solving these equations are obtained from the continuity conditions between the motions in the two phases: $Y_j^{v*}(0)=Y_j^v(t_F^+)$, $Y_j^{g*}(0)=Y_j^g(t_F^+)$, $\bar{y}_r^*(0)=\bar{y}_r(t_F^+)$, $\bar{\theta}_r^*(0)=\bar{\theta}_r(t_F^+)$, $\dot{Y}_j^{v*}(0)=\dot{Y}_j^v(t_F^+)$, $\dot{Y}_j^{g*}(0)=\dot{Y}_j^g(t_F^+)$, $\dot{\bar{y}}_r^*(0)=\dot{\bar{y}}_r(t_F^+)$, $\dot{\bar{\theta}}_r^*(0)=\dot{\bar{\theta}}_r(t_F^+)$, and $\lambda_1^*(0)=\lambda_1(t_F^+)$.

4.1.4 Dynamic responses of vehicle and guideway

The governing equations given in sections 4.1.2 and 4.1.3 are a set of coupled second order differential nonlinear equations. They can be expressed in the following vector form

$$\boldsymbol{G}_d\left(t, \mathbf{Y}, \dot{\mathbf{Y}}, \ddot{\mathbf{Y}}, \boldsymbol{\lambda}\right) = \mathbf{0} \tag{4.20}$$

where $\mathbf{Y}$, $\dot{\mathbf{Y}}$, $\ddot{\mathbf{Y}}$ and $\boldsymbol{\lambda}$ are generalized coordinate, velocity, acceleration vectors and Lagrange multiplier vector, respectively.

$$\mathbf{Y} = [\mathbf{Y}^v, \mathbf{Y}^g, \bar{y}_r, \bar{\theta}_r]^T \tag{4.21}$$

$$\mathbf{Y}^v = \left[Y_1^v, Y_2^v, ..., Y_i^v, ..., Y_N^v\right]$$
$$\mathbf{Y}^g = \left[Y_1^g, Y_2^g, ..., Y_i^g, ..., Y_N^g\right]$$

To solve for Eq. (4.20) by the Petzold-Gear BDF method [37], one has to reduce the set of the second order differential equations to a set of the first ordinary differential equations. Hence, we define

$$\mathbf{Z} = [\mathbf{Z}_u \mid \mathbf{Z}_m \mid \mathbf{Z}_d]^T = \left[\mathbf{Y}^v, \mathbf{Y}^g, \bar{y}_r, \bar{\theta}_r \mid \dot{\mathbf{Y}}^v, \dot{\mathbf{Y}}^g, \dot{\bar{y}}_r, \dot{\bar{\theta}}_r \mid \boldsymbol{\lambda}\right]^T \tag{4.22}$$

where

$$\mathbf{Z}_u = \mathbf{Y} \tag{4.23a}$$
$$\mathbf{Z}_m = \dot{\mathbf{Y}} \tag{4.23b}$$
$$\mathbf{Z}_d = \boldsymbol{\lambda} \tag{4.23c}$$

$$\dot{\mathbf{Z}}_u = \mathbf{Z}_m \tag{4.24}$$

Then, Eqs. (4.20) and (4.24) can be rewritten as

$$\mathbf{G} = [\mathbf{G}_u \mid \mathbf{G}_d]^T = \mathbf{0} \tag{4.25}$$

where,

$$\mathbf{G}_u = \dot{\mathbf{Z}}_u - \mathbf{Z}_m \tag{4.26}$$

Equation (4.26) contains $2N + 2$ independent equations. In the two-shoe contact phase and the tip-off phase, $\boldsymbol{\lambda} = [\lambda_1, \lambda_2]$ and $\boldsymbol{\lambda} = [\lambda_1]$, respectively. Equation (4.20) consists of $2N + 4$ and $2N + 3$ independent equations in the two phases, respectively. Consequently, Eq. (4.25) consists of $4N + 6$ and $4N + 5$ equations in the two phases, respectively. Then, solves a first order differential-algebraic system of equations, $\mathbf{G}(t, \mathbf{Z}, \dot{\mathbf{Z}}, \boldsymbol{\lambda}) = \mathbf{0}$, using the Petzold-Gear BDF method.

After $\mathbf{Y}$ and $\dot{\mathbf{Y}}$ have been determined, the transverse displacement and velocity of the center of gravity of the vehicle can be determined by applying the following equations, respectively;

$$w\left(d_G, t\right) = \bar{y}_r(t) + w_v\left(d_G, t\right) = \bar{y}_r(t) + \sum_{j=1}^{N} \phi_j(d_G) Y_j^v(t) \tag{4.27}$$

$$\dot{w}\left(d_G, t\right) = \dot{\bar{y}}_r(t) + \dot{w}_v\left(d_G, t\right) = \dot{\bar{y}}_r(t) + \sum_{j=1}^{N} \left[\phi_j(d_G) \dot{Y}_j^v(t) + \dot{\zeta} \phi_j^{'}(d_G) Y_j^v(t)\right] \tag{4.28}$$

The pitch angle and pitch rate of the vehicle are found, respectively, by applying

$$\theta\left(t\right) = \bar{\theta}_r\left(t\right) + \sin^{-1}\left\{\frac{1}{d} \sum_{j=1}^{N} \left[\phi_j(d_F) - \phi_j(d_R)\right] Y_j^v(t)\right\} \tag{4.29}$$

$$\begin{aligned}\dot{\theta}\left(t\right) = \dot{\bar{\theta}}_r\left(t\right) + \frac{1}{d\cos\left[\theta\left(t\right) - \bar{\theta}_r\left(t\right)\right]} \sum_{j=1}^{N} \Bigg\{ &\left[\phi_j(d_F) - \phi_j(d_R)\right] \dot{Y}_j^v(t) \\ &+ \dot{\zeta}\left[\phi_j^{'}(d_F) - \phi_j^{'}(d_R)\right] Y_j^v(t)\Bigg\}\end{aligned} \tag{4.30}$$

4.2 Numerical validation and examples

This section considers three case studies to validate the proposed solutions, and the results herein are compared with the results published by Yao and Zhang [34] and the results shown in Chapter three. As shown in Chapters two and three, two typical models were applied to study the tip-off phenomenon of a vehicle when it moved along its guideway. Yao and Zhang [34] utilized the model of a rigid vehicle's moving along a rigid guideway (R.R. model), while Chou *et al.* [35] adopted the model of a rigid vehicle's moving on an elastic guideway (R.E. model). In this chapter, the vehicle and guideway are assumed to be elastic, and the model is denoted by E.E. model. Without special mention, the material properties and geometric parameters of the vehicle and guideway and the parameters defining a typical thrust-time diagram (Fig. 2.3) given in Table 4.1 were used in the following. Ten modes ($N = 10$ in Eq. (4.3)) and a time increment of 0.0001s were used to obtain the present results.

Table 4.1: Parameters of the vehicle launch system.

	Design value of launch system	
Parameters	Vehicle	Guideway
E_*I_*	1.2×10^7 N $\cdot$ m^2	1.2×10^7 N $\cdot$ m^2
$\rho_* A_*$	4.0×10^2 kg/m	1.5×10^2 kg/m
ξ_*	0.03	0.03
L_*	4.0 m	8.0 m
$\theta_{_E}$	-	0.5 rad
d	3.7 m	-
$r_1 d$	2.5 m	-
$\zeta_{_R}$	-	0.1 m
$\zeta_{_F}$	-	4.2 m
$t_{_b}$	0.1 s	-
$P_{\max}$	7.0×10^4 N	-
Δt	0.0001 s	-

$_*$ denote the subscript of vehicle (v) and guideway (g).

4.2.1 Case 1: displacement of contact points between vehicle and guideway

Figure 4.4 shows a comparison of the time histories of the transverse displacement of the contact point of the moving mass obtained by Wu [11] and those obtained from the E.E. model. The result shows the time histories of displacement of R.E. model without considering Coriolis and centrifugal force is near to the result presented in Wu's [11] study. In E.E. model analysis, the formulations are derived including the Coriolis and centrifugal force. The results show the time histories of displacement of R.E. model with considering Coriolis and centrifugal force is near to the E.E. model analysis. The figure shows that the difference between the results is negligible.

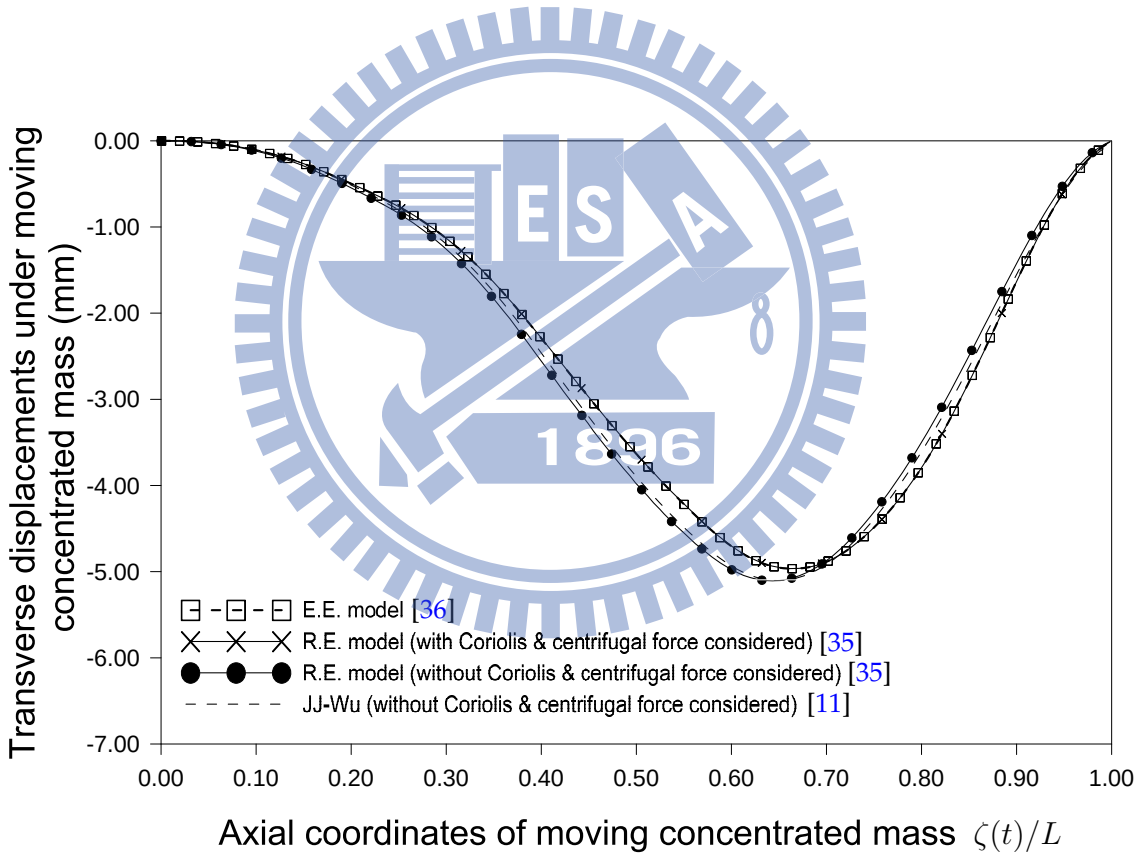

Figure 4.4: Time histories of transverse displacements under simulated moving concentrated mass.

Although the technique proposed in this chapter is meant for the dynamic analysis of an inclined guideway with contact points with a moving vehicle, it can be

used for a horizontal beam if the angle of inclination of the guideway is considered to be close to zero. At the same time, the distance between two contact points is considered to be close to zero $(1 \times 10^{-15}\ \mathrm{m})$ to simulate the single moving mass problem. Wu [11] studied the influence of the effects of the inertial force, Coriolis force, and centrifugal force induced by the moving mass on the dynamic response of a simply supported inclined beam. Wu also validated an example of a horizontal undamped pinned-pinned beam under a moving concentrated mass. The concentrated mass $m = 21.8\ kg$ is assumed to move from the left end to the right end of the beam with a constant speed $V = 27.49\ m/s$. The size and physical constants of the uniform undamped beam studied by Wu [11] are as follows: a rectangular cross-section with width $b = 0.018113\ \mathrm{m}$ and thickness $h = 0.072322\ \mathrm{m}$; moment of inertia, $I = 5.71 \times 10^{-7}\ \mathrm{m}^4$; total length, $L = 4.352\ \mathrm{m}$; mass density, $\rho = 15267.1756\ \mathrm{kg/m}^3$; Young's modulus, $E = 2020.797216 \times 10^8\ \mathrm{N/m}^2$; $\Delta t = 0.001\ \mathrm{s}$; and $\xi = 0.005$.

4.2.2 Case 2: Two shoes constraint condition verification

If the proposed solutions are correct, the computed displacement and velocity of two shoes of the vehicle must also satisfy the constraints condition. Figure 4.5 shows the time histories of the transverse displacement, velocity and acceleration of the two shoes of vehicle relative to the guideway. The results were obtained by using 10 modes. These relative displacement, velocity and acceleration are theoretically zero in the two-shoe contact phase according to the constraint conditions from G_1 to G_6, respectively. To check the velocity constraints G_3 and G_4 and acceleration constrains G_5 and G_6 at the rear shoe and front shoe, Eqs. (4.9d) and (4.9e) are differentiated once and twice with respect to time to obtain these constraints. Figure 4.5 demonstrates the present solutions satisfy the constraint conditions from G_1 to G_6, respectively. Notably, the transverse displacement and velocity are still near to zero in tip-off phase, whereas small values of the relative accelerations are observed at this phase. The relative accelerations in the tip-off phase mote closely satisfy the constraint when more modes are

used to determine the relative accelerations (see Fig. 4.6).

Table 4.2: Comparison of pitch angles of vehicle obtained using different models.

	Pitch angles of vehicle (°)		
Time (s)	E.E.	R.E.	R.R.
0.5000	$2.9900E-09$	$-8.0295E-10$	$0.0000E+00$
0.5100	$2.6181E-09$	$-7.5991E-10$	$0.0000E+00$
0.5136	$-8.1001E-07$	$-9.2237E-08$	$-9.1492E-08$
0.5250	$-1.0819E-02$	$-1.0505E-02$	$-1.0506E-02$
0.5500	$-1.0856E-01$	$-1.0753E-01$	$-1.0770E-01$
0.5750	$-3.0806E-01$	$-3.0619E-01$	$-3.0758E-01$
0.6000	$-6.0949E-01$	$-6.0648E-01$	$-6.1194E-01$
0.6250	$-1.0112E+00$	$-1.0084E+00$	$-1.0235E+00$
0.6500	$-1.5193E+00$	$-1.5120E+00$	$-1.5461E+00$
0.6750	$-2.1288E+00$	$-2.1172E+00$	$-2.1843E+00$
0.6876	$-2.4725E+00$	$-2.4607E+00$	$-2.5546E+00$

Table 4.3: Comparison of pitch rates of vehicle obtained using different models.

	Pitch rates of vehicle ($°/s$)		
Time (s)	E.E.	R.E.	R.R.
0.5000	$2.0902E-08$	$1.3295E-09$	$0.0000E+00$
0.5100	$2.2225E-08$	$1.4172E-09$	$0.0000E+00$
0.5136	$-1.6232E-02$	$5.4549E-03$	$5.4549E-03$
0.5250	$-1.8539E+00$	$-1.8321E+00$	$-1.8489E+00$
0.5500	$-5.9375E+00$	$-5.9137E+00$	$-5.9325E+00$
0.5750	$-1.0011E+01$	$-9.9791E+00$	$-1.0070E+01$
0.6000	$-1.4094E+01$	$-1.4044E+01$	$-1.4298E+01$
0.6250	$-1.8192E+01$	$-1.8110E+01$	$-1.8655E+01$
0.6500	$-2.2310E+01$	$-2.2175E+01$	$-2.3180E+01$
0.6750	$-2.6454E+01$	$-2.6241E+01$	$-2.7914E+01$
0.6876	$-2.8538E+01$	$-2.8289E+01$	$-3.0413E+01$

4.2.3 Case 3: A rigid vehicle moves along a rigid guideway

In this case, the flexural rigidities of the vehicle and guideway were again assumed to be $1.2 \times 10^{15}\ \mathrm{N \cdot m^2}$ to simulate the behavior of a pseudo-rigid body. Figures 4.7

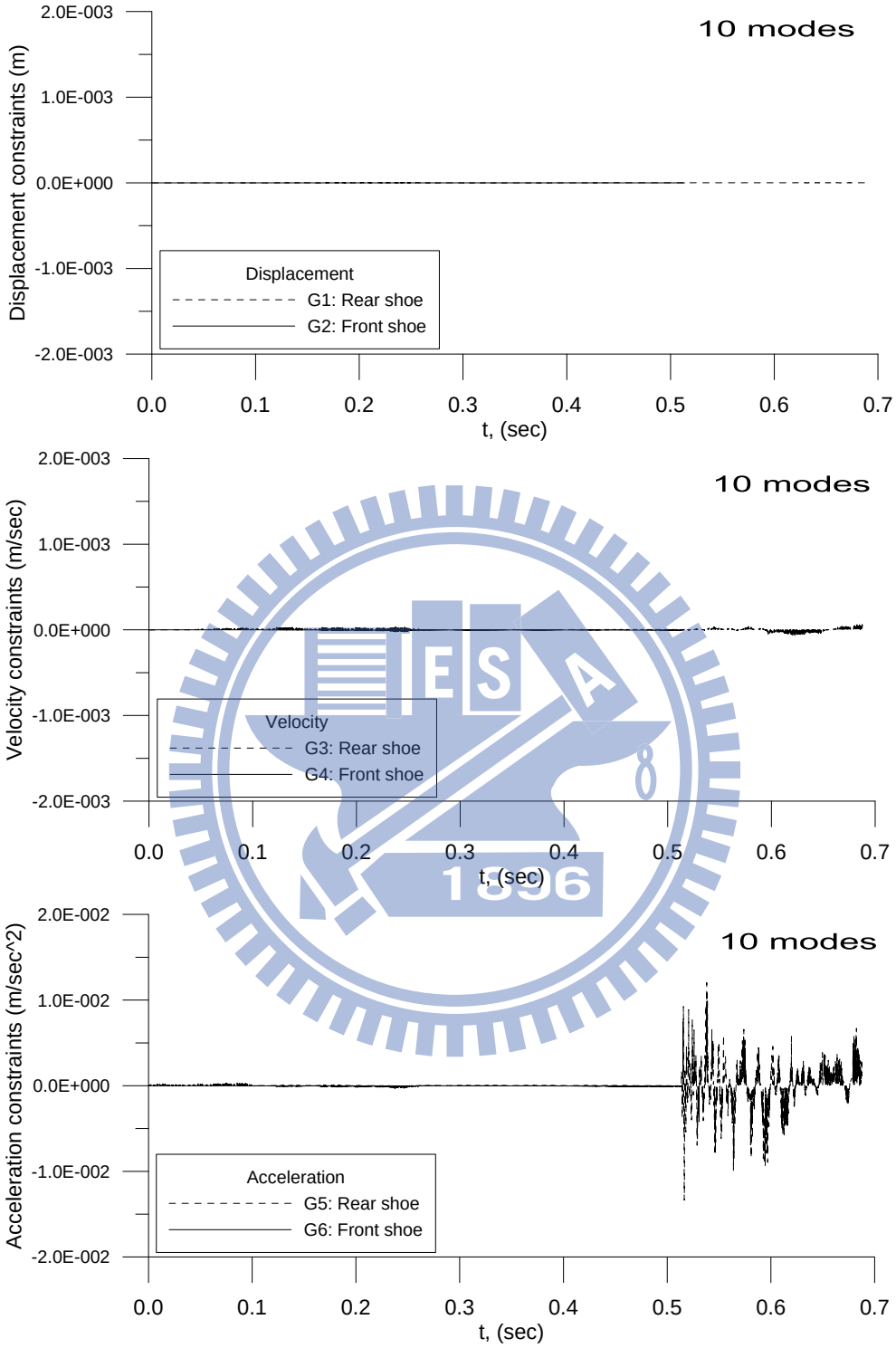

Figure 4.5: Verification of constraint conditions of the two shoes of the vehicle relative to the guideway.

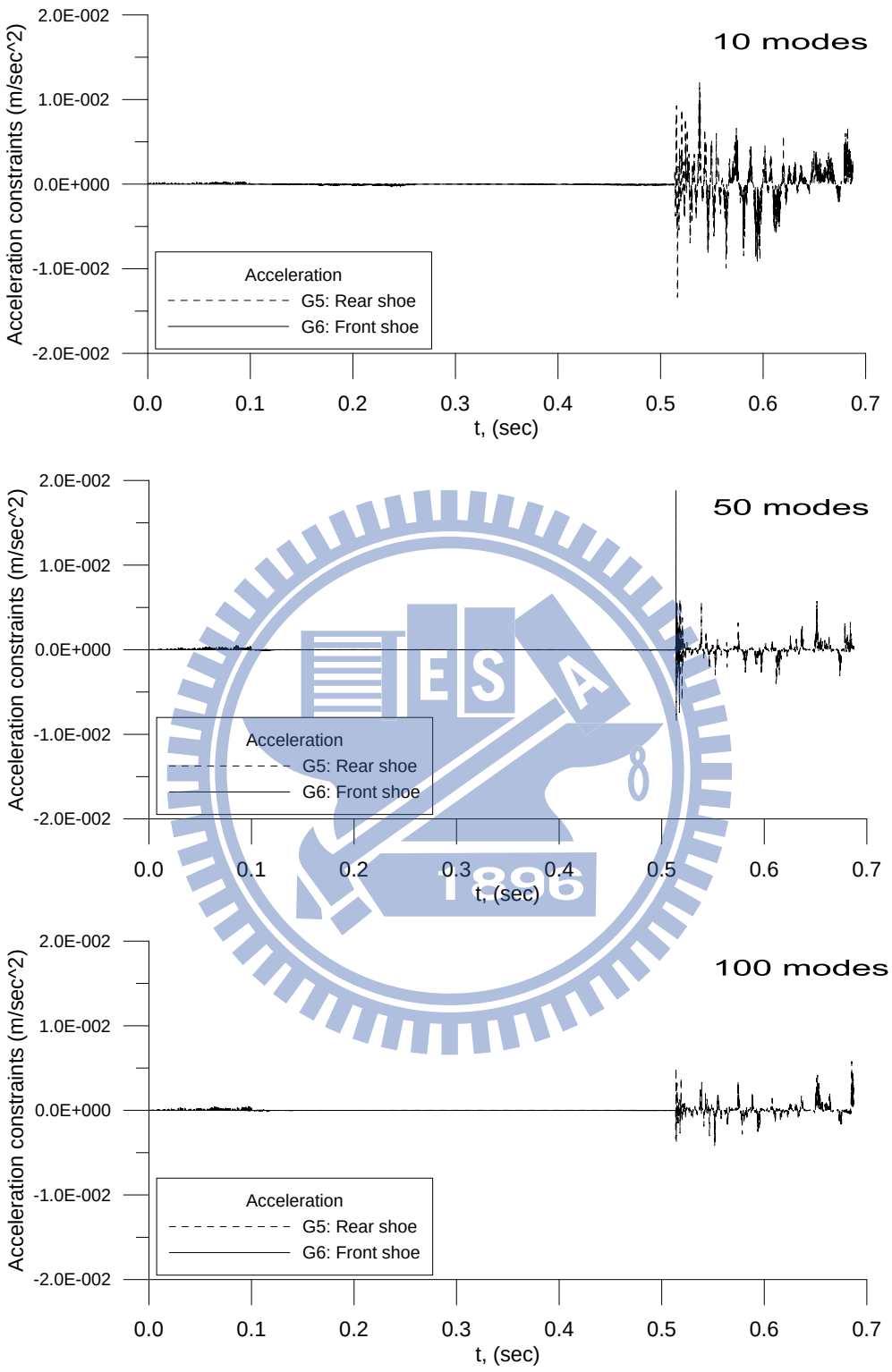

Figure 4.6: Verification of acceleration constraint using different numbers of modes.

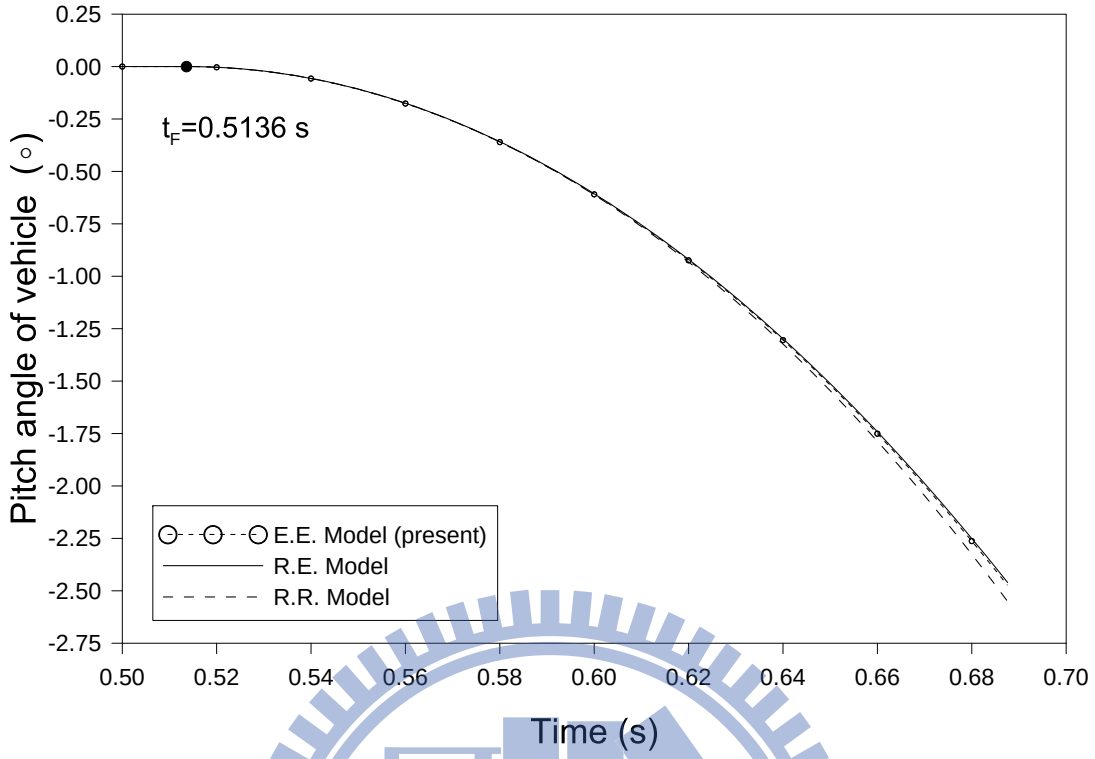

Figure 4.7: Comparisons of pitch angles $\theta - t$ of vehicle obtained using different models.

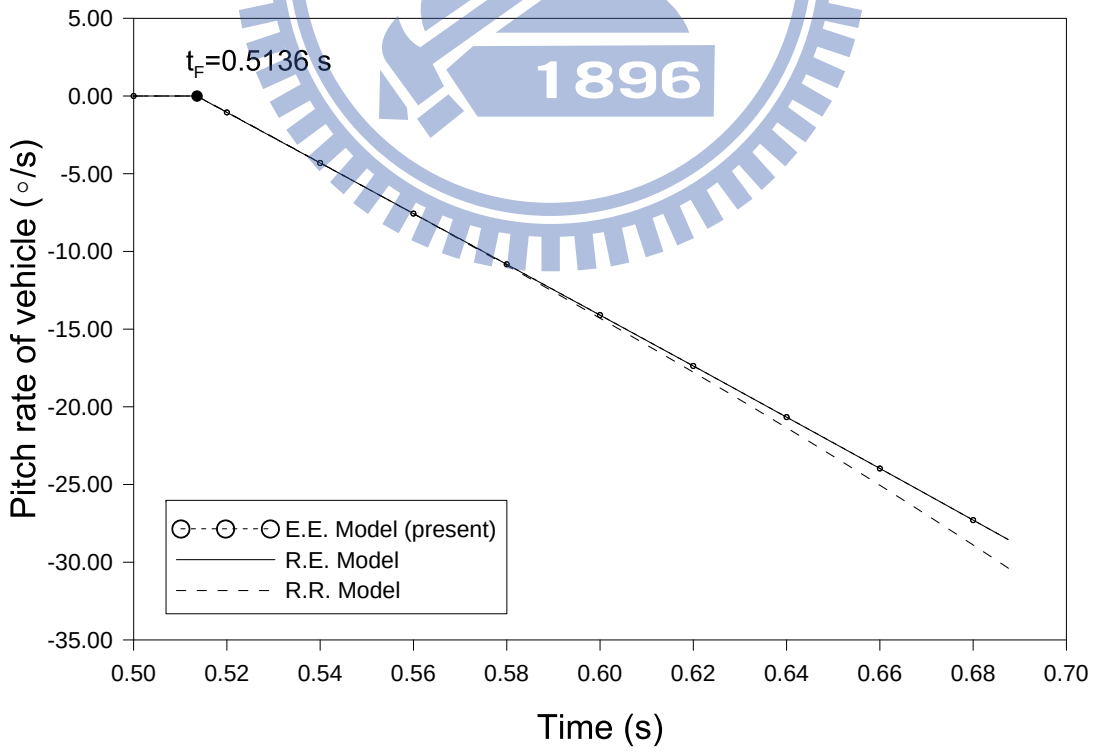

Figure 4.8: Comparisons of pitch rates $\dot{\theta} - t$ of vehicle obtained using different models.

and 4.8 display the numerical results concerning the pitch angle and the pitch rate of the vehicle obtained using three models, respectively. Tables 4.2 and 4.3 present detailed comparative results. In the two-shoe contact phase, the pitch angle and the pitch rate of the vehicle in the R.R. model are theoretically zero, while in the R.E. and E.E. models, they have very small values, because the vehicle and guideway had very large flexural rigidities. The results in Tables 4.2 and 4.3 reflect these facts.

The results of Yao and Zhang [34] (R. R. model) in the tip-off phase differ significantly from the results based on the other models. As mentioned before, the results of Yao and Zhang are somewhat inconsistent with a theoretical physical phenomenon. A rigid vehicle should maintain its uniform rotational acceleration about its rear shoe when the front shoe loses contact with the rigid guideway. Consequently, the slope of the pitch rate in Fig. 4.8 should be constant. A nearly straight line was obtained by both the present results and those of Chou *et al.* [35], whereas the results of Yao and Zhang [34] did not yield a straight line.

4.2.4 Case 4: A rigid vehicle moves along an elastic guideway

Figures 4.9 and 4.10 plot the time histories of the pitch angle and pitch rate of vehicle according to the R.E. and E.E. models. For comparison, the flexural rigidity of the vehicle is set equal to $1.2 \times 10^{15}\ \mathrm{N \cdot m^2}$ in the E.E. model. The pitch angles and the pitch rates of the vehicle are directly obtained from Eqs. (4.29) and (4.30), which are called the "vehicle formulation". Notably, the pitch angles and the pitch rates of the vehicle in the R.E. model were indirectly determined from the displacements of the guideway at the points of contact with the shoes of the vehicle [35]. This approach is called "guideway formulation". For consistency, the pitch angles and the pitch rates of the vehicle in the E.E. model were also computed using the "guideway formulation".

The excellent agreement between the results of the R.E. model and the results of the E.E. model that are based on the "guideway formulation" further confirm the correctness of the proposed solutions. The considerable differences in the tip-off phase be-

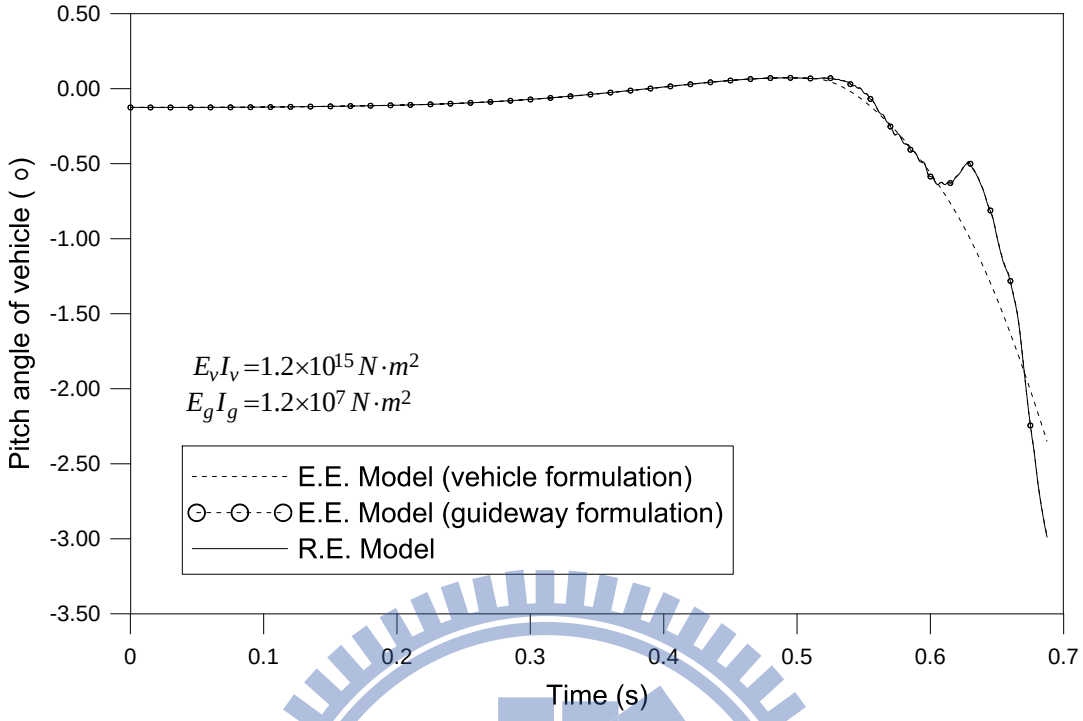

Figure 4.9: Comparisons of pitch angles $\theta - t$ of vehicle obtained using different models and formulations.

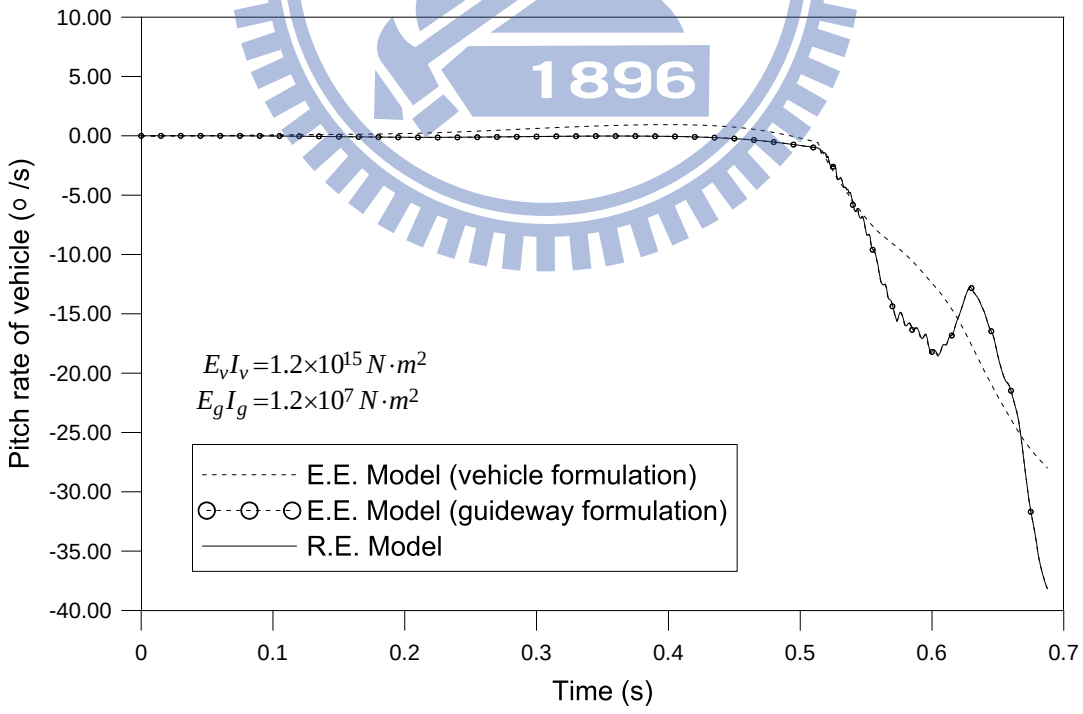

Figure 4.10: Comparisons of pitch rates $\dot{\theta} - t$ of vehicle obtained using different models and formulations.

tween the results of the R.E. model and the results of the E.E. model based on the "vehicle formulation" indicates the importance of the present solution in predicting the dynamic responses of the vehicle.

4.2.5 Case 5: An elastic vehicle moves along an elastic guideway

Case 3 concerns the motion of an elastic vehicle along an elastic guideway. Table 4.1 presents the material properties and geometric parameters of the vehicle and the guideway. To demonstrate the accuracy of the results obtained herein using ten modes and a time increment of 0.0001s, Fig. 4.11 compares the pitch angles and pitch rates of the vehicle obtained by using one mode, ten modes and 50 modes, while Fig. 4.12 compares those obtained using $\Delta t = 0.01, 0.001, 0.0001$ and 0.00001s. The excellent agreement between the results obtained using 10 and 50 modes in Fig. 4.11 demonstrates that solutions obtained using ten modes are sufficiently accurate. Similarly, the consistency between the results obtained using $\Delta t = 0.0001$ and 0.00001s in Fig. 4.12 reveals the accuracy of the solutions obtained herein using ten modes and $\Delta t = 0.0001$s.

Figures 4.13 and 4.14 compare the pitch angles and pitch rates of the vehicle obtained using three models - R.R., R.E. and E.E.. The tip-off phase starts at $t_{_F} = 0.5136$ s and ends at $t_{_R} = 0.6876$ s. In the two-shoe contact phase, the R.R. model only considers rigid body motions so that the pitch angle and pitch rate of the vehicle equal to zero, and underestimates the magnitude of the pitch angle of the vehicle, while the E.E. model includes the elastic deformations of the vehicle and guideway and yields a higher results pitch rate of the vehicle than do the other two models. In the tip-off phase, the agreement between the results obtained using the R.R. and E.E. models are better than that between the results obtained using the R.E. and E.E. models.

The maximum difference in pitch angle between the results of the R.E. and E.E. models is 0.5780° at $t = 0.6350$ s, while the maximum difference in pitch rate is $10.2670^\circ/\text{s}$ at $t = 0.6876$ s. The considerable differences between the results obtained using the R.E. and E.E. models are because, as shown in Section 3.2, different formu-

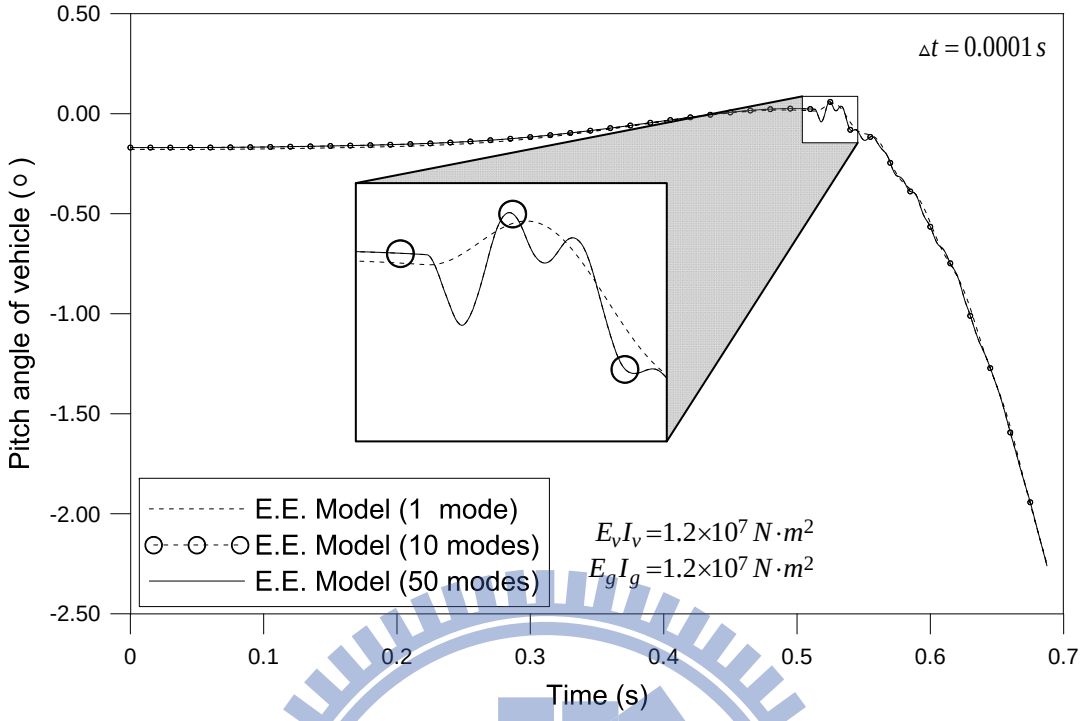

Figure 4.11: Comparisons of pitch angles of vehicle obtained using different numbers of modes.

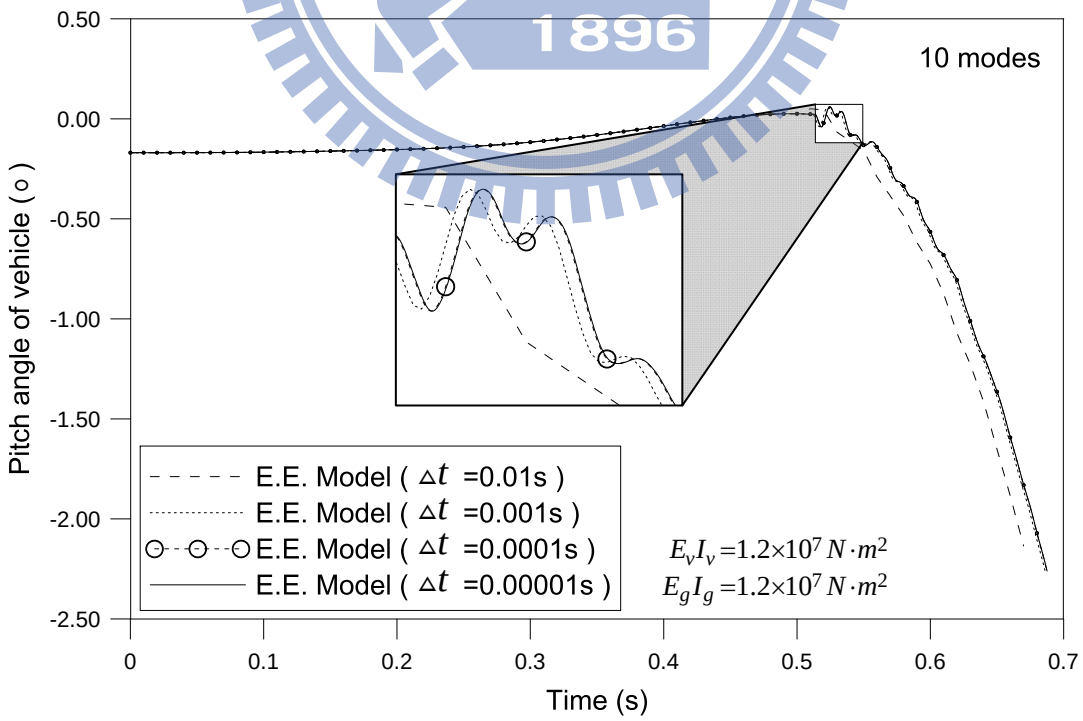

Figure 4.12: Comparisons of pitch angles of vehicle obtained using different time increment.

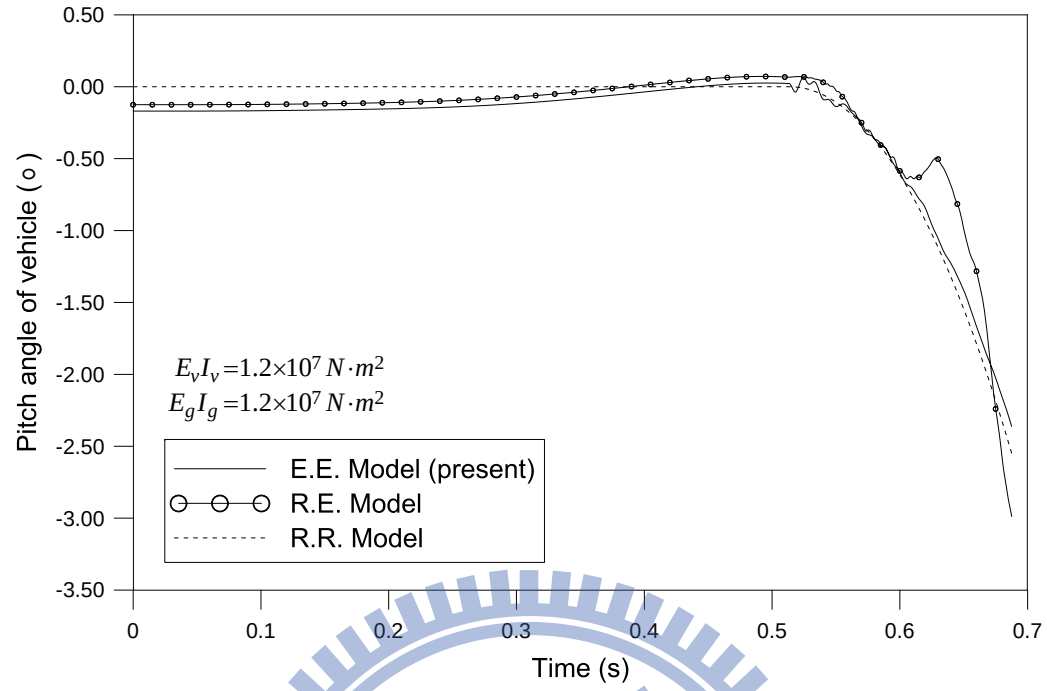

Figure 4.13: Comparison of pitch angles of vehicle obtained using different models.

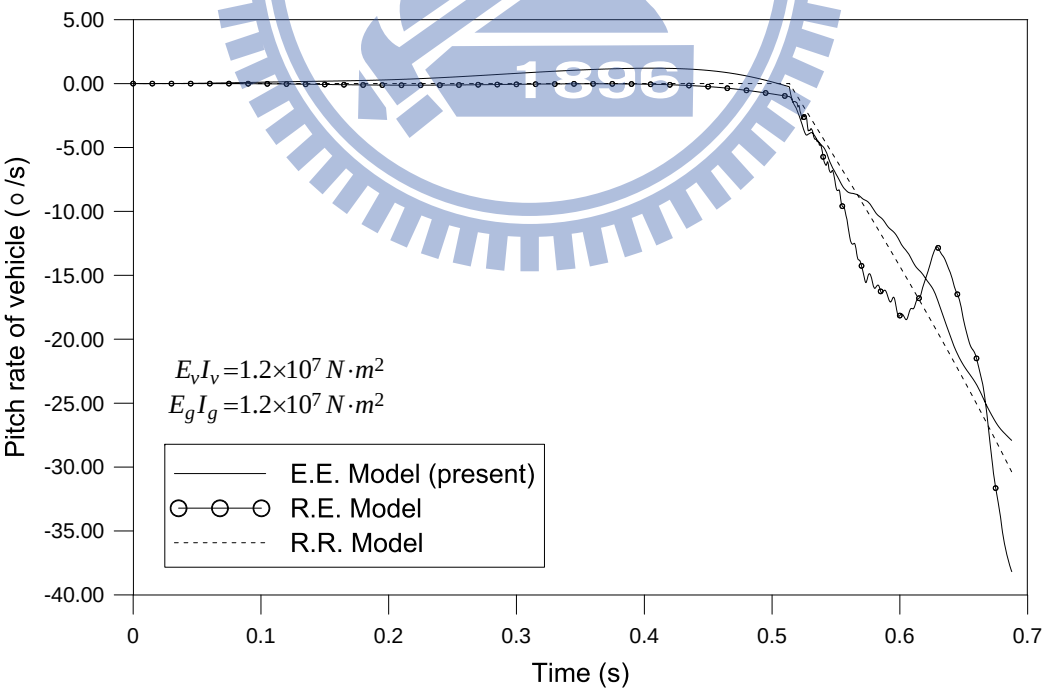

Figure 4.14: Comparison of pitch rates of vehicle obtained using different models.

lations were employed to determine the pitch angles and pitch rates of the vehicle. However, at the end of the tip-off phase ($t = 0.6876$ s), the E.E., R.E. and R.R. models yield pitch angles of the vehicle of $-2.3622°$, $-2.9886°$ and $-2.5546°$, respectively, and pitch rates of $-27.914°/\text{s}$, $-38.181°/\text{s}$ and $-30.41°/\text{s}$. These differences significantly influence the trajectory of the vehicle after the vehicle leaves the guideway.

4.3 Parametric Study

After the accuracy of the proposed approach was confirmed, the solutions are utilized to examine the effects of some important parameters on the pitch angle and pitch rate of the vehicle at take-off. The important parameters of interest are the length of the guideway, L_g; the distance between the shoes of the vehicle, d, the mass ratio, M_r, defined as $\frac{\rho_v A_v L_v}{\rho_g A_g L_g}$, and the flexural rigidity ratio, R_r, defined as $\frac{E_v I_v}{E_g I_g}$. In control engineering, the pitch angle and pitch rate of a vehicle at take-off are the main concerns because they are the factors that dominate the trajectory of the vehicle after it has left the guideway.

4.3.1 Influence of length of guideway

The length of the guideway affects the duration of a vehicle's moving along the guideway. Increasing the length of the guideway increases the period for which the two shoes are in contact with the guideway. Increasing the length of the guideway also increases the velocity of the vehicle when it enters the tip-off phase, because of increasing the period for which the motor thrust acts, and reduces the duration t_R - t_F. Consequently, the length of the guideway substantially affects the tip-off responses of the vehicle.

Table 4.4 presents three combinations of flexural rigidities of the vehicle and the guideway that are considered herein. Case EI01 involves a flexible vehicle and a flexible guideway; case EI02 involves a rigid vehicle and a flexible guideway, while case EI03 involves a rigid vehicle and a rigid guideway.

Figures 4.15 and 4.16, respectively, display the variations of the pitch angle and the pitch rate of vehicle at take-off with the length of the guideway between 4 m and 12 m. Tables 4.1 and 4.4 present the other parameters that must be known to solve for the dynamic responses of the vehicle and the guideway. Both the pitch angle and the pitch rate of the vehicle at take-off generally decrease as the length of the guideway increases, because the duration t_R - t_F decreases. Accordingly, a longer guideway is associated with a weaker vehicle tip-off effect. Nevertheless, the length of the guideway must still be selected to fit the spatial limits on the launcher system.

Table 4.4: Combinations of flexural rigidities of vehicle and guideway.

	Flexural rigidity $(N \cdot m^2)$	
Case	$E_v I_v$	$E_g I_g$
EI01	1.2×10^{06}	1.2×10^{07}
EI02	1.2×10^{15}	1.2×10^{06}
EI03	1.2×10^{15}	1.2×10^{15}

The results given in Figs. 4.15 and 4.16 also reveal that the flexural rigidity combination EI02 always yields a smaller pitch angle and pitch rate of the vehicle than the combination EI03. Combination EI01 yields results that may be larger or smaller than obtained using the other two combinations of flexural rigidity, depending on the length of the guideway. Consequently, the results imply that the vehicle should be to the maximum extent possible stiffer than the guideway.

4.3.2 Influence of distance between shoes of vehicle

As stated in the previous section, the value of t_R - t_F significantly affects the tip-off response. The distance between the shoes of the vehicle is a design factor that critically influences t_R - t_F. Hence, it is worth showing the variations of pitch angle and pitch

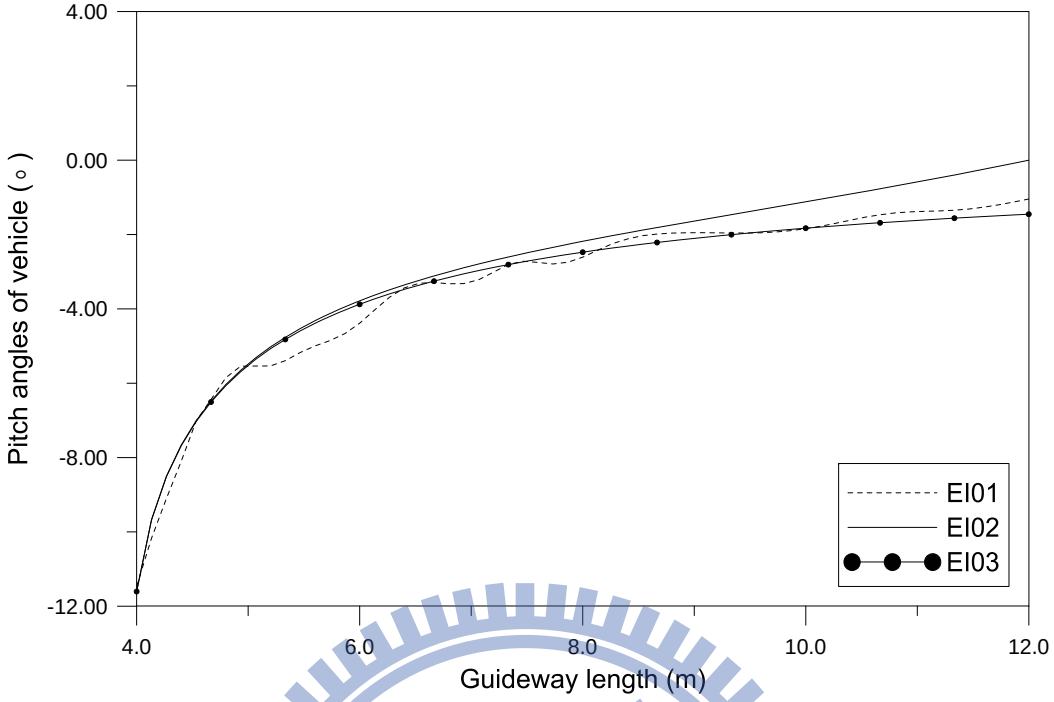

Figure 4.15: Effect of length of guideway on pitch angle of vehicle at take-off ($\theta - L_g$ diagram).

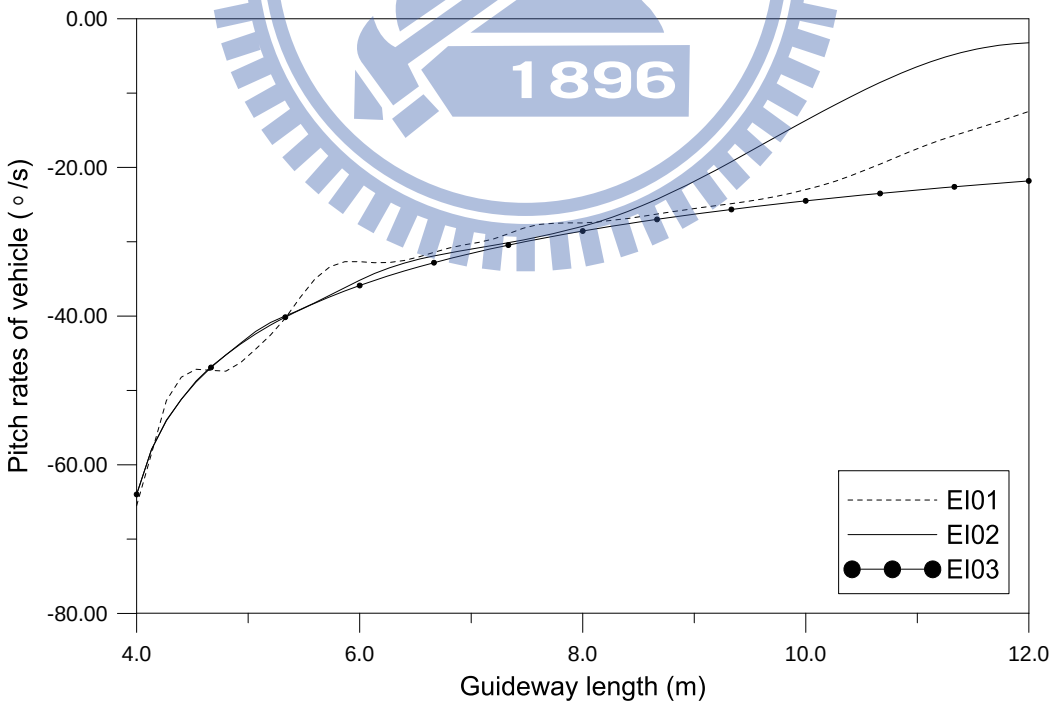

Figure 4.16: Effect of length of guideway on pitch rate of vehicle at take-off ($\dot{\theta} - L_g$ diagram).

rate of the vehicle at take-off with the distance between the shoes of the vehicle. The three combinations of flexural rigidities of the vehicle and the guideway in Table 4.4 are also considered here.

Figures 4.17 and 4.18, respectively, plot the variations of the pitch angle and pitch rate of the vehicle at take-off with the distance between the shoes of the vehicle from 2 m to 4 m. As expected, as the distance between the shoes of the vehicle increases, the magnitudes of the pitch angle and the pitch rate of the vehicle at take-off increases. Again, the vehicle and the guideway with the flexural rigidity combination EI02 always gives a smaller pitch angle and pitch rate of the vehicle than does combination EI03. Combination EI01 yields a larger pitch angle than does combination EI02.

4.3.3 Influence of mass ratio and flexural rigidity ratio

The mass ratio M_r and flexural rigidity ratio R_r can be designed for various real applications. The effects of these two ratios on the pitch angle and pitch rate of the vehicle at take-off is of interest. These two ratios are changed herein by changing the mass and flexural rigidity, respectively, of the guideway only.

Figures 4.19 and 4.20 plot the variations of pitch angle and pitch rate of the vehicle at take-off with M_r and R_r, respectively. Each figure displays three-dimensional plots and contours. Figure 4.19 reveals that the pitch angle decreases as R_r increases but a change in M_r has no significant effect. Figure 4.20 indicates that as both R_r and M_r increase, the pitch rate of the vehicle at take-off decreases. The contour plots are very useful for selecting a set of optimum parameters of launch systems.

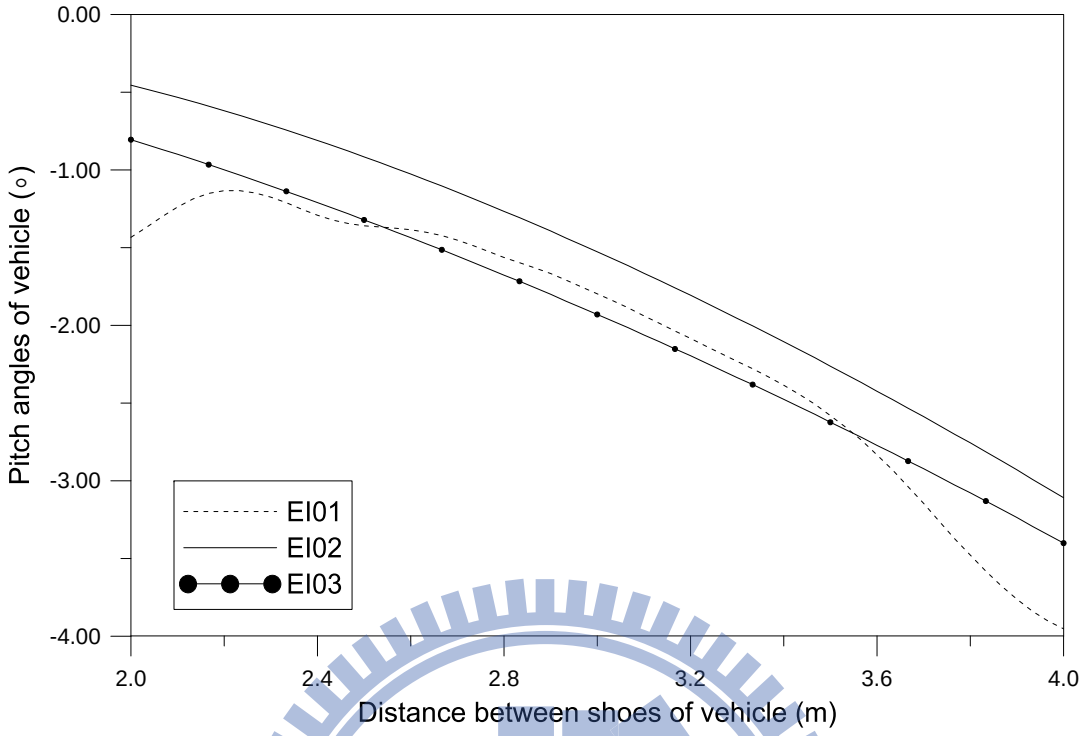

Figure 4.17: Effect of distance between shoes of vehicle on pitch angle of vehicle at take-off.

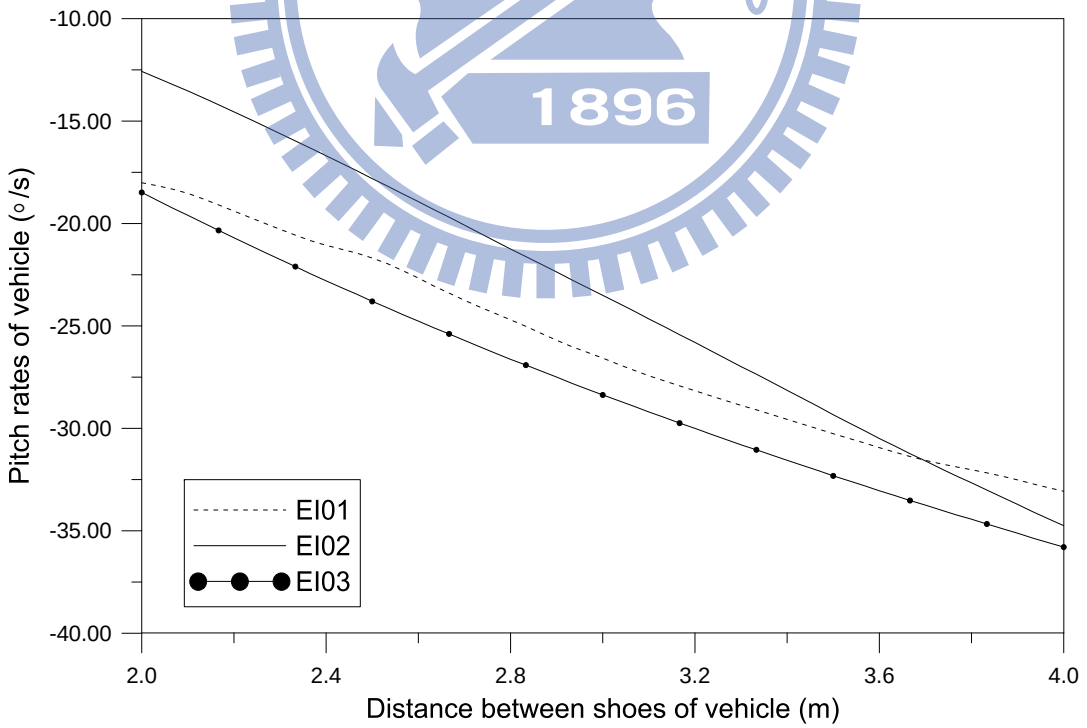

Figure 4.18: Effect of distance between shoes of vehicle on pitch rate of vehicle at take-off.

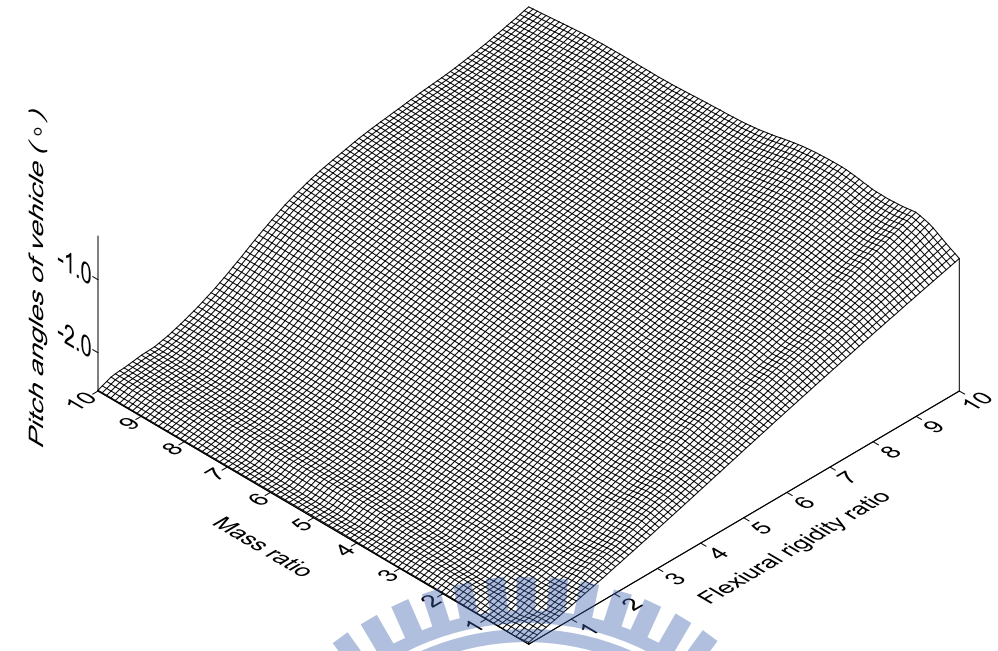

(a)

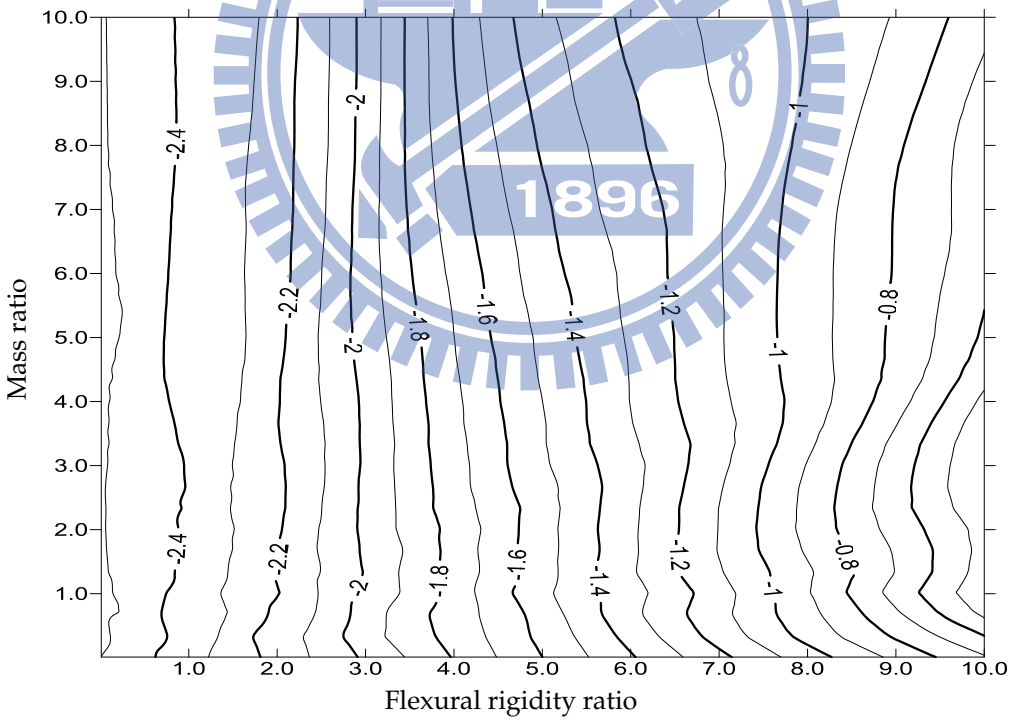

(b)

Figure 4.19: Effect of mass ratio and flexural rigidity ratio on pitch angle of vehicle: (a) 3D plot (b) contour plot.

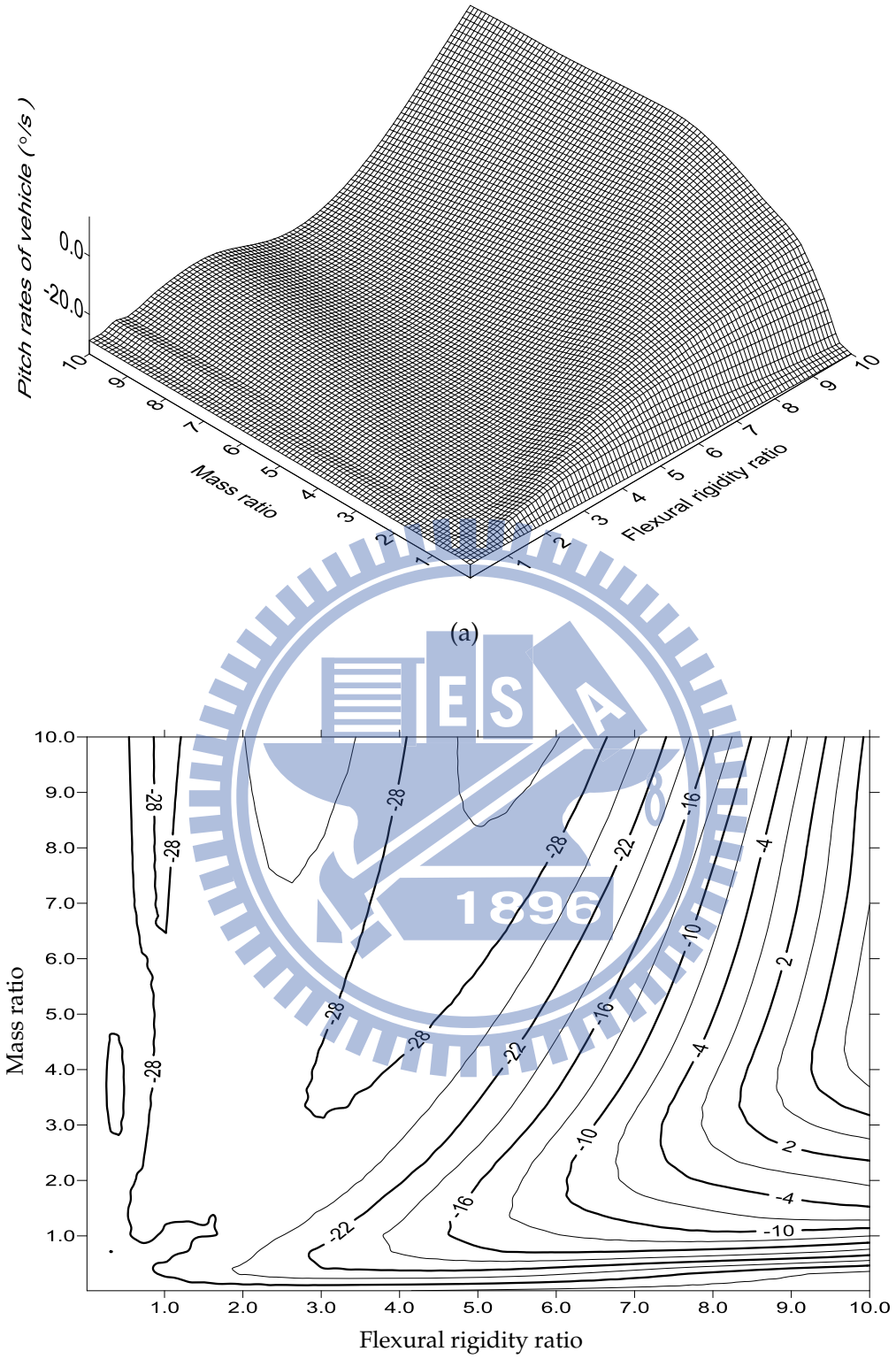

Figure 4.20: Effect of mass ratio and flexural rigidity ratio on pitch rate of vehicle: (a) 3D plot (b) contour plot.

CHAPTER FIVE

Conclusions and Future works

5.1 Conclusions

This study investigated the tip-off dynamic responses of a vehicle moving along its guideway. Two models were developed to determine those dynamic responses, namely, R.E. model and E.E. model. In the R.E. model, the vehicle is assumed rigid and its guideway is modeled as a flexible beam, while both of the vehicle and guideway are modeled as flexible beams in the E.E. model. The inertia, Coriolis, and centrifugal forces are considered in these models. Theoretically, the proposed models capture more closely the practical reality than the commonly used R.R. model which assumes both of the vehicle and the guideway rigid.

The governing equations of the proposed models were reduced to a set of nonlinear ordinary differential equations via the modal superposition method along with the Lagrangian approach. Then, the set of nonlinear differential equations were solved using the Petzold-Gear BDF method. The proposed solutions were validated through the convergence studies using various numbers of modes and time increments and by comparing them with published results for the special cases of a rigid vehicle moving along a rigid guideway. The excellent agreement between the published results and the present results confirmed the correctness of the proposed solutions.

The proposed solutions were further employed to investigate the pitch angle and the pitch rate of the vehicle at take-off influenced by the length of the guideway L,

the distance between the shoes of the vehicle d, the damping ratio ξ, the angle of inclination θ_E, the mass ratio M_r and the flexural rigidity ratio R_r of the vehicle to the guideway. The numerical results revealed several facts, which are useful in designing a launch system, as follows:

1. Increasing in the length of the guideway reduces the pitch angle and the pitch rate of the vehicle at take-off. Reducing the distance between the shoes of the vehicle has a similar effect.

2. Increasing the flexural rigidity ratio of the vehicle to the guideway also reduces the pitch angle and the pitch rate of the vehicle at take-off, while increasing only the mass ratio significantly reduces the pitch rate.

3. When the damping ratio of the guideway is less than 0.01, the tip-off responses of the vehicle are too sensitive. Therefore, it would be preferable to select appropriate guideway materials or heavily damped guideways to minimize the dynamic responses when designing launch systems.

4. The tip-off dynamic responses of a vehicle under the action of the Coriolis force and centrifugal force are approximately 2.0% greater than those in the absence of these forces. In this study, the initial speed of the launched vehicle before take-off is only approximately one-tenth of that of a high-speed train. Therefore, the effects of the Coriolis force and centrifugal force are not significant

5. The dynamic responses obtained from an elastic guideway model could be 30% greater than that obtained from the R.R. model. This highlights the importance of adopting an elastic guideway model when designing actual launch systems.

6. The models of elastic vehicle and elastic guideway, rigid vehicle and elastic guideway, and rigid vehicle and rigid guideway yield significant different values of pitch angle and pitch rate of the vehicle at take-off, which are very important for controlling the trajectory of the vehicle after it has left the guideway.

5.2 Future works

1. In real applications, the guideway are exactly simply supported. To simulate the reality, the vehicle and the guideway can be both modeled as free-free beams, and the shoes of the vehicle and the supports of the guideway are modeled by appropriate springs.

2. The movement of a vehicle along its guideway is more complex than the present study due to thrust asymmetry and manufacturing defects, which can induce the vehicle to rotate, pitch, or yaw. Therefore, a more rigorous analysis of the dynamic interactions is required.

3. When a vehicle-guideway system locates in a moving warship, the angle of inclination of guideway is a time-dependent function ($\theta_E(t)$), which depends on the movement of the warship including rotating, pitching, or yawing. New solutions have to further develop to accurately determine the behaviors in the tip-off phase.

Bibliography

[1] Subcommittee on Vibration Problems Associated with Flexural Members on Transit Systems Committee on Flexural Members of the Committee on Metals of the Structural Division. "Dynamics of Steel Elevated Guideways-An Overview". Journal of Structural Engineering, ASCE, 111(9):1873–1898, 1984.

[2] G. G. Stokes. "Discussion of a Differential Equation relating to the Breaking of Railway Bridges". Part 5:707–735, 1849.

[3] S. P. Timoshenko and D. H. Young. Vibration Problems in Engineering. D. Van Nostrand Co., New York, 3rd ed. edition, 1955.

[4] R. S. Ayre, G. Ford, and L. S. Jacobsen. "Transverse vibration of a two-span beam under action of a moving constant force". Journal of Applied Mechanics, 17(1):1–12, 1950.

[5] N. Sridharan and A. K. Mallik. "Numerical analysis of vibration of beams subjected to moving loads". Journal of Sound and Vibration, 65(1):147–150, 1979.

[6] K. Henchi, M. Fafard, G. Dhatt, and M. Talbot. "Dynamic behaviour of multi-span beams under moving loads". Journal of Sound and Vibration, 199(1):33–50, 1997.

[7] H. H. Jeffcott. "On the vibrations of beams under the action of moving loads". Phil. Magazine Ser. 7, 8(48):66–97, 1929.

[8] Milomir M. Stanišić and Jay C. Hardin. "On the response of beams to an arbitrary number of concentrated moving masses". Journal of the Franklin Institute, 287(2):115–123, 1969.

[9] J. E. Akin and M. Mofid. "Numerical solution for response of beams with moving mass". Journal of Structural Engineering, ASCE, 115(1):120–131, 1989.

[10] M. Dehestani, M. Mofid, and A. Vafai. "Investigation of critical influential speed for moving mass problems on beams". Applied Mathematical Modelling, 33(10):3885–3895, 2009.

[11] J. J. Wu. "Dynamic analysis of an inclined beam due to moving loads". Journal of Sound and Vibration, 288(1-2):107–131, 2005.

[12] Arturo O. Cifuentes. "Dynamic response of a beam excited by a moving mass". Finite Elements in Analysis and Design, 5(3):237–246, 1989.

[13] G. Michaltsos, D. Sophianopoulos, and A. N. Kounadis. "The effect of a moving mass and other parameters on the dynamic response of a simply supported beam". Journal of Sound and Vibration, 191(3):357–362, 1996.

[14] H. P. Lee. "Dynamic response of a beam with a moving mass". Journal of Sound and Vibration, 191(2):289–294, 1996.

[15] H. P. Lee. "Transverse vibration of a Timoshenko beam acted on by an accelerating mass". Applied Acoustics, 47(4):319–330, 1996.

[16] G. T. Michaltsos. "Dynamic behaviour of a single-span beam subjected to loads moving with variable speeds". Journal of Sound and Vibration, 258(2):359–372, 2002.

[17] Ladislav Frýba. Vibration of Solids and Structures under Moving Loads. Thomas Telford, third edition, 1999.

[18] J. M. Biggs. Introduction to Structural Dynamics. McGraw-Hill, New York, N.Y., 1964.

[19] Alexander V. Pesterev and Lawrence A. Bergman. "Response of elastic continuum carrying moving linear oscillator". Journal of Engineering Mechanics, 123(8):878–884, 1997.

[20] Y. B. Yang and Y. S. Wu. "A versatile element for analyzing vehicle-bridge interaction response". Engineering Structures, 23(5):452–469, 2001.

[21] Yeong-Bin Yang, Jong-Dar Yau, and Lin-Ching Hsu. "Vibration of simple beams due to trains moving at high speeds". Engineering Structures, 19(11):936–944, 1997.

[22] R. Moreno Delgado and S. M. dos Santos R.C. "Modelling of railway bridge-vehicle interaction on high speed tracks". Computers and Structures, 63(3):511–523, 1997.

[23] Jianzhong Li and Mubiao Su. "The resonant vibration for a simply supported girder bridge under high-speed trains". Journal of Sound and Vibration, 224(5):897–915, 1999.

[24] Qi-Lin Zhang, A. Vrouwenvelder, and J. Wardenier. "Numerical simulation of train-bridge interactive dynamics". Computers and Structures, 79(10):1059–1075, 2001.

[25] P. Museros, M. L. Romero, A. Poy, and E. Alarc "Advances in the analysis of short span railway bridges for high-speed lines". Computers and Structures, 80(27-30):2121–2132, 2002.

[26] He Xia, Nan Zhang, and Guido De Roeck. "Dynamic analysis of high speed railway bridge under articulated trains". Computers and Structures, 81(26-27):2467–2478, 2003.

[27] Eugenia C. Cojocaru, Hans Irschik, and Hubert Gattringer. "Dynamic response of an elastic bridge due to a moving elastic beam". Computers and Structures, 82(11-12):931–943, 2004.

[28] He Xia and Nan Zhang. Dynamic interaction of vehicles and structures. Beijing, Science press, 2005.

[29] Zhang Tao and Zheng Gang-Tie. "Vibration Analysis of an Elastic Beam Subjected to a Moving Beam with Flexible Connections". Journal of Engineering Mechanics, 136(1):120–130, 2010.

[30] T. R. Sreeram and N. T. Sivaneri. "FE-analysis of a moving beam using Lagrangian multiplier method". International Journal of Solids and Structures, 35(28-29):3675–3694, 1998.

[31] Kim Seong-Min. "Vibration and stability of axial loaded beams on elastic foundation under moving harmonic loads". Engineering Structures, 26(1):95–105, 2004.

[32] Li-Qun Chen, Xiao-Dong Yang, and Chang-Jun Cheng. "Dynamic stability of an axially accelerating viscoelastic beam". European Journal of Mechanics - A/Solids, 23(4):659–666, 2004.

[33] R. F. Fung, P. Y. Lu, and C. C. Tseng. "Non-linearly dynamic modelling of an axially moving beam with a tip mass". Journal of Sound and Vibration, 218(4):559–571, 1998.

[34] Chang-Ren Yao and Po Zhang. Rocket and guided missile launcher device design. Beigin Institute of Technology Press, 1998.

[35] S. N. Chou, F. P. Cheng, and C. S. Huang. "Tip-off effect analysis of a vehicle moving along an inclined guideway by considering dynamic interactions". Journal of The Chinese Institute of Engineers, Vol. 36, 2013.

[36] S. N. Chou, F. P. Cheng, and C. S. Huang. "Dynamic analyses of a flexible vehicle moving along a flexible guideway considering the tip-off effect".

International Journal of Structural Stability and Dynamics, Vol. 13, No. 1, 2013.

[37] C.W. Gear and L. R. Petzold. "ODE methods for the solutions of differential/algebraic equations". SIAM Journal Numerical Analysis, 21(4):716–728, 1984.

[38] Singiresu S. Rao. Vibration of continuous systems. Department of Mechanical and Aerospace Engineering. John Wiley Sons, Inc., Hoboken, New Jersey, 2007.

[39] Ray W. Clough and Joseph Penzien. Dynamics of structures. Computers and Structures, Inc., Berkeley, 2003.

Appendix

A.1 Derivation of $\widetilde{H}_i^a$, $\widetilde{H}_i^b$, $\widetilde{H}_i^c$, $\widetilde{H}_i^d$.

The mode shape functions of free-free beam are

$$\phi_i(x_1) = \cos(\beta_{vi}x_1) + \cosh(\beta_{vi}x_1) - \Upsilon_i\left[\sin(\beta_{vi}x_1) + \sinh(\beta_{vi}x_1)\right] \tag{A.1}$$

where $i = 1, 2, ..., N$

$$\beta_{vi}^4 = \omega_{vi}^2 \cdot \frac{\rho_v A_v}{E_v I_v}, \quad \Upsilon_i = \frac{\cos(\beta_{vi}L_v) - \cosh(\beta_{vi}L_v)}{\sin(\beta_{vi}L_v) - \sinh(\beta_{vi}L_v)}, \quad \beta_{vi}L_v \approx \left(i + \frac{1}{2}\right)\pi \tag{A.2}$$

Accordingly, $\phi_i'(x_1)$ and $\phi_i''(x_1)$ are

$$\phi_i'(x_1) = \beta_{vi}\left\{-\sin(\beta_{vi}x_1) + \sinh(\beta_{vi}x_1) - \Upsilon_i\left[\cos(\beta_{vi}x_1) + \cosh(\beta_{vi}x_1)\right]\right\} \tag{A.3a}$$

$$\phi_i''(x_1) = \beta_{vi}^2\left\{-\cos(\beta_{vi}x_1) + \cosh(\beta_{vi}x_1) + \Upsilon_i\left[\sin(\beta_{vi}x_1) - \sinh(\beta_{vi}x_1)\right]\right\} \tag{A.3b}$$

■ $\widetilde{H}_i^a \equiv \int_0^{L_v} \phi_i(x_1)\phi_i(x_1)dx_1$

$$= \int_0^{L_v} \left\{ \cos(\beta_{vi}x_1) + \cosh(\beta_{vi}x_1) - \Upsilon_i \left[\sin(\beta_{vi}x_1) + \sinh(\beta_{vi}x_1) \right] \right\}^2 dx_1$$

$$= \int_0^{L_v} \Big[\cos^2(\beta_{vi}x_1) + 2\cos(\beta_{vi}x_1)\cosh(\beta_{vi}x_1) + \cosh^2(\beta_{vi}x_1)$$
$$- 2\Upsilon_i \cos(\beta_{vi}x_1)\sin(\beta_{vi}x_1) - 2\Upsilon_i \cosh(\beta_{vi}x_1)\sin(\beta_{vi}x_1)$$
$$- 2\Upsilon_i \cos(\beta_{vi}x_1)\sinh(\beta_{vi}x_1) - 2\Upsilon_i \cosh(\beta_{vi}x_1)\sinh(\beta_{vi}x_1)$$
$$+ \Upsilon_i^2 \sin^2(\beta_{vi}x_1) + 2\Upsilon_i^2 \sin(\beta_{vi}x_1)\sinh(\beta_{vi}x_1)$$
$$+ \Upsilon_i^2 \sinh^2(\beta_{vi}x_1) \Big] dx_1$$

$$= \frac{1}{4\beta_{vi}} \Big\{ 4\beta_{vi}x_1 + 4\cosh(\beta_{vi}x_1)\sin(\beta_{vi}x_1) + \sin(2\beta_{vi}x_1)$$
$$+ 4\cos(\beta_{vi}x_1)\sinh(\beta_{vi}x_1) + \sinh(2\beta_{vi}x_1) - 4\left[\sin(\beta_{vi}x_1) + \sinh(\beta_{vi}x_1) \right]^2 \Upsilon_i$$
$$+ \Big[4\cosh(\beta_{vi}x_1)\sin(\beta_{vi}x_1) - \sin(2\beta_{vi}x_1) - 4\cos(\beta_{vi}x_1)\sinh(\beta_{vi}x_1)$$
$$+ \sinh(2\beta_{vi}x_1) \Big] \Upsilon_i^2 \Big\} \Big|_0^{L_v}$$

$$= \frac{1}{4\beta_{vi}} \Big\{ 4\beta_{vi}L_v + 4\cosh(\beta_{vi}L_v)\sin(\beta_{vi}L_v) + \sin(2\beta_{vi}L_v)$$
$$+ 4\cos(\beta_{vi}L_v)\sinh(\beta_{vi}L_v) + \sinh(2\beta_{vi}L_v) - 4\left[\sin(\beta_{vi}L_v) + \sinh(\beta_{vi}L_v) \right]^2 \Upsilon_i$$
$$+ \Big[4\cosh(\beta_{vi}L_v)\sin(\beta_{vi}L_v) - \sin(2\beta_{vi}L_v) - 4\cos(\beta_{vi}L_v)\sinh(\beta_{vi}L_v)$$
$$+ \sinh(2\beta_{vi}L_v) \Big] \Upsilon_i^2 \Big\} \qquad \text{(A.4)}$$

Using $\sin(2\beta_{vi}L_v) = 2\sin(\beta_{vi}L_v)\cos(\beta_{vi}L_v)$, $\sinh(2\beta_{vi}L_v) = 2\sinh(\beta_{vi}L_v)\cosh(\beta_{vi}L_v)$, $\cos(\beta_{vi}L_v) = 0$, and $\sinh^2(\beta_{vi}L_v) = \cosh^2(\beta_{vi}L_v) - 1$, one can simplify Eq. (A.4) as

$$\widetilde{H}_i^a = \int_0^{L_v} \phi_i(x_1)\phi_i(x_1)dx_1$$
$$= \frac{1}{2\beta_{vi}} \Big[\left(\Upsilon_i^2 + 1\right) \cosh\left(\beta_{vi}L_v\right) \sinh\left(\beta_{vi}L_v\right) - 2\Upsilon_i \cosh^2\left(\beta_{vi}L_v\right)$$
$$+ 2\left(\Upsilon_i^2 + 1\right) \sin\left(\beta_{vi}L_v\right) \cosh\left(\beta_{vi}L_v\right) + 2\beta_{vi}L_v$$
$$-4\Upsilon_i \sin\left(\beta_{vi}L_v\right) \sinh\left(\beta_{vi}L_v\right) \Big] \tag{A.5}$$

■ $$\widetilde{H}_i^b \equiv \int_0^{L_v} \phi_i^{'}(x_1)\phi_i(x_1)dx_1$$
$$= \int_0^{L_v} \beta_{vi} \left\{ -\sin\left(\beta_{vi}x_1\right) + \sinh\left(\beta_{vi}x_1\right) - \Upsilon_i \left[\cos\left(\beta_{vi}x_1\right) + \cosh\left(\beta_{vi}x_1\right) \right] \right\}$$
$$\cdot \left\{ \cos\left(\beta_{vi}x_1\right) + \cosh\left(\beta_{vi}x_1\right) - \Upsilon_i \left[\sin\left(\beta_{vi}x_1\right) + \sinh\left(\beta_{vi}x_1\right) \right] \right\} dx_1$$
$$= \int_0^{L_v} \beta_{vi} \Big[-\cos\left(\beta_{vi}x_1\right) \sin\left(\beta_{vi}x_1\right) - \cosh\left(\beta_{vi}x_1\right) \sin\left(\beta_{vi}x_1\right)$$
$$+ \cos\left(\beta_{vi}x_1\right) \sinh\left(\beta_{vi}x_1\right) + \cosh\left(\beta_{vi}x_1\right) \sinh\left(\beta_{vi}x_1\right) - \Upsilon_i \cos^2\left(\beta_{vi}x_1\right)$$
$$- 2\Upsilon_i \cos\left(\beta_{vi}x_1\right) \cosh\left(\beta_{vi}x_1\right) - \Upsilon_i \cosh^2\left(\beta_{vi}x_1\right) + \Upsilon_i \sin^2\left(\beta_{vi}x_1\right)$$
$$- \Upsilon_i \sinh^2\left(\beta_{vi}x_1\right) + \Upsilon_i^2 \cos\left(\beta_{vi}x_1\right) \sin\left(\beta_{vi}x_1\right) + \Upsilon_i^2 \cosh\left(\beta_{vi}x_1\right) \sin\left(\beta_{vi}x_1\right)$$
$$+\Upsilon_i^2 \cos\left(\beta_{vi}x_1\right) \sinh\left(\beta_{vi}x_1\right) + \Upsilon_i^2 \cosh\left(\beta_{vi}x_1\right) \sinh\left(\beta_{vi}x_1\right) \Big] dx_1$$
$$= \frac{1}{4} \Bigg\{ \cos\left(2\beta_{vi}x_1\right) + 4\cos\left(2\beta_{vi}x_1\right) \cosh\left(2\beta_{vi}x_1\right) + \cosh\left(2\beta_{vi}x_1\right)$$
$$-2\Upsilon_i \Big[2\cosh\left(\beta_{vi}x_1\right) \sin\left(\beta_{vi}x_1\right) + \sin\left(2\beta_{vi}x_1\right) + 2\cos\left(\beta_{vi}x_1\right) \sinh\left(\beta_{vi}x_1\right)$$
$$+ \sinh\left(2\beta_{vi}x_1\right) \Big] + 2\Upsilon_i^2 \left[\sin\left(\beta_{vi}x_1\right) + \sinh\left(\beta_{vi}x_1\right) \right]^2 \Bigg\} \Bigg|_0^{L_v}$$
$$= \frac{1}{4} \Bigg\{ -6 + \cos\left(2\beta_{vi}L_v\right) + 4\cos\left(\beta_{vi}L_v\right) \cosh\left(\beta_{vi}L_v\right) + \cosh\left(2\beta_{vi}L_v\right)$$
$$+ 2\Upsilon_i \left[\sin\left(\beta_{vi}L_v\right) + \sinh\left(\beta_{vi}L_v\right) \right] \left\{ -2 \left[\cos\left(\beta_{vi}L_v\right) + \cosh\left(\beta_{vi}L_v\right) \right] \right.$$
$$\left. + \Upsilon_i \left[\sin\left(\beta_{vi}L_v\right) + \sinh\left(\beta_{vi}L_v\right) \right] \right\} \Bigg\} \tag{A.6}$$

Using $\cos(2\beta_{vi}L_v) = 2\cos^2(\beta_{vi}L_v) - 1$, $\sinh^2(\beta_{vi}L_v) = \cosh^2(\beta_{vi}L_v) - 1$, $\cosh(2\beta_{vi}L_v) = \cosh^2(\beta_{vi}L_v) + \sinh^2(\beta_{vi}L_v)$ and $\cos(\beta_{vi}L_v) = 0$, one can simplify Eq. (A.6) as

$$\begin{aligned}
\widetilde{H}_i^b &= \frac{1}{4}\Bigg\{2\cosh^2(\beta_{vi}L_v) + 2\Upsilon_i\Big[\sin(\beta_{vi}L_v) + \sinh(\beta_{vi}L_v)\Big] \\
&\quad \cdot\Bigg\{\Upsilon_i\Big[\sin(\beta_{vi}L_v) + \sinh(\beta_{vi}L_v)\Big] - 2\cosh(\beta_{vi}L_v)\Bigg\} - 8\Bigg\} \\
&= \frac{1}{2}\left(\Upsilon_i^2 + 1\right)\cosh^2(\beta_{vi}L_v) - \Upsilon_i\cosh(\beta_{vi}L_v)\sin(\beta_{vi}L_v) - 2 \\
&\quad - \Upsilon_i\cosh(\beta_{vi}L_v)\sinh(\beta_{vi}L_v) + \Upsilon_i^2\sin(\beta_{vi}L_v)\sinh(\beta_{vi}L_v) \qquad \text{(A.7)}
\end{aligned}$$

■ $$\begin{aligned}
\widetilde{H}_i^c &\equiv \int_0^{L_v} \phi_i''(x_1)\phi_i(x_1)dx_1 \\
&= \int_0^{L_v} \beta_{vi}^2\Bigg\{-\cos(\beta_{vi}x_1) + \cosh(\beta_{vi}x_1) + \Upsilon_i\Big[\sin(\beta_{vi}x_1) - \sinh(\beta_{vi}x_1)\Big]\Bigg\} \\
&\quad \Bigg\{\cos(\beta_{vi}x_1) + \cosh(\beta_{vi}x_1) - \Upsilon_i\Big[\sin(\beta_{vi}x_1) + \sinh(\beta_{vi}x_1)\Big]\Bigg\}dx_1 \\
&= \int_0^{L_v} \beta_{vi}^2\Big[-\cos^2(\beta_{vi}x_1) + \cosh^2(\beta_{vi}x_1) + 2\Upsilon_i\cos(\beta_{vi}x_1)\sin(\beta_{vi}x_1) \\
&\quad -2\Upsilon_i\cosh(\beta_{vi}x_1)\sinh(\beta_{vi}x_1) - \Upsilon_i^2\sin^2(\beta_{vi}x_1) + \Upsilon_i^2\sinh^2(\beta_{vi}x_1)\Big]dx_1 \\
&= \frac{1}{4}\beta_{vi}\Big[-\sin(2\beta_{vi}x_1) + \sinh(2\beta_{vi}x_1) - 4\Upsilon_i\cos^2(\beta_{vi}x_1) - 4\Upsilon_i\cosh^2(\beta_{vi}x_1) \\
&\quad -4\Upsilon_i^2\beta_{vi}x_1 + \Upsilon_i^2\sin(2\beta_{vi}x_1) + \Upsilon_i^2\sinh(2\beta_{vi}x_1)\Big]\Big|_0^{L_v} \\
&= \frac{1}{4}\beta_{vi}\Bigg\{\sinh(2\beta_{vi}L_v) - \sin(2\beta_{vi}L_v) + 2\Upsilon_i\Big[2 - \cos(2\beta_{vi}L_v) - \cosh(2\beta_{vi}L_v)\Big] \\
&\quad -\Upsilon_i^2\Big[4\beta_{vi}L_v - \sin(2\beta_{vi}L_v) - \sinh(2\beta_{vi}L_v)\Big]\Bigg\} \qquad \text{(A.8)}
\end{aligned}$$

Using $\sin(2\beta_{vi}L_v) = 2\sin(\beta_{vi}L_v)\cos(\beta_{vi}L_v)$, $\cos(2\beta_{vi}L_v) = 2\cos^2(\beta_{vi}L_v) - 1$, $\cosh(2\beta_{vi}L_v) = 2\cosh^2(\beta_{vi}L_v) - 1$, and $\sinh(2\beta_{vi}L_v) = 2\sinh(\beta_{vi}L_v)\cosh(\beta_{vi}L_v)$, one can simplify Eq. (A.8) as

$$\widetilde{H}_i^c = -\frac{1}{4}\beta_{vi}\left\{2\cos\left(\beta_{vi}L_v\right)\sin\left(\beta_{vi}L_v\right) - 2\cosh\left(\beta_{vi}L_v\right)\sinh\left(\beta_{vi}L_v\right)\right.$$
$$+ 2\Upsilon_i\left[-4 + 2\cos^2\left(\beta_{vi}L_v\right) + 2\cosh^2\left(\beta_{vi}L_v\right)\right] - \Upsilon_i^2\left[-4\beta_{vi}L_v\right.$$
$$\left.\left.+2\cos\left(\beta_{vi}L_v\right)\sin\left(\beta_{vi}L_v\right) + 2\cosh\left(\beta_{vi}L_v\right)\sinh\left(\beta_{vi}L_v\right)\right]\right\} \quad \text{(A.9)}$$

Using $\cos(\beta_{vi}L_v) = 0$, one can simplify Eq. (A.9) as

$$\widetilde{H}_i^c = \frac{1}{2}\beta_{vi}\left[\left(\Upsilon_i^2 + 1\right)\cosh\left(\beta_{vi}L_v\right)\sinh\left(\beta_{vi}L_v\right) - 2\Upsilon_i\cosh^2\left(\beta_{vi}L_v\right)\right.$$
$$\left.+4\Upsilon_i - 2\beta_{vi}L_v\Upsilon_i^2\right] \quad \text{(A.10)}$$

■ $$\widetilde{H}_i^d \equiv \int_0^{L_v}\phi_i(x_1)dx_1$$
$$= \int_0^{L_v}\left\{\cos\left(\beta_{vi}x_1\right) + \cosh\left(\beta_{vi}x_1\right) - \Upsilon_i\left[\sin\left(\beta_{vi}x_1\right) + \sinh\left(\beta_{vi}x_1\right)\right]\right\}dx_1$$
$$= \frac{1}{\beta_{vi}}\left\{\sin\left(\beta_{vi}x_1\right) + \sinh\left(\beta_{vi}x_1\right) + \Upsilon_i\left[\cos\left(\beta_{vi}x_1\right) - \cosh\left(\beta_{vi}x_1\right)\right]\right\}\Big|_0^{L_v}$$
$$= \frac{1}{\beta_{vi}}\left\{\sin\left(\beta_{vi}L_v\right) + \sinh\left(\beta_{vi}L_v\right) + \Upsilon_i\left[\cos\left(\beta_{vi}L_v\right) - \cosh\left(\beta_{vi}L_v\right)\right]\right\} \quad \text{(A.11)}$$

Using $\cos(\beta_{vi}L_v) = 0$, one can simplify Eq. (A.11) as

$$\widetilde{H}_i^d = \frac{1}{\beta_{vi}}\left[\sin\left(\beta_{vi}L_v\right) + \sinh\left(\beta_{vi}L_v\right) - \Upsilon_i\cosh\left(\beta_{vi}L_v\right)\right] \quad \text{(A.12)}$$

About the Author

姓名： 周勝男　Sheng-Nan Chou

生日： 48.11.24

籍貫： 台灣省桃園縣

學歷： 私立逢甲大學土木工程系學士

私立淡江大學土木工程系碩士班　結構組

國立交通大學土木工程系博士班　結構組

經歷： 中山科學研究院系統發展中心　助理研究員

中山科學研究院系統發展中心　副研究員

中山科學研究院系統發展中心　雄風計畫　計畫管理組副組長

中山科學研究院系統發展中心　雄風計畫　產品管理組組長

中山科學研究院系統發展中心　雄風計畫　總工程師

學術著作清單：

1. S. N. Chou and F. P. Cheng. "A Study of Tip-off Problem for Dynamical Interactions between a Launched Vehicle and Its Guideway System". *International Conference on Aerospace Engineering and Information Technology* (AEIT) Pages:164-169 (2011).

2. S. N. Chou, F. P. Cheng, and C. S. Huang. "Tip-off effect analysis of a vehicle moving along an inclined guideway by considering dynamic interactions". *Journal of The Chinese Institute of Engineers*, Vol. 36(2013).

3. S. N. Chou, F. P. Cheng, and C. S. Huang. "Dynamic analyses of a flexible vehicle moving along a flexible guideway considering the tip-off effect". *International Journal of Structural Stability and Dynamics*, Vol. 13, No.1 (2013).